Physics – Uspekhi **58** (3) 209 – 251 (2015)

REVIEWS OF TOPICAL PROBLEMS PACS numbers: 72.80.Tm, 73.61.Ph, 73.63.Fg

Electrical characteristics of carbon nanotube-doped composites

A V Eletskii, A A Knizhnik, B V Potapkin, J M Kenny

DOI: 10.3367/UFNe.0185.201503a.0225

Contents

Abstract. This paper reviews research into the electrical properties that are imparted to composite materials by introducing carbon nanotubes (CNTs) into their polymer matrices. Due to the large aspect ratio of CNTs, even a small amount of doping (at a level of 0.01 – 0.1%) is enough to increase the conductivity of the material by more than ten orders of magnitude, thus changing it from an insulator to a conductor. At low doping, charge transfer is of a percolation nature in the sense that nanotubes that are in contact with each other form conducting channels in the material. Importantly, the conductivity has a threshold nature, so that the conduction jump occurs upon an arbitrarily small increase in a doping level above the critical value. This paper summarizes experimental data on the position of the percolation threshold and the maximum magnitude of the conductivity for composites obtained using various polymer types and a variety of CNT geometries. Factors affecting the electrical characteristics of composites produced by distinct methods are analyzed. Methods for and basic results obtained from the simulation of the percolation conductivity of CNT-doped composites are discussed. Particular attention is given to contact phenomena that occur at adjacent nanotube boundaries and which determine the conductivity of CNT-doped composites.

Keywords: polymers, composites, carbon nanotubes, electrical properties

A V Eletskii National Research University
'Moscow Power Engineering Institute',
ul. Krasnokazarmennaya 14, 111250 Moscow, Russian Federation
E-mail: eletskii@mail.ru
A A Knizhnik, B V Potapkin National Research Centre
'Kurchatov Institute'; Kintechlab Limited,
pl. Akademika Kurchatova 1, 123182 Moscow, Russian Federation
E-mail: knizhnik@kintechlab.com
J M Kenny Department of Civil and Environmental Engineering,
University of Perugia,
Strada di Pentima 4, 05100 Terni (TR) Italy;
Institute of Polymer Science and Technology, ICTP-CSIC,
Calle Juan de la Cierva 3, 28006 Madrid, Spain;
Institute of Macromolecular Compounds, Russian Academy of Sciences,
V.O. Bol'shoi pr. 31, 199004 St. Petersburg, Russian Federation

Received 10 October 2014, revised 8 November 2014
Uspekhi Fizicheskikh Nauk **185** (3) 225 – 270 (2015)
DOI: 10.3367/UFNr.0185.201503a.0225
Translated by A V Eletskii; edited by A Radzig

1. Introduction

Polymer materials are finding applications in many technological processes and engineering systems due to their good mechanical characteristics, high plasticity, and relatively low cost. One of the widespread approaches to improving the characteristics of such materials is based on the use of fillers. Specifically, adding carbon nanotubes (CNTs) into a polymer matrix imparts new properties to the material due to the unique characteristics of CNTs. Young's modulus of a single-walled nanotube reaches a magnitude of order terapascal (TPa) [1] which is a record quantity for all known materials. This offers a possibility of developing the composite materials on the base of polymers possessing improved mechanical properties due to the addition of CNTs.

The main difficulty arising in the solution of the above-noted problem relates to the necessity of providing a quite reliable mechanical conjugation between the nanotube's surface and the matrix material. In the absence of such a conjugation, the nanotubes behave inside a composite like a hair in a pie, moving freely inside the matrix under mechanical loading. In this case, the addition of nanotubes results in a decrease rather than an increase in the mechanical strength of the composite. This problem can be overcome by providing a linkage between the nanotube surface and the matrix material, which is achieved through the functionalization of CNTs. Efforts of tens of laboratories in the world are focused on the solution to this problem.

Along with extraordinary mechanical properties, CNTs possess good electrical conductivity: therefore, adding those into a polymer matrix imparts electrical conducting properties to the composite material. This extends considerably the area of possible applications of composite materials and is attracting many researchers to investigate the electrical properties of such materials. The scientific community's increasing interest in studies of CNTs and composite materials with CNT fillers can be seen from the diagram presented in Fig. 1 [2]. As evident from this diagram, the annual number of publications in these areas has increased by tens of percent per year, reaching in 2010 5500 for CNTs and 1300 for composites filled with CNTs. Some fall in the number of publications in 2010 is obviously due to a lack of data relating to this last year of the period under analysis in paper [2].

The specific electrical conductivity of CNTs reaches magnitudes on the order of 10^6 S m^{-1} [3, 4], which exceeds the characteristic values for the majority of polymer materials by 15–20 orders of magnitude [5]. With such a great difference in the conductivity, just a small quantity of added CNT filler is sufficient to make a polymer conductive. One of the advantages concerning the usage of CNTs as a conductive addition to composite materials is related to the high aspect ratio η (ratio of the length l to the diameter D) for these nanoobjects. Due to such a feature, the addition of about 0.1% CNTs to a polymer matrix results in an enhancement of the conductivity of the composite by 8–10 orders of magnitude, which transforms the material from an insulator into a conductor. Then, a percolation character of the conductivity of the material appears, in accordance with which at low filler loading the charge transport occurs through a few number of conducting channels forming at the contacts of filler particles.

The percolation threshold, conventionally defined as the filler content sufficient for emerging the electrical conductivity of the material, depends on such factors as the structure of the filler particles, the sort of a polymer material, the aspect ratio, and the degree of ordering of filler particles in the composites. The dependence of the percolation threshold on the aspect ratio of the filler particles is particularly significant when CNTs are used as filler particles having an aspect ratio of order $10^3 - 10^4$. In this case, the position of the percolation threshold is inversely proportional to the aspect ratio [6] and can be found within the range of 0.01–0.1%. This important feature is attracting the interest of researchers to the problem of the development of conductive polymer-based composites with a CNT addition.

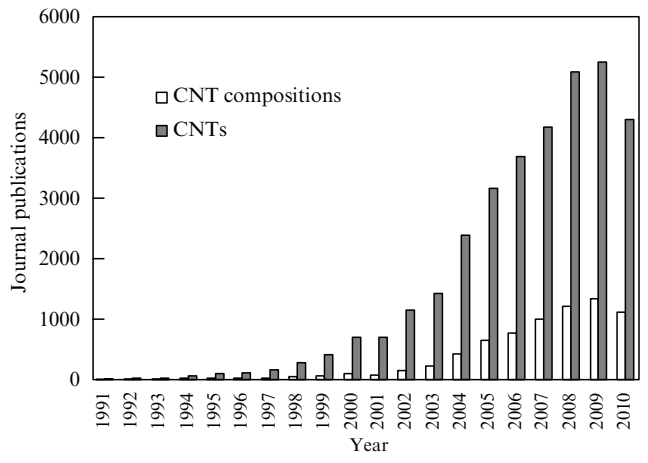

Figure 1. Change in the number of journal publications devoted to investigations in the field of CNTs (gray bars) and CNT-based composites (white bars) [2].

The properties of such materials are determined mainly by both the aspect ratio and the character of the contact between adjacent nanotube surfaces and between a nanotube and the polymer matrix. These properties have been the subject of active experimental and theoretical investigations performed in recent years. The present review contains a brief consideration of the approaches applied in those investigations and an analysis of the results obtained.

2. Experimental studies of the electrical conductivity of composites filled with CNTs

The percolation conductivity of composite materials consisting of a nonconducting matrix doped with a conducting component addition has been studied in detail by many authors (see, e.g., reviews [6–10]). Interest in investigations of the conductivity of composites on the base of polymers doped with CNTs was stimulated by the work of Coleman et al. [11], where the percolation character of the charge transport in such a material was first demonstrated. In this work, poly-*p*-phenylenevinylene-co-2.5-dioxy-*m*-phenylenevinylene (PMPV) was used as a polymer matrix. CNTs were synthesized by the standard electric arc method. Samples of the composite with various contents of CNTs were sealed with toluene and ultrasonicated. The mixture was held for 3 days until the soot precipitated. For performance of electrical measurements, a film several hundred nm thick and 4 mm^2 in area was plated on a platinum electrode deposited onto a glass substrate. The second platinum electrode was deposited from above the film. To improve the contact, the electrodes were covered with a conducting dye. The electrical conductivity of the films was measured by means of the standard two-probe method.

The measurements performed indicate a ten-order-of-magnitude enhancement in the conductivity of the composite from the initial value of $\sim 2 \times 10^{-10}$ S m^{-1} as a result of its filling with CNTs. The most abrupt increase in the conductivity (8 orders of magnitude, from 10^{-9} up to 10^{-1} S m^{-1}) was observed upon increasing the CNT content from 7 to 11%. The further increase in the filler content is accompanied by a relatively smooth rise in the composite conductivity which reaches the value of 3 S m^{-1} at the CNT content of 36%.

The observed dependence of the composite conductivity on the filler loading corresponds to the percolation behavior of the system. The treatment of those dependences on the basis of standard theoretical approaches has resulted in the percolation threshold position $p_c = 8.4\%$. Such a high value can be caused by a rather low content of nanotubes (at a level of about several percent) in the soot produced as a result of the thermal sputtering of graphite. An analysis of the experimental data implies that the effective (averaged over the volume) value of the carrier concentration below the percolation threshold is about $10^{11} - 10^{12}$ cm^{-3}, while this quantity reaches $\sim 10^{17}$ cm^{-3} upon a filler loading exceeding the percolation threshold.

Subsequent studies have shown that the electrical properties of polymer-based composites doped with CNTs depend considerably not only on the sort of polymer and type and

geometry of nanotubes (single-walled, multiwalled, aspect ratio), but also on the procedure of preparation of the composite. This is related to the high sensitivity of the electrical properties of such materials to the degree of homogeneity of the CNT distribution inside the polymer matrix. This sensitivity is most clearly defined in the vicinity of the percolation threshold. An inhomogeneous distribution of nanotubes inside the polymer results in a notable spread in values of the specific conductivity of the composite, as well as in the position of the percolation threshold.

2.1 Results of measurements of the percolation conductivity

Early publications concerned with investigations of the electrical and mechanical properties of polymer-based composites doped with CNTs have been reviewed in Refs [12, 13]. Table 1 presents the results of numerous experiments addressing the measurement of electrical conductivity of such composites. The table contains experimental data collected in Ref. [12, 13] and supplemented with the results published recently. The polymer matrices are presented in alphabetical order in the table, which contains, along with the designation of the polymer material, indications of the sort of CNTs (single-walled, multiwalled), the method of their production, the conditions of processing, the method of inserting CNTs into the polymer matrix, the position of percolation threshold p_c, the power index t determining the dependence of the conductivity from the excess of CNTs loading over the percolation threshold (5), the maximum value σ_{max} of the conductivity, and the relevant magnitude of the CNT content.

It should be noted that the main parameter characterizing the composite is the CNT content. Two various definitions of this parameter are used: volumetric content p, and mass content Φ. Due to the difference in the densities of polymers ($\rho \sim 1.2-1.5$ g cm^{-3}) and CNTs ($\rho \sim 2.2-2.3$ g cm^{-3}), these quantities are related by the formula $\Phi \approx 1.5p$.

An analysis of the data presented in Table 1 permits drawing the following inferences about the features of the percolation behavior of polymer-based composites doped with CNTs [11].

(1) The position of the percolation threshold and the value of the maximum conductivity are very sensitive to both the method of CNT processing and the conditions of CNT preparation. Moreover, the quantities characterizing the percolation threshold position and the maximum conductivity measured in various laboratories for similar samples produced by applying the same fabrication method can differ considerably from each other.

(2) The percolation threshold p_c of a composite depends on the aspect ratio η of nanotubes. In the case of the homogeneous filling of a polymer matrix with nanotubes, this dependence takes the form $p_c \sim 1/\eta$ [6], which corresponds to the mechanism of statistical percolation. In this regard, the influence of the CNT structures on the percolation characteristics of a composite is less prominent than the influence of the polymer type and the CNT dispersion method.

(3) Inserting nonentangled multiwalled CNTs into a polymer matrix results in a considerably higher conductivity (about 50-fold) than the same quantity of entangled ones.

(4) For the specific type of polymer matrix, the percolation threshold position increases as the maximum conductivity goes up.

(5) If the conductivity of a composite is lower than that following from the expression $\sigma = 500p^{2.7}$ S m^{-1} (p is the mass content of CNTs), the main mechanism of the electrical conductivity is determined by electron tunneling through a barrier formed by a polymer material in the gap between the neighboring nanotubes.

(6) Experimental results with a high value of the percolation threshold, $p_c \sim 1\%$, indicate an inhomogeneous distribution of CNTs inside the composite, while lower values of p_c point to the clusterization of homogeneously dispersed nanotubes (kinetic percolation).

(7) The power index t involved in expression (5), which describes the percolation behavior of a composite, does not depend on the geometric characteristics of CNTs or other parameters characterizing the composite.

Below, the main physical features of the percolation behavior of samples of polymer composites doped with CNTs will be considered on the basis of analyses of several experimental studies.

2.2 Percolation conductivity in an alternating field

As the electric field frequency increases, the role of percolation contacts in the charge transport decreases. This is due to the contribution from the reactive component of the impedance to the charge transport. Conductive particles inside the composite material play the role of capacitor plates that charge and discharge periodically in an alternating field, providing the charge transfer effect. These phenomena have manifested themselves in the experimental results obtained by various authors.

The electrical properties of polyamide 6 (PA6) doped with multiwalled CNTs were studied in detail in a set of publications [58, 185]. PA6 pellets doped with 20 wt.% CNTs were used as the initial material. The diameter D of CNTs was about 10 nm, and their length l exceeded 10 μm, which corresponds to the aspect ratio of $l/D \sim 1000$. For the preparation of samples with a lower content of CNTs, the initial samples were melted and mixed with the necessary quantity of the melted polymer PA6. The viscous fluid obtained was moulded under pressure. The samples PA6/MWCNT to be studied had the form of platelets about 0.5 mm thick.

The electrical properties of the samples were determined using the dielectric relaxation spectroscopy (DRS) method. In doing so, the sample under investigation with deposited gold electrodes was placed between capacitor plates and underwent the action of an alternating electric field with the frequency varied within the range of $10^{-2}-10^{6}$ Hz. This permitted the measurement of the complex impedance of the sample $Z^* = Z' - iZ''$, on which basis the frequency dependence of the complex permittivity $\varepsilon^* = \varepsilon' - i\varepsilon''$ was determined, using the well-known relation

$$\varepsilon(\omega) = \frac{1}{i\omega Z^*(\omega)\, C_0}\,. \qquad (1)$$

Here, $\omega = 2\pi f$ is the angular frequency of the electric field alternation, f is the circular frequency, and C_0 is the equivalent capacity of the free space. The conductivity of a sample in an alternating field is expressed in a standard manner through the imaginary part of the complex permittivity $\varepsilon''(\omega)$:

$$\sigma' = \varepsilon_0 \omega \varepsilon''(\omega)\,, \qquad (2)$$

Table 1. Measurement data on the percolation threshold of CNT-doped polymer composites. The data relating to a specific polymer are arranged in order of increasing the percolation threshold Φ_c. In the 'Filler' column, the CNT preparation method is shown in parentheses. In the σ_{max} column, the weight content of CNTs, corresponding to this maximum value of the conductivity, is given in parentheses. The t parameter defines the power dependence of the conductivity on the CNT content according to Eqn (5). The 'Treatment' column relates to the procedure of CNT preparation; the 'Solution' and 'Dispersion' columns specify the procedure of composite preparation.

Polymer	Filler	Treatment	l/D	Solution	Dispersion	Φ_c, wt.%	t	σ_{max}, S m^{-1} (Φ)	References
ASTAM	SWNT * (HiPco)	HCl	—	C_4H_9NO	Sonication, stirring	0.035	—	10^{-7} (0.08)	[14]
EMMA					Solution stirring			10 (10)	[15]
Rubber	SWNT				Ball milling	2 – 3		1 (10)	[16]
Nafion	SWNT				Solution stirring			3.2×10^3 (18)	[17]
Epoxy	MWNT # (CVD)	—	200	—	Heating	0.0021	1.8	10^{-3} (0.01)	[18]
Epoxy	MWNT # (CVD)	—	340	—	Heating	0.0025	1.2	2 (1)	[19]
Epoxy	MWNT # (CVD)	—	10^3	—	Heating	0.0025	—	0.4 (0.5)	[20]
Epoxy	MWNT # (CVD)	—	860	—	Heating	0.0039	1.7	2×10^{-4} (0.01)	[18]
Epoxy	SWNT * (laser)	Purified	400	C_6H_8O	Sonication	0.005	2.7	0.02 (0.1)	[21]
Epoxy	SWNT * (HiPco)	Purified	150	C_6H_8O	Sonication	0.009	3.1	10^{-5} (0.04)	[22]
Epoxy	SWNT * (laser)	Purified	400	C_6H_8O	Sonication	0.01	1.6	5×10^{-3} (0.4)	[21]
Epoxy	MWNT * (CVD)	—	10^3	—	Heat stirring	0.011	1.7	0.4 (1)	[22]
Epoxy	SWNT * (HiPco)	Purified	150	C_6H_8O	Sonication	0.023	3.2	2×10^{-4} (0.2)	[21]
Epoxy	MWNT * (CVD)	—	10^3	—	Heat stirring	0.024	1.7	0.3 (1)	[21]
Epoxy	MWNT * (CVD)		100	C_2H_6O	Sonication, stirring	0.03	—	0.1 (0.15)	[23]
Epoxy	MWNT * (CVD)		10^3	—	Stirring, calendering	0.03	—	0.01 (0.3)	[24]
Epoxy	MCHT * (CVD)	HNO_3, centrifugation, C_3H_6O	10^3	OP	Sonication	0.034	1.7	0.1 (2)	[25]
Epoxy	SWNT (arc)	—	—	C_3H_6O	Sonication, stirring	0.04	1.7	10 (4)	[26]

Table 1. (continued)

Polymer	Filler	Treatment	l/D	Solution	Dispersion	Φ_c, wt.%	t	σ_{max}, S m^{-1} (Φ)	References
Epoxy	SWNT (CVD)	—	10^3	—	Stirring, calendering	0.04	—	0.001 (0.4)	[24]
Epoxy	MWNT * (CVD)	H_2O_2/NH_4OH, centrifugation, C_3H_6O	10^3	OP	Sonication	0.042	1.8	1 (2)	[25]
Epoxy	SWNT (CVD)	—	—	C_2H_6O, NaOH	Sonication, heating	0.05	—	0.03 (0.5)	[20]
Epoxy	SWNT * (arc)	Heating, oxidation, chemical treatment	5×10^3	C_2H_6O	Sonication, vacuum pumping	0.074	1.3	10^{-3} (0.2)	[21]
Epoxy	MWNT * (CVD)	—	10^3	—	Stirring, heating	0.08	2.0	0.04 (0.6)	[22]
Epoxy	SWNT (CVD)	HCl	—	H_2O	Stirring	0.08	—	0.02 (0.4)	[28]
Epoxy	CNF	Heating, purification (CH_2Cl_2, H_2O)	300 – 1000		Sonication, stirring	0.1	1.8	10^{-3} (2)	[29]
Epoxy	SWNT * (HiPco)	HCl	—	—	Sonication	0.1	—	—	[30]
Epoxy	MWNT * (CVD)		10^3	C_3H_6O	Sonication	0.1	—	0.2 (1)	[31]
Epoxy	MWNT		100		Stirring	0.1	1.8	0.01 (0.12)	[32]
Epoxy	DWNT * (CVD)		10^3		Stirring, calendering	0.15	—	0.01 (0.6)	[24]
Epoxy	SWNT (CVD)				Milling, heating	0.23	—	10^{-3} (0.5)	[20]
Epoxy	MWNT * (CVD)	NH_2 functionalization	—	—	Milling, calendering	0.25	—	10^{-4} (0.4)	[24]
Epoxy	DWNT * (CVD)	NH_2 functionalization	—	—	Milling, calendering	0.25		10^{-4} (0.6)	[24]
Epoxy	MWNT * (CVD)	UV/O_2	10^3	C_3H_6O	Sonication	0.27	—	0.02 (1)	[31]
Epoxy	SWNT * (HiPco)	—	—	—	PMMA removal, resin infiltration	0.3	0.5	(3)	[33]
Epoxy	SWNT (CVD)	—	—	C_2H_6O	Sonication, stirring	0.3	1.4	0.01 (2.5)	[28]
Epoxy	MWNT * (CVD)	—	10^3	—	Stirring	0.4	—	0.02 (1)	[31]
Epoxy	MWNT * (CVD)	—	—	—	Vacuum stirring, calendering	< 0.5	—	0.03 (2)	[31]
Epoxy	MWNT * (CVD)	—	400	CH_4O	Stirring	0.5	—	5 (3)	[34]

Table 1. (continued)

Polymer	Filler	Treatment	l/D	Solution	Dispersion	Φ_c, wt.%	t	σ_{max}, S m^{-1} (Φ)	References
Epoxy	SWNT * (arc)	—	10^3	—	Manual stirring	0.6		0.01 (14)	[35]
Epoxy	MWNT (CVD)	—	100	C_3H_6O	Stirring	0.6	2.9	0.005 (10)	[36]
Epoxy	MWNT * (CVD)	—	> 500	CH_4O	Sonication, hot calendering	0.7	—	5 (4)	[37]
Epoxy	SWNT * (arc)	HNO_3	—	C_3H_6O	Sonication, stirring	1	2.4	0.1 (7.5)	[29]
Epoxy	MWNT (CVD)	—	80	CH_4O	Stirring, filtration	1.5	—	0.001 (3)	[37]
Epoxy	MWNT * (CVD)	HNO_3	20	C_3H_6O	Sonication, stirring	3.5	—	10^{-5} (8)	[38]
Epoxy	CNT				Solution stirring	0.3	1.44	0.013 (2.5)	[28]
Epoxy	CNT	Palm acid			Stirring	0.05 – 0.1		6.9×10^{-3} (0.8)	[39]
Epoxy	SWNT				Sonication	0.074	1.3	1.25×10^{-3} (0.21)	[27]
Epoxy	MWNT				Solution stirring	0.5		0.5 (1.4)	[40]
Epoxy	SWNT/DWNT				Solution stirring		2.28	0.01 (0.4)	[28]
Epoxy	SWNT				Solution stirring	0.062	2.68	10 (15)	[41]
Epoxy	MWNT				Rolling	< 0.1		50 (5)	[42]
Epoxy	MWNT				Stirring			2.5×10^{-7} (0.5)	[43]
Epoxy	MWNT oxide				Solution stirring	0.012		0.01 (1)	[44]
Epoxy					Solution stirring			0.01 (1)	[45]
Epoxy	MWNT (arc)	—	100	—	Manual stirring	4	—	10^{-3} (16)	[38]
Epoxy	MWNT * (CVD)	—	> 20	C_3H_6O	Sonication, stirring	5	—	2×10^{-5} (20)	[46]
Epoxy	MWNT (CVD)	HNO_3	20	C_3H_6O, tergitol	Sonication, stirring	5	—	10^{-5} (8)	[38]
Epoxy	MWNT * (CVD)	—	—	—	Stirring, calendering	< 0.5	—	0.03 (2)	[47]
Nylon-6	MWNT				Melt stirring	2 – 3		10^{-3} (2)	[48]
Nylon-6	MWNT	Sodium aminohexanoic acid salt				0 – 0.5		10^{-2} (2)	[49]
Nylon-6	MWNT				Melt stirring	2 – 2.5		0.1 (5)	[49]

Table 1. (continued)

Polymer	Filler	Treatment	l/D	Solution	Dispersion	Φ_c, wt.%	t	σ_{max}, S m^{-1} (Φ)	References
Nylon-66	MWNT				Melt stirring	0.5 – 1		0.1 (5)	[49]
Nylon-610 modified	MWNT	Acylchloride			Polymerization			6.1×10^{-10} (0.1)	[50]
P(BuA)/ Latex	SWNT * (arc)	PVA functionaliza-tion	—	H_2O	Sonication	0.27	—	5 (1)	[51]
P3HT	MWNT * (CVD)	—	< 100	$CHCl_3$	Sonication, CH_4O coagulation	0.1	1.7	0.5 (20)	[52]
P3HT	MWNT				Polymerization, oxidation			0.36 (8)	[53]
P3HT	SWNT				Solution stirring	2	1.5	10^{-4} (30)	[54]
P3HT	MWNT				Solution stirring/moulding	10.6		70 (36)	[55]
P3OT	SWNT * (arc)	HCl, centrifugation	100	$CHCl_3$	Sonication	4	2.0	0.05 (35)	[39]
P3OT	SWNT * (arc)	—	100	$CHCl_3$	Sonication	11	2.0	0.001 (35)	[56]
PA	SWNT				Pressing/moulding			10^2 (13)	[57]
PA6	MWNT (CVD)	—	60	—	Liquid stirring, pressing	2.5	8.4	0.1 (22)	[58]
PA6	MWNT * (CVD)	—	$< 10^3$	H_2O, Na – AHA	Sonication, hot pressing	2.5	—	0.03 (4)	[48]
PA6	MWNT * (CVD)	—	—	—	Extrusion	7	—	10 (16)	[59]
PAN (nano-particles)	MWNT (oxidized)				Solution stirring, chemical tailoring			2.9 (10)	[60]
PANI	SWNT * (HiPco)	—	—	—	Sonication	0.3	2.1	3000 (15)	[61]
PANI	SWNT * (HiPco)	—	—	C_8H_{10}	Sonication	0.3	2.1	300 (20)	[62]
PANI	SWNT * (laser)	—	—	C_8H_{10}	Sonication	0.3	2.1	300 (20)	[55]
PANI	MWNT	—	500	—	Stirring, hot pressing	4	—	1000 (80)	[63]
PANI	MWNT	—	—	—	Polymerization			0.26 (10)	[64]
PANI	SWNT				Electrochemical polymerization			1.6×10^{-2} (8)	[65]
PANI	MWNT				Polymerization			10 (50)	[66]
PAT	MWNT # (CVD)	HNO_3, CCl_3	> 200	C_6H_{12}, $CHCl_3$	Sonication	12	2.6	50 (35)	[55]

Table 1. (continued)

Polymer	Filler	Treatment	l/D	Solution	Dispersion	Φ_c, wt.%	t	σ_{max}, S m^{-1} (Φ)	References
PBT	SWNT * (HiPco)	Oxidation	—	—	Sonication, extrusion	0.2	—	10^{-8} (0.2)	[63]
PC	SWNT * (HiPco)	PEE functionalization	—	$CHCl_3$	Sonication, stirring	0.1	2.8	500 (7)	[67]
PC	MWNT	—	150	—	—	0.1		10 (5)	[68]
PC	SWNT * (HiPco)	—	—	—	Extrusion	0.3	—	0.1 (1)	[69]
PC	SWNT * (arc)	—	—	C_6H_8O, $CHCl_3$, C_2H_6O	Sonication, filtration, hot pressing	0.5	—	30 (17)	[70]
PC	SWNT * (HiPco)	—	—	C_6H_8O, $CHCl_3$, C_2H_6O	Sonication, filtration, hot pressing	0.5	—	10 (1)	[70]
PC	SWNT * (HiPco)	—	—	—	Extrusion	0.5	3.8	0.1 (2)	[70]
PC	MWNT * (CVD)	—	10^3	—	Extrusion	1	3.8	5 (3)	[71]
PC	MWNT * (CVD)		> 100	—	Extrusion	1.44	2.1	2 (5)	[72]
PC	SWNT * (arc)	—	—	—	Extrusion	1.9	—	0.1 (10)	[70]
PC	SWNT * (arc)	—	—	$CHCl_3$	Sonication, extrusion	1.9	—	0.1 (4)	[70]
PC	SWNT * (arc)	—	—	—	Extrusion	2.5	—	0.1 (7)	[70]
PC	MWNT * (CVD)	HCl	10^3	—	Extrusion	5	—	10^{-4} (15)	[73]
PC	MWNT * (CVD)	—	> 100	—	Extrusion	1 – 2	—	10 (15)	[74]
PC	SWNT * (HiPco)	Annealing, $SOCl_2$, centrifugation	—	—	Extrusion	—	—	0.1 (1)	[47]
PC	SWNT * (arc)	Annealing, $SOCl_2$, centrifugation	—	—	Extrusion	> 5	—	0.1 (7)	[69]
PC	MWNT				Melt stirring	1 – 1.5		10^3 (15)	[75]
PC	MWNT				Melt stirring	1.5		10^{-1} (15)	[76]
PC	SWNT MWNT				Melt stirring	0.25 – 0.5 1.5		10^{-2} 10 (5)	[77]
PC	MWNT				Extrusion	< 2		100 (15)	[78]

Table 1. (continued)

Polymer	Filler	Treatment	l/D	Solution	Dispersion	Φ_c, wt.%	t	σ_{max}, S m^{-1} (Φ)	References
PC	MWNT with P3HT-g-PCL							64 (5)	[79]
PCL	SWNT * (HiPco)	Purification	—	C_7H_8, ADA	Sonication	0.09	1.5	10^{-3} (3)	[80]
PCL	MWNT (CVD)	—	10^3	—	Sonication, stirring	1.5	—	10 (7)	[81]
PCL	MWNT * (CVD)	HNO_3, filtration	10^3	—	Sonication, stirring	4	—	1 (7)	[81]
PDMS	SWNT				Solution stirring			100 (1.2)	[82]
PDMS	MWNT				Sonication	1.5		0.02 (2.5)	[83]
PE (UHMW)	MWNT # (CVD)	—	100	H_2O, SDS	Sonication, dry stirring, hot pressing	0.045	2.6	50 (1)	[84]
PE (UHMW)	MWNT (CVD)	NaOH, HCl	> 100	—	Sonication, hot pressing	0.07	2.1	0.01 (0.7)	[85]
PE (UHMW)	SWNT * (arc)	—	—	C_6H_8O	Sonication, dry stirring, hot pressing	0.19	2.7	100 (1)	[86]
PE (UHMW)	MWNT (CVD)	NaOH, HCl	> 100	—	Stirring	0.14	1.8	0.1 (0.7)	[85]
PE (UHMW)	MWNT # (CVD)	—	100	C_6H_8O	Sonication, dry stirring, hot pressing	0.19	2.7	100 (1)	[84]
PE (UHMW)	SWNT * (arc)	—	—	C_6H_8O	Sonication, dry stirring, hot pressing	0.25	2.2	0.5 (3)	[84]
PE (UHMW)	MWNT # (CVD)	—	5×10^3		Dry stirring, hot pressing	0.28	2.7	10 (1)	[84]
PE (UHMW)	SWNT * (arc)	—	—	—	Dry stirring, hot pressing	0.6	2.2	0.005 (3)	[84]
PE (UHMW)	SWNT * (arc)	—	—	—	Dry stirring, hot pressing	1.1	2.3	0.5 (30)	[84]
PE (UHMW)	SWNT * (arc)	—	—	—	Dry stirring, hot pressing	1.2	2.2	0.005 (3)	[84]
PE (UHMW)	MWNT	—	—	—	Solution stirring			0.6 (15)	[86]
PE (UHMW)	MWNT	—	—	—	Solution stirring			0.5	[15]
PE (UHMW)	MWNT	—	—	—	Solution stirring	3	1.9	6 (15)	[87]
PE (UHMW)	MWNT	—	—	—	Solution stirring			10.7 (10)	[88]
PE (UHMW/ LMW = 1:1)	MWNT	—	—	—	Solution stirring			1.5 (10)	[88]

Table 1. (continued)

Polymer	Filler	Treatment	l/D	Solution	Dispersion	Φ_c, wt.%	t	σ_{max}, S m^{-1} (Φ)	References
PE (UHMW/ LMW = 1:2)	MWNT	—	—	—	Solution stirring			0.7 (10)	[88]
PE (UHMW/ LMW = 6:1)	MWNT	—	—	—	Solution stirring			0.1 (10)	[15]
PE(LD)	MWNT * (CVD)	HCl, HNO_3, centrifugation	$< 10^3$	—	Milling, hot pressing	2	—	3 (10)	[89]
PE(HD)	SWNT * (HiPco)	Purification	—	H_2O, SDS	Centrifugation, sonication, extrusion	4	—	0.5 (6)	[90]
PE(HD)	SWNT				Solution crystallization	0.13		70 (8)	[91]
PE(MD)	MWNT (CVD)	HCl	> 100	—	Extrusion	7.5	—	0.01 (10)	[92]
PE(LD)	MWNT * (CVD)	—	100	C_8H_{10}	Sonication, liquid stirring	15	—	5×10^{-6} (30)	[93]
PEI	SWNT				Solution stirring, coagulation			2×10^4 (75)	[94]
PEMA	SWNT				Polymerization	3		0.4 (23)	[95]
Polyether imide	MWNT				Ball milling		1 – 2	2×10^{-3} (10)	[96]
Polyimide-sodium salts	SWNT				Polymerization			1 (10)	[97]
PEO	MWNT (CVD)	—	$< 10^3$	H_2O, GA	Sonication, stirring	0.45	1.3		[98]
PEO	MWNT (CVD)	HNO_3	—	C_3H_8O	Stirring	15 – 50	—	700 (50)	[99]
PEO	SWNT				Solution stirring		0.24	0.03 (0.5)	[100]
PET	SWNT * (arc)	—	10^3	—	Extrusion, hat pressing	0.7	—	10^{-2} (2)	[101]
PET	MWNT * (CVD)	HCl	10^3	ODCB-C_6H_6O	Sonication	0.9	2.2	0.03 (9)	[102]
PET	SWNT	—			Melting	$\leqslant 2$		10^{-4} (5)	[101]
PET	SWNT				Melt stirring	0.024		1 (3)	[103]
PETI	MWNT				Ball milling			4×10^{-3} (15)	[104]
PFA	MWNT (CVD)	Annealing	< 30	—	Sonication, stirring	8	—	10 (15)	[105]
PI	SWNT * (laser)	—	> 300	C_3H_8O	Sonication, stirring	0.05	1.5	10^{-4} (1)	[106]
PI	MWNT * (CVD)	—	—	C_4H_9NO	Sonication, stirring	0.3	1.6	10 (7.4)	[107]
PI	MWNT				Polymerization	0.27	1.56	10 (6.7)	[107]

Table 1. (continued)

Polymer	Filler	Treatment	l/D	Solution	Dispersion	Φ_c, wt.%	t	σ_{max}, S m^{-1} (Φ)	References
PI	MWNT				Solution stirring	0.5		10 (3)	[108]
PI(LMW)	SWNT				Solution stirring	< 0.1		2.9×10^{-8} (1)	[109]
PI(HMW)	SWNT				Solution stirring	< 0.5		1.6×10^{-6} (1)	[109]
PI	MWNT				Solution stirring			2.4×10^{-3} (7)	[110]
PI	MWNT	Acid						3.8×10^{-6} (7)	[110]
PI	MWNT	Ammonia						5.8×10^{-6} (7)	[110]
PI	MWNT (CVD)	H_2SO_4, HNO_3, centrifugation	100	C_4H_9NO	Sonication	9.5	—	0.002 (12)	[111]
PLLA	MWNT				Solution stirring	13.5		0.4 (20)	[112]
PLLA/PCL (30:70)	MWNT oxide				Melt stirring	1		10^{-5} (3)	[113]
PMMA	MWNT # (CVD)	—	—	$C_8H_{18}O_4$	Stirring	0.084	1.8	200 (1.5)	[114]
PMMA	MWNT	—	10^3	$C_2HF_3O_2$	Sonication	0.12	—	0.8 (1.5)	[115]
PMMA	SWNT * (HiPco)	$SOCl_2$	—	$CHCl_3$	Stirring	0.17	2.2	10^4 (10)	[116]
PMMA	SWNT * (HiPco)	—	—	$CHCl_3$	Stirring	0.17	1.3	2000 (10)	[116]
PMMA	MWNT * (CVD)	—	—	C_7H_8	Sonication, stirring				[117]
PMMA	SWNT * (arc)	—	—	C_7H_8	Sonication	0.33	2.1	50 (8)	[118]
PMMA	SWNT * (HiPco)	HCl, CH_4O, annealing	45	C_6H_8O	Sonication, H_2O, hot pressing	0.37	—	0.05 (2)	[119]
PMMA	SWNT * (HiPco)	HCl	—	C_6H_8O	Sonication, H_2O, hot pressing	0.39	2.3	0.001 (2)	[120]
PMMA	SWNT * (arc)	HNO_3	$> 10^3$	C_6H_8O	Sonication, hot pressing	0.5	—	0.1 (7), parallel	[121]
PMMA	SWNT * (arc)	HNO_3	$> 10^3$	C_6H_8O	Sonication, hot pressing	0.5	—	10^{-5} (7), perpendicular	[122]
PMMA	MWNT	C_6H_8O, $C_2HF_3O_2$, centrifugation	100	C_6H_8O, $C_2HF_3O_2$	Sonication	0.65	—	0.08 (1.5)	[115]
PMMA	SWNT * (arc)	—	—	H_2O, SDS	Sonication, centrifugation, hot pressing	0.7	2.0	0.1 (1.5)	[122]
PMMA	SWNT * (HiPco)	HCl, CH_4O, annealing	—	C_6H_8O	Sonication, H_2O, hot pressing	1.3	—	0.01 (2)	[123]
PMMA	SWNT * (HiPco)	$SOCl_2$	—	$CHCl_3$	Sonication, hot pressing	< 0.1	—	50 (0.5)	[124]

Table 1. (continued)

Polymer	Filler	Treatment	l/D	Solution	Dispersion	Φ_c, wt.%	t	σ_{max}, S m^{-1} (Φ)	References
PMMA	MWNT	—	—	—	Stirring	10^{-3}		0.5 (16)	[125]
PMMA	MWNT	—	—	—	Solution stirring	0.003	2.2	3000 (0.4)	[126]
PMMA	SWNT	—			Solution stirring	0.003		1000 (0.3)	[127]
PMMA	SWNT	—	—	—	Solution stirring	0.429	2.1	50 (10.4)	[128]
PMMA	MWNT	—	—	–	Electrospinning			0.053 (2)	[129]
PMMA	MWNT array	—	—	—	Drop moulding			1250	[130]
PmPV	MWNT * (arc)	—	—	C_7H_8	Sonication	0.06	1.4	10^{-5} (4)	[131]
PmPV	MWNT * (arc)	—	> 25	C_7H_8	Sonication	7.5	—	0.002 (35)	[132]
PmPV	MWNT * (arc)	—	—	C_7H_8	Sonication	8	—	3 (36)	[12]
PmPV	MWNT				Solution stirring			0.01 (0.35)	[132]
PmPV	CNT				Solution stirring	8.4		3 (10)	[133]
PP	MWNT # (CVD)	—	10^3	—	Extrusion	0.07	—	—	[134]
PP	MWNT (CVD)	—	—	—	Sonication, extrusion	0.4	—	0.1 (0.07)	[135]
PP	MWNT	—	—	—	Extrusion, hot pressing	0.44	—	2 (9)	[136]
PP	MWNT * (CVD)	H_2SO_4, HNO_3, filtration	10^3	—	Extrusion, hot pressing	1.5	—	0.2 (5)	[137]
PP	MWNT (CVD)	HF, HCl	—	—	Extrusion, hot pressing	2	—	0.5 (10)	[138]
PP	SWNT	—	—	—	Hot pressing	5.25		8 (10.4)	[57]
PP	MWNT	—	—	—	Stirring	1.1		4.6 (10.7)	[139]
PP	MWNT	—	—	—	Extrusion, hot pressing	2.62	—	10^{-4} (2.5)	[136]
PP	MWNT	—	—	—	Injection, moulding	3.8	3.8	180 (12)	[2]
PPS	MWNT				Stirring, powder pressing	0.4	3.55	10^3 (5.4)	[140]
PPV	SWNT * (laser)	—	—	—	Sonication	1.8	2.0	1000 (64)	[141]
PPy	CNT				Polymerization			1.6×10^3 (50)	[142]
PPy	CNT				Polymerization with oxidation			2.3×10^3 (25)	[143]
PPy	MWNT				Microemulsion			40 (30)	[144]
PPy	MWNT				Polymerization with oxidation			390 (3)	[145]
PS	SWNT * (HiPco)	PEE functionalization	—	$CHCl_3$	Sonication, stirring	0.05	1.5	7 (7)	[67]

Table 1. (continued)

Polymer	Filler	Treatment	l/D	Solution	Dispersion	Φ_c, wt.%	t	σ_{max}, S m^{-1} (Φ)	References
PS	MWNT * (CVD)	—	< 60	C_6H_8O	Sonication, stirring	0.16	—	—	[146]
PS	SWNT * (arc)	Annealing	—	$C_6H_4Cl_2$	Sonication stirring	0.27	2.0	0.001 (1)	[147]
PS	SWNT				Solution, stirring	0.3	—	1 (1.5)	[148]
PS	SWNT with PMPV covering				Solution stirring	0.17	2	2×10^{-7} (1.5)	[149]
PS	SWNT				Solution stirring	0.1	2	0.45	[150]
PS	MWNT array				Drop moulding			1330	[130]
PS	SWNT * (arc)	—	—	H_2O, SDS	Sonication, centrifugation, hot pressing	0.28	1.6	1 (1.5)	[122]
PS	SWNT * (arc)	—	—	$C_6H_4Cl_2$	Sonication, stirring	0.44	3.6	3×10^{-6} (2)	[147]
PS	MWNT # (CVD)	—	10^3	—	Extrusion	0.45	—	—	[134]
PS	MWNT * (CVD)	HNO_3, HCl	—	—	Sonication	0.8	—	0.02 (2)	[89]
PS	SWNT * (arc)	—	—	H_2O, GA	Sonication, centrifugation, hot pressing	—	—	10^{-6} (3)	[151]
PS	MWNT * (arc)	C_3H_6O, filtration	—	C_7H_8	Sonication, hot pressing	< 12	—	10^4 (25)	[152]
PS	MWNT * (arc)	C_3H_6O, filtration	—	C_7H_8	Sonication, hot pressing	< 12	—	300 (25)	[153]
PS–latex	SWNT *	HF, filtration	2000	H_2O, AIBN, C_5H_8, SDBS	Sonication, stirring	0.2	7.3	10^{-4} (3)	[154]
PS–latex	SWNT *	HF, filtration	2000	H_2O, AIBN, C_5H_8, SDBS	Sonication, stirring	0.2	7.6	5×10^{-5} (3)	[154]
PS–latex	MWNT * (CVD)	HNO_3	> 100	H_2O, SDBS	Sonication	0.36	1.7	10 (6)	[155]
PS–latex	MWNT * (CVD)	HNO_3	> 100	H_2O, SDBS	Sonication, cold drying, hot pressing	0.9	3.9	0.1 (6)	[155]
PS–latex	SWNT * (arc)	—	10^3	H_2O, SDS	Sonication, centrifugation, hot pressing	1.5	4.9	0.005 (5)	[155]
PS–latex	MWNT (CVD)	—	—	H_2O, SDBS	Sonication, centrifugation, stirring	2.5	—	10 (15)	[156]
PS-b-EB-bS	MWNT				Melt stirring	1.25–2.5		516 (15)	[157]
PTh	SWNT				Oxidation, chemical polymerization			41 (50)	[158]
PU	MWNT * (CVD)	Oxidation	10^3	MEK, BKC	Sonication, stirring, pressing	0.018	1.5	8 (8)	[159]

Table 1. (continued)

Polymer	Filler	Treatment	l/D	Solution	Dispersion	Φ_c, wt.%	t	σ_{max}, S m^{-1} (Φ)	References
PU	MWNT	—	> 100	C_4H_8O	Stirring	1	3.1	200 (15)	[160]
PU	MWNT				Stirring/casting			0.1 (5)	[161]
PU	MWNT				Polymerization			30 (3)	[162]
PUF	MWNT	Crushing, sonication, H_2O_2			Stirring, moulding	0.01	—	2.5 (0.03)	[163]
PVA	MWNT #	H_2SO_4, HNO_3, filtration	—	C_4H_8O	Sonication, stirring, electrospinning	0.2	—	10 (5)	[164]
PVA	MWNT * (CVD)	H_2SO_4, HNO_3, filtration	—	H_2O	Stirring	< 10	—	100 (60)	[165]
PVA	MWNT				Solution stirring	0.72	2.7	0.27 (22)	[166]
PVAc	SWNT	GA			Emulsion stirring	0.04		20 (4)	[167]
PVAc	MWNT				Melt stirring			2.9×10^{-6} (5)	[168]
PVA – latex	SWNT * (HiPco)	—	—	H_2O, GA	Sonication, stirring, filtration	0.038	1.9	100 (4)	[167]
PVC	MWNT (CVD)	—	10^3	—	Sonication, crushing, hot pressing	0.094	3.3	0.01 (1.4)	[169]
PVDF	SWNT	H_2SO_4	$> 10^3$	C_6H_8O	Spinning	0.02	—	3×10^{-4} (0.05)	[170]
PVDF	MWNT	Trifluorophenyl			Solution stirring	0.144	1.54	0.01 (0.32)	[171]
PVDF	MWNT	—	—	C_6H_8O	Sonication, hot pressing	3.2	0.9	2×10^{-4} (4)	[172]
SBA	MWNT				Suspension stirring			20 (5.4)	[173]
SBR	MWNT				Moulding	0.25–0.50		200 (12)	[174]
SE	MWNT/ SWNT mixture				Stirring, milling			3.6 (3.8)	[175]
SE	CNT mat				Spin coating			4×10^{-4} (0.4)	[176]
SE	MWNT	Octenyltrichlo-rosilane func-tionalization			Stirring	< 2		10 (5)	[177]
SIBS	SWNT				Stirring, moulding			850 (0.3)	[178]
SPPA	MWNT	—	—	—	Sonication	3.5	—	0.2 (20)	[179]
UPR	MWNT * (CVD)		160		Annealing	0.026	2.5	0.13 (0.3)	[180]
UPR	MWNT (CVD)	Annealing	—	—	Sonication, magnet	< 1	—	0.1 (1), parallel	[181]
UPR	MWNT (CVD)	Annealing			Sonication, magnet	< 1	—	0.005 (1)	[181]
VE	MWNT (CVD)	NaOH, HCl, K_2MnO_4	—	—	Sonication, stirring	< 0.5	—	0.04 (2)	[182]

Table 1. (completed)

Polymer	Filler	Treatment	l/D	Solution	Dispersion	Φ_c, wt.%	t	σ_{max}, S m^{-1} (Φ)	References
VMQ	MWNT	APTS functionalization	500	—	Hot pressing	2.4	2.9	4×10^{-4} (5)	[183]
WBPU	MWNT	HNO_3			Stirring, moulding			0.08 (1.5)	[184]

Notations: SWNT — single-walled carbon nanotubes; MWNT — multiwalled carbon nanotubes; DWNT — double-walled carbon nanotubes; CNF — carbon nanofibers; ADA — aminododecane acid; AHA — aminohexanvic acid; AIBN — azoisobuthyronytrile; APTS — aminipropyltriethoxy silane; ASTAA — alkoxysilane-terminated amide acid; BKC — benzalkonium chloride; EMMA — poly-ethyl-methylmetacrilate; GA — gummiarabic; MEK — methylethylketone; OP — polyoxyethylene octil phenyl ether; P3HT — poly-3-hexylthiophen; P3OT — poly-3-okthylthiophene; PA-6 — polyamide-6; PAN — polyacrilonitrile; PANI — polyaniline; PARMAX — poly(benzoil1-1,4-phenylene)-co-(1,3-phenylene); PAT — polyhexadecyl thiophene; PBT — polybuthylene terephtalate; P(BuA) — polybuthyle acrylate; PC — polycarbonate; PCL — polycaprolactone; PDMS — polydimethylsiloxane; PE — polyethylene; PE(UHMW) — ultra-high molecular weight polyethylene; PE(LMW) — low molecular weight polyethylene; PE(LD) — low-density polyethylene; PE(MD) — medium-density polyethylene; PE(HD) — high-density polyethylene; PPE — polyphenylene ether; PEI — poly(ethyleneimine); PEMA — poly(ethyl methacrylate); PEO — polyethylene oxide; PET — polyethylene tetraphthalate; PETI — phenylethynyl-terminated imide; PFA — polyfurfuryl alcohol; PI — polyimide; PLLA — poly(l-lactic) acid; PMMA — polymethylmethacrylate; PmPV — poly-m-phenylene vinylene; PP — polypropylene; PPS — polyphenylene sulphide; PPV — polyparaphenylene vinylene; PPy — polypyrrole; PS — polystyrene; PS-b-EB-bS — poly(styrene-b-ethylene-co-buthylene)-b-styrene; PTh — polythiophene; PU — polyurethane; PUF — polyurethane foam; PVA — polyvinylacetate; PVC — polyvinylchloride; PVDF — poly(vinylene difluoride); SE — silicon elastomer; SBA — polystyrobuthylacrylate; SBR — styrene-butadiene rubber; SDBS — sodium dodecylbenzosulphonate; SDS — sodium dodecylsulphate; SIBS — poly(styrene-b-isobuthylene-b-styrene); SPPA — sulpho-poly-phenylacethylene; UPR — unsaturated polyesther resin; VE — vinylesther; VMQ — methyl-vinyl-silicon rubber; WBPU — waterborne polyurethane; * — nanotubes are entangled; # — nanotubes are not entangled; CVD — chemical vapor deposition, and HiPco — CNT production by high-pressure thermocatalytic CO decomposition.

where $\varepsilon_0 = 8.85 \times 10^{-12}$ F m^{-1} is the dielectric constant of a free space. Along with the notions of complex conductivity and permittivity, the notion of the electrical modulus (M^*) is used, being expressed through ε^* in the following manner:

$$M^* = M' + \mathrm{i}M'' = \frac{1}{\varepsilon^*} = \frac{\varepsilon'}{\varepsilon'^2 + \varepsilon''^2} + \mathrm{i}\frac{\varepsilon''}{\varepsilon'^2 + \varepsilon''^2}\,. \qquad (3)$$

The results of measuring the electrical characteristics of PA/MWCNT composites of various contents are given in Fig. 2 [58, 185]. Panel 2a in this figure presents the frequency dependences of the conductivity σ_{ac} of samples that have been obtained on the basis of processing the experimental data according to expressions (1) and (2). The frequency range where the conductivity does not depend on the frequency corresponds to the electrostatic field conductivity. The frequency dependence of the electrical conductivity is usually represented as

$$\sigma'(\omega) = \sigma(0) + \sigma_{ac}(\omega) = \sigma_{dc} + A\omega^s\,, \qquad (4)$$

where σ_{dc} is the electrostatic field conductivity of a material, and A and s are the fitting parameters.

Table 2 presents the parameters in expression (4), which were obtained on the basis of processing the data collected in Fig. 2. Here, the critical frequency f_c corresponds to the passage of the conductivity from the electrostatic field value to a growing frequency dependence. As is seen from the data presented in Fig. 2 and Table 2, increasing the CNT content in a sample results in an increase of both the absolute magnitude of the conductivity and the value of f_c corresponding to the passage from the electrostatic field value of conductivity to a frequency-dependent function.

Figure 2b plots the dependence of the electrostatic field conductivity ($\sigma_{dc} = \sigma'(\omega \to 0)$) of nanocomposite PA6/MWCNT on the volumetric content of CNTs retrieved on the basis of measurements by the dielectric relaxation spectroscopy (DRS) method [58]. This dependence is expressed quite well by the following relation [7–10]:

$$\sigma_{dc}(p) = \sigma_0(p - p_c)^t\,, \qquad (5)$$

where the power index $t = 8.4 \pm 0.4$ considerably exceeds the value of $t \approx 2.0$, which follows from the statistical theory of percolation [7–10]. A similar result has also been reported in some other publications ($t = 8$ for the polyehylene-polyoxymethylene composite doped with iron articles [186], and $t = 6.27$ for the polyethylene-graphite composite [187]). The deviation of the power index entering into dependence (5) from the value of $t \approx 2.0$ inherent in the above-mentioned composites points to a more complex character of charge transfer in these materials. Specifically, if the direct contact between neighboring conducting particles of the filler is absent, the electrical conductivity can be provided due to tunneling of charge carriers from one particle to the other [188, 189]. In this case, the interparticle distance is characterized by a considerable spread, so that expression (5) loses its universal character and the parameter t is no more a unique characteristic of the composites under consideration.

Table. 2. Values of conductivity σ_{dc}, critical frequency f_c, and power index s retrieved according to Eqn (4) from the measurement data for PA6/MWCNT samples of various compositions [58, 185].

Sample	σ_{dc}, S m^{-1}	f_c, Hz	s
PA/5 wt.% CNT	9.69×10^{-10}	0.42	0.73
PA/6.25 wt.% CNT	4.16×10^{-8}	16.52	0.68
PA/7.5 wt.% CNT	$9/42 \times 10^{-8}$	38.87	0.68
PA/8.75 wt.% CNT	1.53×10^{-6}	412.95	0.68
PA/10.0 wt.% CNT	1.1×10^{-5}	3519.00	0.68
PA/20.0 wt.% CNT	1.34×10^{-4}	—	—

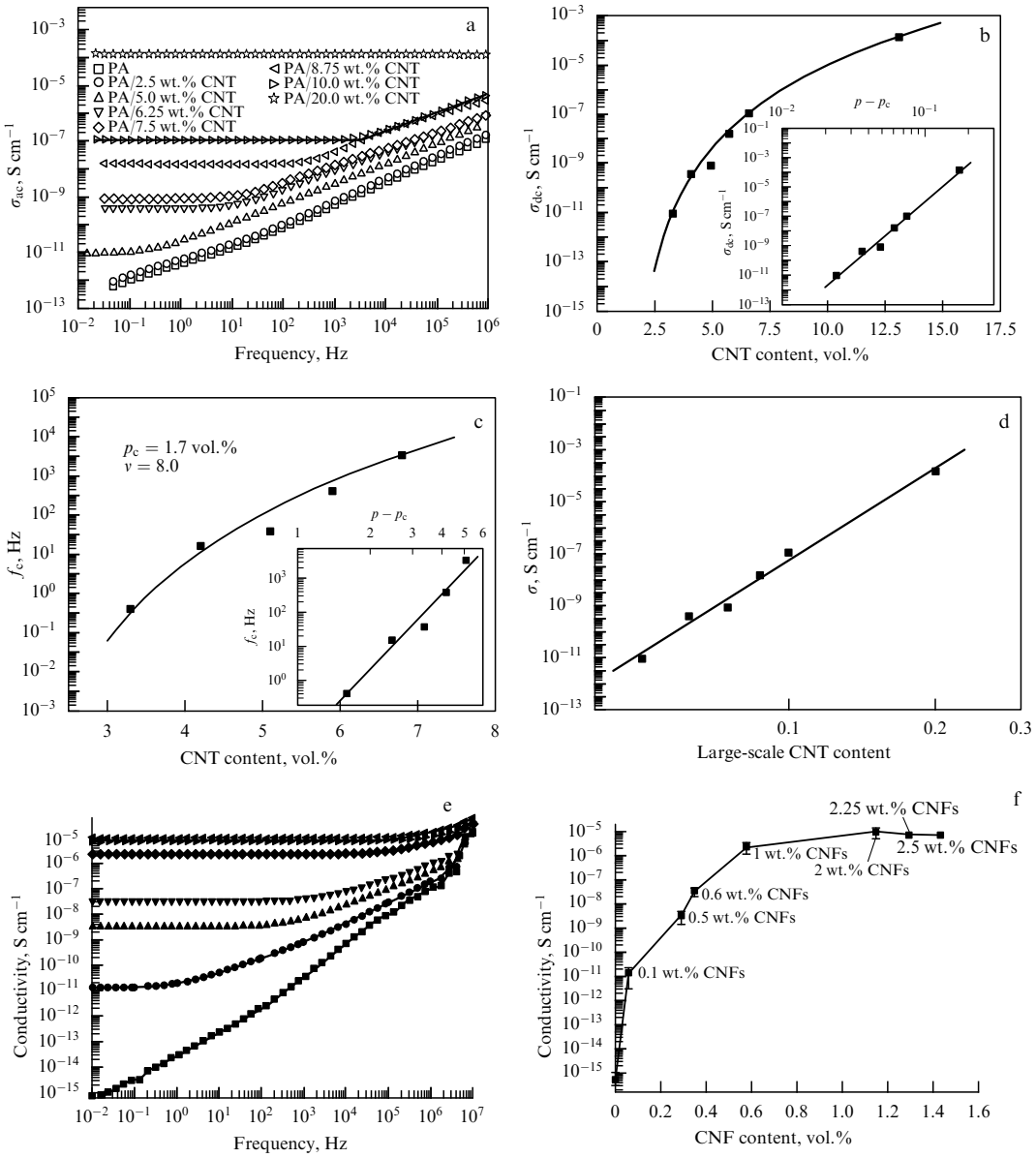

Figure 2. Results of measuring the electrical properties of samples of CNT- and CNF-doped composites of various compositions at room temperature: (a) frequency dependences of the conductivity of a CNT-doped composite on the basis of polyamide (PA) [58]; dependence (4) retrieved for the PA/10.0 wt.% CNT sample is shown by the solid line; (b) the dependence of the conductivity of PA6/MWCNT composite from the volumetrical content of CNTs. The inset displays the same dependence in log-log coordinates, permitting the determination of the power index $t = 8.4$ in the percolation expression (5) and the percolation threshold position $p_c = 1.7$ vol.% [58]; (c) the dependence of the critical frequency f_c on CNT volume loading (p) [58]. The inset presents the same dependence in relative units p/p_c. The straight line corresponds to Eqn (6) with the fitting parameters $v = 8.0$ and $p_c = 1.7$ vol.% providing the best agreement between the experimental data and expression (6); (d) the dependence of the conductivity of the PA6/MWCNT composite on the CNT weight loading represented in log-log coordinates according to Eqn (8) [58]; (e) the frequency dependence of the conductivity of CNF-doped epoxy-based composites of various compositions: ■ pure resin; ● 0.1% CNF; (▲) 0.5% CNF, (▼) 0.6% CNF, (◆) 1% CNF, (◀) 2% CNF, (▶) 2.25% CNF, and (∗) 2.5% CNF [29]; (f) the dependence of the DC conductivity of CNF-doped epoxy-based composites on CNT loading [29].

The absence of an electrical contact between CNTs in the PA6/MWCNT composite is explained by the formation of a thin polymer layer covering the nanotubes [185]. Therefore, the results of experiments [58, 185] imply the necessity of the construction of the percolation model taking into account a possible tunneling of electrons from one particle to another. The problem of describing the percolation conductivity of composites in the absence of direct surface contact between conducting particles is considered below in sections of the article.

According to the classical percolation model [190, 191], the dependence of the critical frequency f_c on the content of the conducting filler in a composite is described by an expression similar to the above-considered expression (5) proceeded from the assumption of the percolation behavior of the conductivity:

$$f_c(p) \sim (p - p_c)^v . \qquad (6)$$

Here, v is the power index equal to 3.1, as follows from the classical percolation theory [191]. Figure 2c compares the experimental results [58, 185] with the analytical dependence (6). The best fitting is achieved at the following values of the parameters: $v = 8.0 \pm 0.4$ and $p_c = 1.7 \pm 0.1$ vol.%. As is

seen in this case, the power index v also considerably deviates from that corresponding to the percolation theory. Such a deviation again indicates the more complicated mechanism of the percolation conductivity, including possible electron tunneling.

Along with CNTs, carbon nanofibers (CNFs) are also utilized as a filler for polymer materials. Their structure somewhat differs from that of CNTs; nonetheless, these two objects are similar to each other in relation to such physical characteristics as thermal conductivity, electrical conductivity, and chemical and thermal stabilities. The behavior of composites on the basis of epoxy resin doped with CNFs has been studied in Ref. [29]. CNFs between 100 and 200 nm in diameter and between 30 and 100 μm in length were subjected to thermal processing at a temperature up to 3000 °C. In order to remove contaminations, CNF samples were kept in dichloromethane CH_2Cl_2 for 5 days at 35 °C, washed in deionized water, and then repeatedly treated in CH_2Cl_2 for 24 hours. After drying, the CNF samples were stored in anhydrous conditions.

To prepare samples of the desired composition, a suspension of CNFs in dimethylacetamide (DMAc) was ultrasonicated and stirred for an hour and then epoxy resin was put into it. The mixture obtained was ultrasonicated and stirred again for 3 hours. Then, the solution was kept in a vacuum at 80 °C in order to remove DMAc. The liquid produced was poured out into different moulds for further studies. Before carrying out the studies, the samples were heat treated for 2 hours at 125 °C, and then for 2 hours at 177 °C. The content of CNFs in the samples was varied from 0 to 2 wt.%.

The electrical conductivity and permittivity of the composite samples were measured within the frequency range of $10^{-2}-10^{7}$ Hz. The composite samples measuring 1.5×1.5 cm^2 were covered with a thin layer (100 nm thick) of silver to ensure good electrical contact between the electrodes and the sample. The silver electrodes had a circular form 0.5 cm in diameter. The data obtained for 3–4 samples were averaged. For each frequency, the capacity C_p of the sample was measured, which permitted the determination of the dielectric constant according to the trivial relationship $\varepsilon = C_p t/(A\varepsilon_0)$, where $t \sim 0.5$ mm is the thickness of the sample, A is the area of the electrode, and $\varepsilon_0 = 8.85 \times 10^{-12}$ F m^{-1} is the permittivity of a vacuum.

The frequency dependences of the electrical conductivity of epoxy resin composites with various contents of CNFs are plotted in Fig. 2e. As is seen, this dependence has a linear shape for a pure polymer, which is typical for nonconducting materials. For composites filled with CNFs, the conductivity does not depend on the frequency at low frequencies; however, upon exceeding a critical frequency value, it starts increasing with frequency. Enhancement of this critical value, as the content of the CNF filler rises, is representative of a typical behavior of a reactive resistance in an alternating electric field.

Figure 2f depicts the direct current conductivity of composites as a function of the volumetric content of CNFs. This dependence was obtained on the basis of processing the data collected in Fig. 2e [29]. As is seen, the addition of 0.1 wt.% CNFs results in enhancement of the composite conductivity by four orders of magnitude, which is a characteristic feature of the percolation transition. Upon reaching a content of 1 wt.% of the filler, the conductivity of the composite is ten orders of magnitude higher than that for a pure polymer. Further increasing of the filler content barely changes the conductivity, which indicates the formation of a ramified conducting network. The magnitude of the power index t involved in the dependence of the conductivity on loading the filler, $\sigma \sim (p - p_c)^t$, was determined on the basis of the measurement results, amounting to $t = 1.83$.

2.3 Dependence of the percolation threshold on the aspect ratio

It is clear intuitively that in a composite based on a nonconducting polymer filled with conducting particles of an elongated structure, the position of the percolation threshold depends on the aspect ratio (ratio of the length to the diameter) of those particles. Indeed, if the length of a conducting particle is on the order of the sample size, even one such particle is sufficient to make the sample conductive. This conclusion is confirmed by the results of an analysis [192–194] performed on the basis of the classical percolation theory. According to the above-cited studies, the position of the percolation threshold in a composite filled with high-aspect-ratio particles, $l/D \gg 1$, is expressed by the following relation

$$\Phi_c = 1 - \exp\left(-\frac{1.4(\pi/4)\, D^2 l + (\pi/6)\, D^3}{(4\pi/3)\, D^3 + 2\pi D^2 l + (\pi/2)\, D l^2} \right). \quad (7)$$

As is seen, the exponent in formula (7) is much lower than unity at a high aspect ratio, $l/D \gg 1$, which permits representing this relation in a considerably more simple form

$$\frac{l}{D}\, \Phi_c \approx 0.7\,, \quad (7a)$$

which results in the above-noted inversely proportional dependence of the percolation threshold position on the aspect ratio of conducting particles [6]. Such a dependence offers the prospects for using CNTs as a conductive filler for polymer-based composites.

Equation (7) can be applied to estimate the aspect ratio of nanotubes using the measurement data on the percolation threshold position. Thus, according to expression (7), the value of $p_c = 1.7$ vol. % observed in experiments [58, 185] corresponds to the aspect ratio l/D of nanotubes equal approximately to 40. This magnitude is substantially lower than the relevant initial value of $l/D \sim 1000$ estimated on the basis of observations performed by means of a tunneling electron microscope (TEM). One can suppose that such a discrepancy is caused by decreasing the aspect ratio of particles during the preparation of samples. Such decreasing can be evolved from forming the bundles of CNTs, resulting in an increase in the effective diameter of conducting particles, or from shortening the CNTs. The authors of Refs [58, 185] prefer to accept the second reason, taking into account the results of TEM observations. Indeed, the TEM findings indicate the emergence of CNTs about 500 nm in length in the sample, which were not observed in the initial sample. Therefore, the procedure of preparing composite samples based on pressure moulding is accompanied by about a 20-fold shortening of the nanotube length, which results in the production of a composite with a rather high percolation threshold position amounting to $p_c = 1.7$ vol.%.

2.4 Contact resistance

As may be seen from the measurement results presented in Fig. 2b and in Table 2, the maximum magnitude of the

electrical conductivity of samples studied does not exceed 0.1 S m^{-1}. This value is several orders of magnitude lower than the measured conductivity of multiwalled nanotubes, which amounts to $\sim 10^4$ S m^{-1} [3, 195, 196]. Meanwhile, one would expect that at a quite high content of a conductive filler (on the level of several dozen percent), the composite conductivity would approach that of the additive. One of the reasons for this discrepancy is a rather high value of the resistance of the surface contact between adjacent nanotubes.

The model describing the influence of the contact resistance on the conductivity of a composite filled with elongated conducting particles has been developed by Kovacs et al. [22]. The authors considered a composite added with statistically homogeneously distributed hard conducting cylinders, r in radius and l in length. According to the calculations performed within the framework of this model, the dependence of the material conductivity on the mass content Φ of the filler upon loading far from the percolation threshold is expressed by the following relation

$$\sigma = \frac{l}{2\pi r^2} \frac{\Phi^{2\chi+1}}{R + R_c}, \tag{8}$$

where R is the resistivity of a particle, R_c is the resistance of the contact between neighboring particles, and χ is an empirical parameter. Under conditions of a bad contact ($R \ll R_c$), the composite conductivity is obviously determined by the contact resistance and barely depends on the additive resistance R. Processing the results of measurements of the conductivity for samples of various compositions permits the determination of R_c in conditions when the contact resistance considerably exceeds that of individual nanotubes. Figure 2d presents the results of such processing. Taking into consideration the values of $r = 5$ nm and $l = 500$ nm, we obtain $R_c = 10^5$ Ω. This quantity exceeds the typical resistance of an individual CNT by 1–2 orders of magnitude and is of the same order as the resistance of composites based on polycarbonate and epoxy resin filled with multiwalled CNTs [22].

It should be emphasized that the above values of the contact resistance determined from processing the experimental data [22, 58] present the lowest magnitudes of this parameter. In most publications, much higher values of the contact resistance have been obtained. Such high values can be due to the occurrence in a composite of a thin polymer layer covering the nanotube's surface [195]. This layer prevents the transport of carriers (electrons) from one nanotube to another, thus enhancing the contact resistance.

It should also be noted that the above approach to modeling composite conductivity by taking into account the contact resistance is rather approximate, because within the framework of this approach all contacts between nanotubes are characterized by a common value of the contact resistance. In actuality, the contact resistance is characterized by a statistical spread that corresponds to the spread in the thicknesses of the polymer layers separating the adjacent CNTs. The transport of electrons through these layers is governed by the tunneling mechanism, so that the probability of electron passage through the layer decreases abruptly with the thickness of the layer. This complicates the description of the percolation behavior of composites. Peculiarities of the percolation conductivity of a composite filled with CNTs caused by the formation of a polymer layer separating the neighboring nanotubes are also analyzed in Section 2.7 of the present article.

2.5 Temperature dependences and the conduction mechanism

The authors of Refs [58, 185] have measured the temperature dependences of the electrical properties of composite samples of various compositions with the goal of analyzing the conduction mechanism. Thus, the frequency dependences of the imaginary part of the electric modulus (M'') of composite PA6/2.5 wt.% CNTs measured at various temperatures are demonstrated in Fig. 3a. Similar measurements were also performed on pure polymer PA6. The maximum in the measured dependences corresponds to the transition from AC to DC conductivity, so that the position of this maximum (f_{max}) determines the value of the relaxation time (τ) in accordance with the relation $2\pi f_{max}\tau = 1$ [194]. The temperature dependences of the parameter f_{max} are shown in Fig. 3b in comparison with the analytical expression

$$f_{max} = f_0 \exp\left(-\frac{B}{T - T_V}\right). \tag{9}$$

Such a dependence characterizes the transition of the material into a glass phase [197]. Here, f_0 is the pre-exponent factor, B

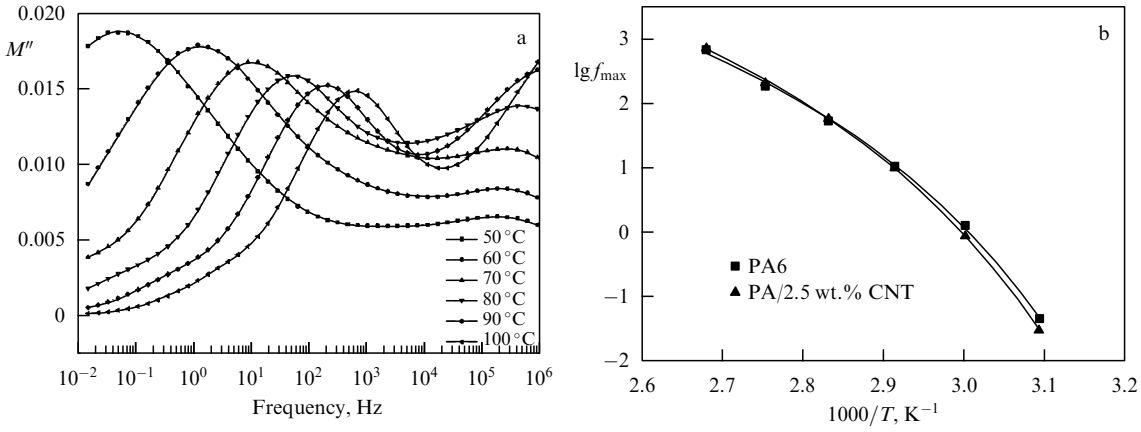

Figure 3. Electrical properties of composite PA6/CNT samples [58, 185]: (a) frequency dependences of the imaginary part of the electric modulus of composite PA6/2.5 CNTs measured at various temperatures; (b) temperature dependences of the parameter f_{max} evaluated on the basis of data of Fig. 3a for pure polymer PA6 and composite PA/2.5 wt.% CNTs. Solid lines correspond to Eqn (9).

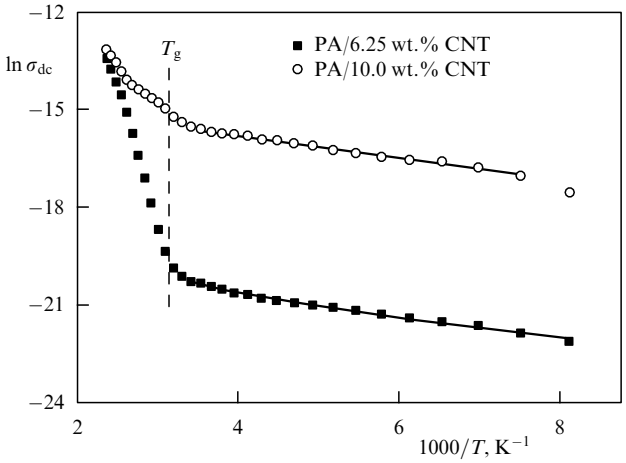

Figure 4. Temperature dependence of $\ln \sigma_{dc}$ vs $1000/T$ measured for samples with various compositions. Solid lines correspond to Eqn (10) [58, 185].

is the fitting parameter, and T_V is the Vogel temperature. The best agreement between the measurement results and formula (9) is reached at $f_0 = 1212$ Hz, $B = 428$ K, $T_V = 274$ K for pure polymer PA6, and $f_0 = 812$ Hz, $B = 390$ K, $T_V = 275$ K for composite PA/2.5 wt.% CNTs. It should be noted that the above-determined value T_V is about 50 °C lower than the glassy phase transition temperature for the same materials [198]. Therefore, the experimental data imply that the main charge transfer mechanism in both nonconducting materials at temperatures exceeding the glassy phase transition point deals with the movement of polymer chains with the characteristic time of order f_0^{-1} [198].

The results of similar measurements performed with conducting composites indicate an increase in the electrical conductivity and the critical frequency f_c, as the temperature rises from −150 °C to 150 °C. Thus, Fig. 4 demonstrates the Arrhenius representation of the temperature dependences of DC conductivity measured for two composite samples with different compositions [58, 185]. As is seen, the character of the temperature dependence of the conductivity changes upon passage through the phase transition point T_g.

In the temperature range below the phase transition point T_g, the conduction mechanism related to electron tunneling induced by thermal fluctuations (FIT) occurs [199, 200]. According to this mechanism, the electrical conduction is due to electron tunneling through a potential barrier varying in height that is determined by local temperature fluctuations. In this case, the temperature dependence of the conductivity is expressed through the following equation

$$\sigma_{dc} = A \exp\left(-\frac{T_1}{T + T_0}\right), \quad T < T_g . \tag{10}$$

Here, the parameter T_1 can be considered as the electron energy sufficient for overcoming the insulating barrier between two nanotubes, T_0 is the temperature whose exceeding makes the overbarrier electron transition possible, and A is the pre-exponent factor. Fitting the experimental data collected in Fig. 4 with expression (10) results in $T_1 = 875$ K, $T_0 = 100$ K for PA6/6.25 wt.% CNT, and $T_1 = 466$ K, $T_0 = 30$ K for PA6/10 wt.% CNT. These values exceed those obtained for polyethylene-terephtalate/charcoal composites [201], which is one more indication of a dependence of the electrical properties of a composite material on the natures of the polymer and conducting filler.

Attempts to explain the experimental data in Fig. 4 within the framework of one-, two-, and three-dimensional hopping conduction models (VRH) have turned out to be less successful [202]. The FIT model is also supported by the linear character of the $\ln \sigma_{dc}$ dependence on $p^{-1/3}$ (p is the mass content of a filler) measured for samples of the same composite and presented in Fig. 5a [58, 185].

The influence of a conducting filler on the mechanism of the dielectric relaxation of a polymer was studied by the dielectric relaxation spectroscopy method. The results of this study are illustrated in Fig. 5b presenting the temperature dependences of the imaginary part (ε'') of the permittivity responsible for the dielectric losses. These data were measured at a frequency of 95 Hz for samples of pure polymer and composite PA6/2.5 wt.% CNT. The measurements could be performed only for samples not possessing DC conduction because the dielectric relaxation is masked by the conduction for conducting samples in which the filler content exceeds the percolation threshold. Two peaks (at −100° and −30°C, respectively) observable in Fig. 5b correspond to γ and β mechanisms of secondary dielectric relaxation in polymer PA6, relating to the local movement of dipoles [203].

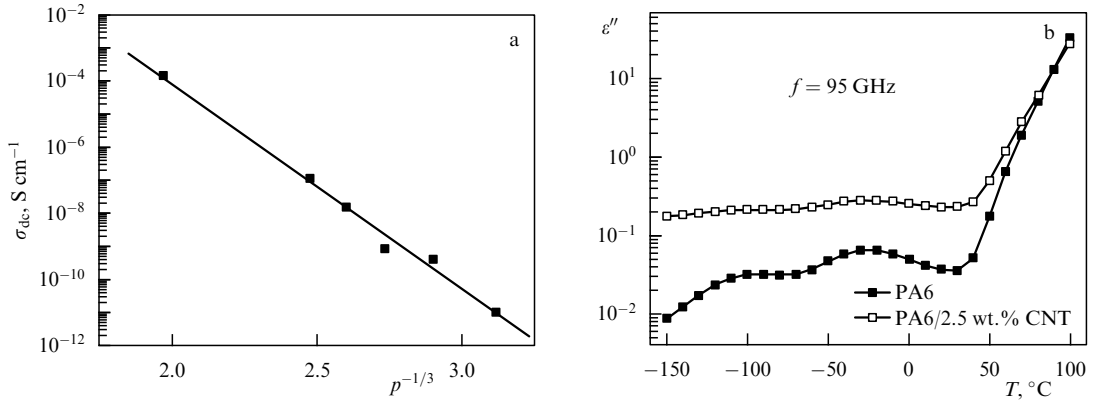

Figure 5. (a) Dependence σ_{dc} on the CNT weight loading, measured at room temperature and represented in the coordinates $\lg \sigma_{dc}(p^{-1/3})$. The linear character of this dependence indicates that the conduction mechanism corresponds to the FIT model [62, 195]; (b) the temperature dependence of the imaginary part (ε'') of the permittivity measured at a frequency of 95 Hz for nonconducting samples of polymer PA6 and composite PA6/CNT [58, 185].

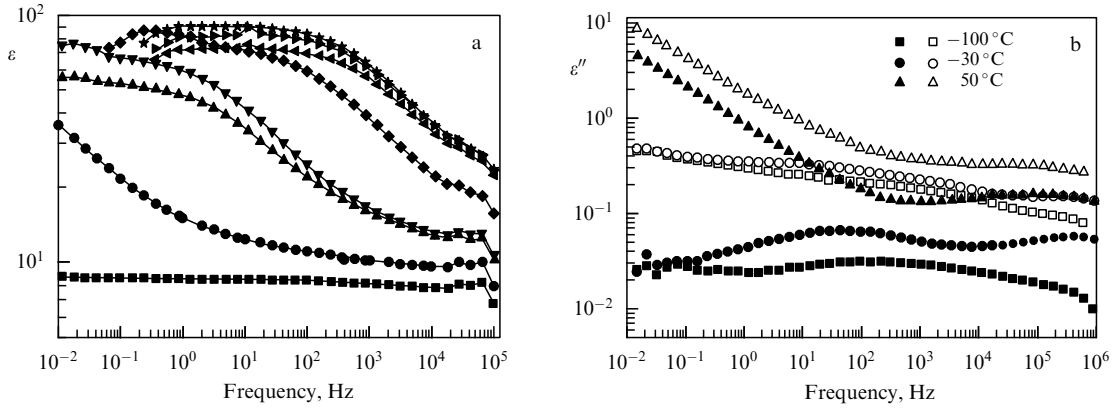

Figure 6. (a) Frequency dependence of the dielectric constant of CNF-doped epoxy resin-based composites [29]: ■ pure resin; ● 0.1% CNF; ▲ 0.5% CNF; ▼ 0.6% CNF; ◆ 1% CNF; ◄ 2% CNF; ► 2.25% CNF; * 2.5% CNF; (b) frequency dependence of the imaginary part (ε'') of the permittivity measured at temperatures −100, −30, and 50 °C [58, 185]. The black and white symbols correspond to the pure polymer PA6 and composite PA6/2.5 wt.% CNT.

Specifically, γ-relaxation relates to the rotational movement of the radical CH_2 added to polar groups, while β-relaxation is caused by the movement of amide bonds [204].

Inserting a conducting filler into a polymer produces changes in both the absolute value of the permittivity and its frequency dependence. Figure 6a displays the results of measurements of the AC permittivity for an epoxy resin-based composite doped with CNFs [29], which present a characteristic example of such changes. In a frequency-fixed electric field, the permittivity ε rises as the filler loading increases. At a fixed filler content, the sample permittivity ε decreases with the frequency, which is caused by shortening the electric field oscillation relative to the characteristic time of the charge exchange of an effective capacitor formed by the neighboring conducting particles. At high frequencies, the capacitor has no time for charge exchanging, so that the sample permittivity approaches the value inherent to a pure polymer without a filler.

Figure 6b presents the frequency dependences of the imaginary part (ε'') of the permittivity measured at temperatures of −100, −30, and 50 °C for nonconducting samples of pure polymer PA6 and composite PA6/2.5 wt.% CNT. The peak observable in a middle part of the frequency region at −100 °C is caused by γ-relaxation. At a higher temperature (−30 °C), this peak shifts toward higher frequencies ($\sim 3 \times 10^5$ Hz), while the peak related to the β-relaxation appears in a low-frequency region (~ 40 Hz). At $T = 50$ °C, the peak responsible for the γ-relaxation shifts out of the frequency region under investigation, while the peak caused by the β-relaxation falls to a high-frequency part of this region. For $f < 10^3$ Hz, ε'' reaches high magnitudes, which is caused by conduction effects.

As is seen from the data given in Fig. 6b, the influence of a CNT filler in a PA6 matrix on the secondary processes of β-and γ-relaxations is hardly essential. The only effect deserving attention is a notable (by an order of magnitude) increase in the parameter ε'' that can be conditioned by strengthening the internal field due to the presence of CNTs.

2.6 Influence of stirring on the composite conductivity

Along with the contact resistance, the absolute magnitude of the electrical conductivity of composites filled with CNTs is determined essentially by the degree of homogeneity of the composite. Experience shows that a thorough stirring of a liquid polymer resin with an admixture of CNTs results in lowering the percolation threshold of the composite. In particular, this effect has been observed by the authors of Ref. [180], who obtained a quite low value of the percolation threshold (0.026 wt.%) for the nanocomposite fabricated by inserting multiwalled CNTs of 90% purity into the matrix of non-saturated polyester. Multiwalled CNTs about 9.5 nm in diameter and ~ 1.5 μm in length were synthesized by the usage of the CVD technique. The samples to be studied were fabricated by the method based on the preliminary preparation of an initial material with enhanced content of CNTs (masterbatch), followed by its dilution with a polymer resin [47, 205]. The CNT content in the samples studied was varied between 0.05 and 0.3 wt.%. Each sample underwent stirring in a laboratory mixer at a temperature of 30 – 35 °C for 7 hours at a frequency of 1000 cpm.

The resulting samples 100 ± 20 μm in thickness were studied by means of optical and scanning electron microscopies. Electrical properties of the samples were measured using the impedance spectroscopy method with the aid of a frequency analyzer. The impedance was measured within the frequency range between 1 Hz and 1 MHz. The conductivity of a sample was determined on the basis of impedance $Z(\omega)$ measurements according to the relation

$$\sigma = \frac{l}{Z(\omega)}\,, \tag{11}$$

where ω is the angular frequency of the electric field, and $l = 3.93$ m^{-1} is a geometric factor characterizing the measuring sensor device. DC conductivity of the material was measured by the two-probe method at a temperature of 20 °C. In these measurements, cylindrical samples 8 mm in diameter and 4 mm in height with the edges coated with a silver-based conducting paint were used.

Figure 7a illustrates the dynamics of changing the resistivity of a liquid resin made up on the base of a nonsaturated ester doped with CNTs in due course of stirring [180]. Let us note that the picture does not contain the similar dependence for $p_c = 0.05\%$, which hardly differs from that for the sample with $p_c = 0.1\%$. However, the occurrence of multiple bubbles when stirring induces considerable noise on the above-mentioned dependence. As is seen, the resistance of the resin filled with a CNT loading of about 0.2–0.3% decreases by more than two orders of magnitude after about 50 min of stirring. The magnitude of the drop, naturally, rises

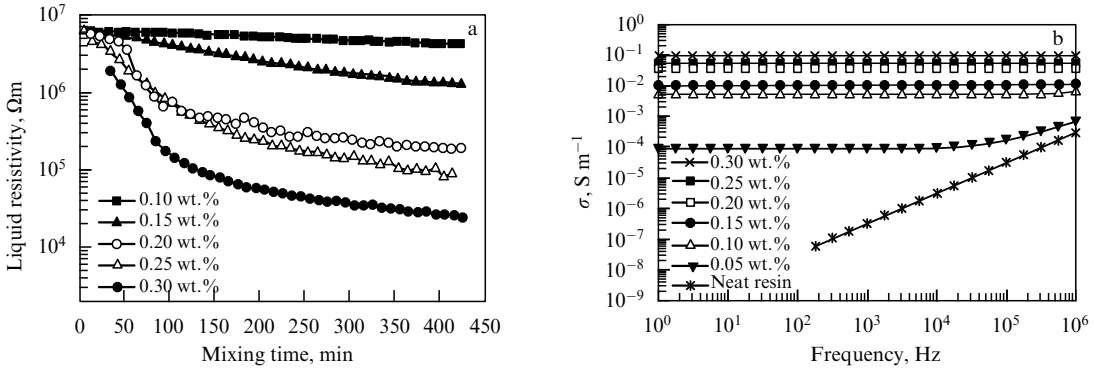

Figure 7. (a) Evolution of the resistivity of liquid nonsaturated polyester resin upon admixing of multiwalled CNTs [180]; (b) frequency dependences of the conductivity measured for samples of various compositions upon completing the fabrication process [180].

as the CNT content increases. Such a long incubation period is required for reaching the percolation threshold, which is possible only upon homogeneous distribution of CNTs over the material. However, even stirring for 420 hours does not ensure the fully homogeneous distribution of CNTs over the sample, because, as is evidenced from the dependences presented in the picture, the drop in the resistivity with time does not terminate.

Figure 7b gives the measurement data on the frequency dependence of the conductivity of solid composite samples with different compositions performed by the impedance spectroscopy method [180]. The frequency dependence of a pure polymer corresponds to the capacitor behavior. The conductivity of a composite filled with 0.05 wt.% CNTs does not depend on the frequency in a frequency range below 10^4 Hz, while at higher frequencies it demonstrates a capacitor behavior. The conductivity of composites with a CNT content exceeding 0.1 wt.% does not really depend on the frequency and notably increases as the CNT content rises.

Figure 8a compares the dependence of AC conductivity of solid composites on the CNT content with the relevant data for liquid composites of the same composition [180]. The conductivity of the pure polymer accounts for about 10^{-12} S m^{-1}. However, inserting CNTs in a quantity as low as 0.05 wt.% results in increasing the conductivity by eight orders of magnitude, to 2.7×10^{-4} S m^{-1}. Further enhancement of the filler loading increases the electrical conductivity to 1.3×10^{-1} S m^{-1}. The values of DC conductivity measured by the two-probe method are in agreement with those measured by impedance spectroscopy. It should be noted that the values of conductivity for liquid and solid composites of the same composition differ from each other by about four orders of magnitude.

Figure 8b presents results of the treatment of the measured dependence of the conductivity on the filler loading in accordance with Eqn (5). These data have been used to evaluate the parameters entering this equation [180]. The treatment has resulted in the percolation threshold position $\Phi_c = 0.026$ wt.% and the parameter $t = 2.55$. It is interesting to compare the above-given value of the percolation threshold with the estimate of this parameter on the basis of the classical percolation theory developed to describe the percolation conductivity of a composite with a minor additive of elongated conducting cylindrical particles D in diameter and l in length. According to this approach, the percolation threshold position is determined by expression (7) [192–194], which is reduced to an approximate relation $\Phi_c \approx 0.7\,D/l$ in the limiting case of a high aspect ratio ($D \ll l$). This relation results in $\Phi_c \approx 0.045\%$ for the composite containing CNTs $D = 9.5$ nm in diameter and $l = 1.5$ μm in length [180]. Therefore, the measured percolation threshold position (0.026%) is about 1.6 times less than the estimate following from the statistical theory. Such a discrepancy is probably explained by the orientation ordering of CNTs in the composite, which enhances the effective aspect ratio of particles involved in percolation charge transport.

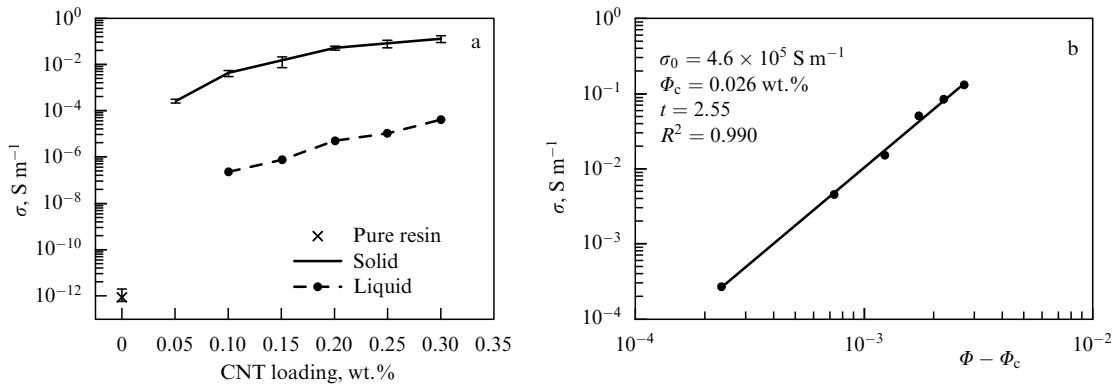

Figure 8. (a) Dependence of DC conductivity of solid (solid line) and liquid composites as measured upon completing the stirring procedure (dotted line) on CNT weight loading [180]; (b) dependence $\sigma(\Phi)$ represented in log-log coordinates permitting the determination of the parameters entering into expression (5) [180].

The measured percolation threshold position is comparable with other relevant data measured for such polymer matrices as epoxy resin, polyurethane, and vinyl ester (see Table 1). However, this value is about 40 times less than that for a composite based on a nonsaturated ester filled with entangled multiwalled CNTs (1%), and one quarter that for the same matrix filled with nonentangled CNTs (0.1%) [206]. Notice that the lowest value of the percolation threshold (0.0021 wt.%) was observed for an epoxy-resin-based composite filled with nonentangled CNTs [18, 23, 207]. We should also note the value of $\Phi_c = 0.005$ wt.% measured for an epoxy-resin-based composite filled with single-walled CNTs [193], and $\Phi_c = 0.011$ wt.% for an epoxy-resin-based composite filled with entangled multiwalled CNTs [22, 23].

The percolation behavior of a polypropylene (PP)-based composite filled with multiwalled CNTs was studied experimentally by the authors of Ref. [2]. Nanocomposite samples of various compositions were prepared with the use of a masterbatch on the basis of polypropylene filled with 20% multiwalled CNTs. Diluting this material with a pure polymer followed by stirring and injection moulding allowed producing composites with various CNT contents. The injection rate was varied from 25 to 178 mm s^{-1}. The electrical conductivity was measured by the standard two-probe method. To this end, rectangular-shaped composite samples of different compositions were fabricated, so that the opposite butt ends of them were coated with a conducting silver-based paint.

Figures 9a, b exemplify the results of measurements of the sample electrical conductivity. Figure 9a presents the dependences of the conductivity of composite samples on the mass CNT content measured for various injection velocities of a liquid composite. The measured data were treated on the basis of the statistical percolation theory [10] describing the dependence of the conductivity on the filler content in the vicinity of the percolation threshold through expression (5). In addition, the experimental data were also treated using a more modern-day approach [192] based on the following relationships:

$$\sigma = 2.70 \times 10^5 (p - p_c)^{3.8} \text{ S m}^{-1}, \quad p > p_c, \tag{12}$$

$$\sigma = 1.0 \times 10^{-9} (p_c - p)^{-0.9} \text{ S m}^{-1}, \quad p < p_c. \tag{13}$$

The parameters of these relationships (factors and power indices) were found to provide the best agreement with the experimental data in Fig. 9. The percolation threshold position evaluated on the basis of the experimental data amounts to $p_c = 3.8$ wt.%. The dependence described by standard relation (5) is also shown there. In this case, the percolation threshold position was equal to the above-evaluated value. A comparison of the dependences determined on the basis of various theoretical approaches indicates that the percolation models of Refs [10] and [192] are equally appropriate for describing experimental data on the conductivity of CNT-doped composites.

The dependences of the reduced conductivity on the injection velocity, measured for samples of various compositions, are plotted in Fig. 9b. As is seen, the injection velocity has an appreciable effect on the percolation behavior of the composites, and this effect can have a nonmonotone character, depending on the sample's composition. The maximum influence of the injection velocity on the composite conductivity is observed for samples with the CNT content at a level of 4.5%. This effect reflects the influence of the injection velocity on the degree of homogeneity of the CNT distribution over the sample. SEM observations in particular indicate that CNTs form aggregates as a result of stirring the composite. These aggregates are distributed randomly over all the material volume. A rise in the injection velocity causes the orientation of these aggregates towards the resin flow, which promotes the formation of percolation paths for electrical conduction. However, these paths can be formed only at quite high filler content. Therefore, the dependences presented in Fig. 9 indicate an inhomogeneous dispersion of the material upon its production by injection followed by moulding. This conclusion is also supported by the extraordinarily high magnitude of the percolation threshold (3.5%) measured for the sample of the above composition.

It should be noted that the percolation threshold position at the level of 3% was also observed for PP/MWNT composites by Liang et al. [208], who used pressure moulding for the composite production. A similar result ($p_c \sim 3\%$) was obtained by So et al. [209], who synthesized the composite on the basis of polyimide doped with multiwalled CNTs using the *in situ* polymerization process.

As an example of a composite possessing a high degree of homogeneity of a conducting filler, we can mention polyurethane foam (PUF) doped with CNTs [163]. This material combines a low density, low thermal conductivity, and good electrical conduction, which makes it attractive for a wide area of applications. With the aim of enhancing the degree of distribution homogeneity, the multiwalled nanotubes utilized

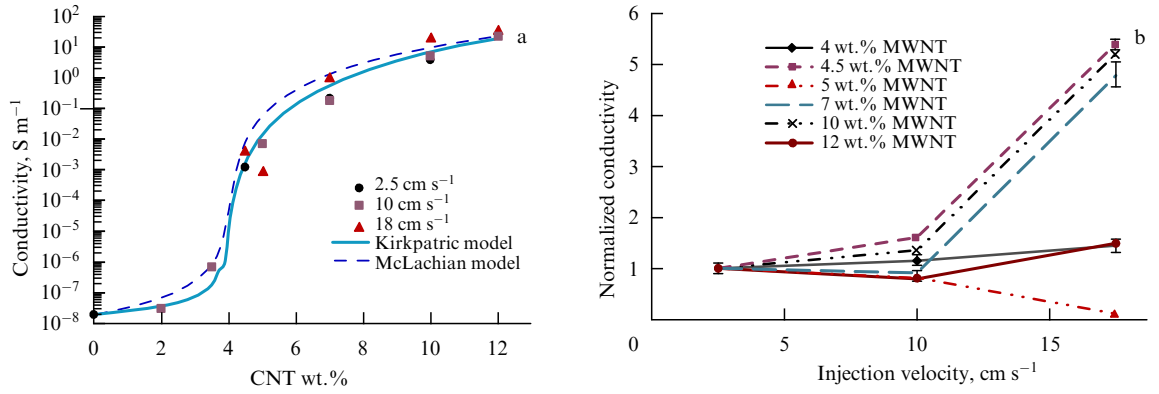

Figure 9. (a) Dependences of the electrical conductivity of composite PP/MWNT on CNT weight loading measured for samples fabricated at various injection velocities [2]; (b) Dependence of the reduced electrical conductivity of composite PP/MWNT of various compositions on the injection velocity [2]. Solid and broken lines correspond to calculations performed in various models.

Table 3. Chemical composition of the mixture utilized for production of polyurethane foam doped with multiwalled CNTs [163].

Component	Name	Weight, g
MDI	4.4-Diphenylmethane diizocianate	143.0
Polyol	Type of polyester	100.0
Surface activator	Type of silicon	2.0
Stabilizer	Cyclopenthane/water	6.0/1.0
Catalyst	Type of amine	1.5
Filler	Multiwalled CNTs	0.01, 0.05, 0.1

for the composite production were subjected to shortening from 3.5 to 1 μm by means of ball milling, followed by functionalization with hydrogen peroxide. In doing so, 1.5 g of CNTs were flooded with 500 ml of a 98% solution of H_2O_2 and ultrasonicated for 90 min at room temperature. Table 3 presents the chemical composition of the mixture utilized for the production of polyurethane foam.

CNTs were introduced into polyol to produce PUF. Stirring was provided by a mechanical mixer, the rate of which was gradually enhanced from 100 rpm to 3000 rpm. The duration of stirring took 5 min. Thereafter, water, catalysts, and the surface activator were added to the solution and the suspension obtained was stirred for 60 s at a rate of 3000 rpm until a homogeneous material formed. Then, MDI was added to the mixture, and experienced stirring at 5000 rpm for 10 s. This procedure resulted in a freely growing foam that was moulded into a form $250 \times 250 \times 250$ mm in size, where it was held at room temperature for 10 min. Thereafter, the foam was extracted from the mould and kept at room temperature for a day. Samples $15 \times 15 \times 5$ mm in size designed for measurement of the composite electrical conductivity were placed between two disk electrodes 30 mm in diameter with a gold coating.

Figure 10 displays the dependence of the electrical conductivity of composites fabricated on the base of polyurethane foam and doped with multiwalled CNTs on the nanotube's content (in units of php = 0.1%) [163]. Notice the low value of the percolation threshold, ~ 0.01 wt.%, whose exceeding leads to a conductivity increase from 0 to 23 S m^{-1} in a jump-like manner. Such a low position of the percolation threshold is due to a high degree of homogeneity of the composite, which was reached, on the one hand, due to the mechanical properties of the polyurethane resin providing good mixing of the polymer filled with CNTs, and, on the other hand, owing to a short length of nanotubes that also promotes more effective mixing. A further increase in the CNT content to 0.05% barely changes the sample's conductivity, while exceeding this content is accompanied by a decline in the conductivity. Such a character of the percolation behavior of the composite is caused by the tendency of CNTs to form entangled clots upon exceeding some content of CNTs in a material.

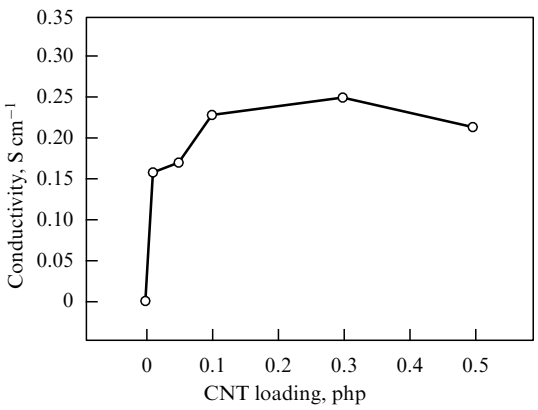

Figure 10. Dependence of the electrical conductivity of multiwalled CNT-doped polyurethane foam-based composites on MWNT loading (php = 0.1 %) [163].

2.7 Influence of the alignment of CNTs on the percolation behavior of composites

Orientation ordering of nanotubes introduced into a composite endows this material with anisotropic electrical properties. The conductivity of the material becomes dependent on the angle between the direction of the electric field and the direction of the prevailing orientation of nanotubes. This dependence has been studied in detail in conditions of percolation conduction, notably in Refs [119, 120]. The studies resulted in the discovery of nonmonotone dependence of the composite conductivity on the degree of CNT alignment.

Composite samples on the basis of polymethylmethacrilate (PMMA) doped with single-walled CNTs were prepared in Refs [119, 120] by taking advantage of the coagulation method [123] providing a homogeneous distribution of nanotubes over the volume. In initial samples, the nanotubes synthesized by the HiPco method were bound into bundles having an average diameter of 6.9 nm and length of ~ 310 nm, which corresponds to the aspect ratio of ~ 45. The degree of orientation ordering was controlled through the variations of the extrusion rate within the range of 1–15 mm min^{-1}, the spinneret diameter (0.5, 1.5, 2.5 mm), and the fiber-drawing speed (1–31 m min^{-1}). The samples lacking CNT alignment were produced by hot pressing of coagulated composites.

The electrical conductivity of filaments fabricated from the composite was measured at room temperature using the two-probe method by means of an impedance electrometer. The degree of orientation ordering was characterized by the full width at half maximum (FWHM) of the nanotube distribution over the orientation angles. This distribution was established from measurements of X-ray radiation by small angle scattering. Increasing FWHMs from 0° (perfectly aligned) to 180° (isotropic) corresponded to increasing SWNT isotropy.

Figure 11 presents the results of measurements of the electrical conductivity of composites [119, 120]. These measurements (see Fig. 11a) allowed determining the percolation threshold position for the isotropic sample at $\Phi_c = 0.365$ wt.%. An interesting peculiarity of the data obtained is the occurrence of the percolation transition upon changing the degree of CNT alignment (Fig. 11b). Thus, for the composite sample containing 2 wt.% CNTs, the longitudinal conductivity $\sigma_{||}$ measured along the alignment direction experienced an abrupt jump from 6.5×10^{-11} up to 4.4×10^{-6} S cm^{-1} when increasing FWHM (lowering the degree of alignment) from 20° to 36°. Such a behavior is caused by decreasing the number of possible contacts between neighboring nanotubes as a result of the enhancement of the degree of alignment upon lowering the CNT content.

Measurements imply that in the vicinity of the percolation transition the dependence of the electrical conductivity on the degree of alignment is described by a power function:

$$\sigma_{||} = \sigma_0(\mathrm{FWHM} - \mathrm{FWHM_c})^{\beta_{or}}, \qquad (14)$$

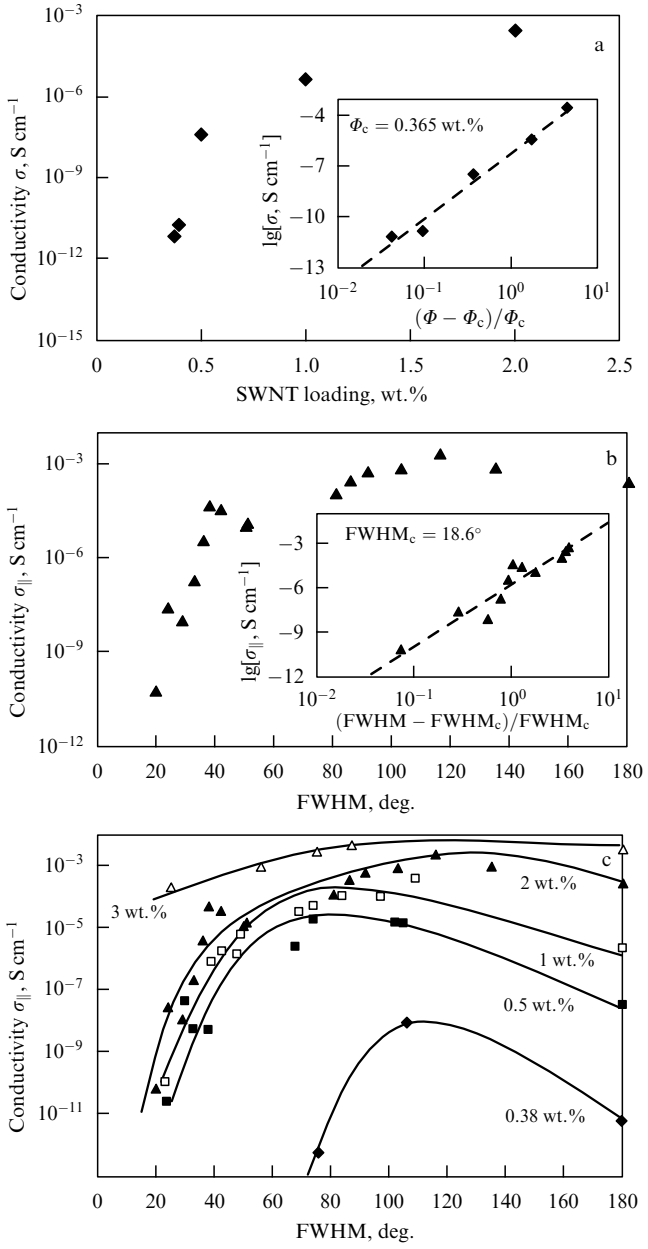

Figure 11. (a) Dependence of the electrical conductivity of isotropic samples of the PMMA/CNT composite on filler loading. The inset shows the same dependence represented in log-log coordinates, which permits the evaluation of the percolation threshold position Φ_c. (b) The dependence of the conductivity of the PMMA/CNT composite with a filler loading of 2 wt.% measured along the alignment direction on the degree of alignment. The inset shows the same dependence represented in log-log coordinates, which permits the evaluation of the critical degree of alignment $FWHW_c$. (c) Dependences of the conductivity of samples of the PMMA/CNT composite with various filler loadings measured along the alignment direction on the degree of alignment (△) 3, (▲) 2, (□) 1, (■) 0.5, and (◆) 0.38 wt.% [119, 129].

which is similar to the percolation dependence (5). In this case, both the threshold value $FWHM_c$ of the alignment degree and the power index β_{or} engaged in expression (14) demonstrate the dependence on CNT loading. Specifically, the measured threshold value is $FWHM_c = 18.60$ at the CNT loading of 2 wt.%. The data shown in Fig. 11c indicate that for a sample of fixed composition the dependence of the electrical conductivity on the degree of filler alignment has a

Table. 4. Conductivity σ_{iso} of the isotropic composite, threshold position FWHMc of the degree of alignment, and the maximum magnitude σ_{max} of the conductivity measured for samples of various compositions at the relevant value of $FWHM_{max}$ [119].

CNT content, wt.%	$FWHM_c$, deg.	$FWHM_{max}$, deg.	σ_{max}, S cm^{-1}	σ_{iso}, S cm^{-1}	$\sigma_{max}/\sigma_{iso}$
0.38	75	116	1.0×10^{-8}	7.0×10^{-11}	1400
0.5	23	109	1.9×10^{-5}	4.0×10^{-8}	470
1	22	80	1.2×10^{-4}	2.5×10^{-6}	46
2	19	106	2.7×10^{-3}	3.5×10^{-4}	8
3	< 19			4.2×10^{-3}	

nonmonotone character, so that the maximum of this dependence also depends on CNT loading in a nonmonotone manner.

Table 4 gives the results of treatment of experimental data obtained for samples with various CNT loadings and demonstrated in Fig. 11c. A sharp enhancement of the maximum electrical conductivity of samples, $\sigma_{max}/\sigma_{iso}$, can be seen as the CNT loading decreases. The high value of this ratio at low loadings indicates that the number of percolation paths forming in a sample with a low degree of anisotropy exceeds that in a fully anisotropic sample. Moreover, the enhancement of the CNT content from 0.38 to 3 wt.% is accompanied by a lowering of the threshold value of $FWHM_c$ from $\sim 75°$ to $\sim 19°$, which corresponds to increasing the threshold value of the CNT alignment degree. The reason is that the number of contacts among nanotubes rises with increasing CNT content, so that the percolation breaks at a higher degree of anisotropy.

The above dependences are in qualitative agreement with the results of a simple numerical model developed in Ref. [211]. The probability of crossing for cylinders with the aspect ratio $l/D = 20$, calculated in this work, for a weak degree of alignment exceeds that for an isotropic system.

Measurements indicate that the nonmonotone character of the dependence of the electrical conductivity on the degree of alignment of the CNT filler is most pronounced at low loadings. At a filler content of 3 wt.%, this dependence begins monotonically increasing, reaching saturation at $FWHM \approx 75°$. Therefore, the weak anisotropy of a composite at such a high CNT loading does not change notably the percolation behavior, because the number of contacts among CNTs in the sample is quite high. On the other hand, at a lower filler loading, a percolation network containing a few conducting paths is subjected to essential changes as a result of a modest alignment of filler particles, because it impacts notably on the percolation network structure. Continuing their research initiated in Ref. [109], the members of the same team studied the dependence of the electrical conductivity and thermal conductivity of polyethylene-based composites doped with single-walled CNTs on the degree of alignment of polymer matrix molecules [210].

Low- and high-density polyethylene with crystallinities of 33% and 78%, respectively, was utilized as a polymer matrix. Single-walled CNTs were synthesized by the laser ablation method. Composite samples with various degrees of alignment of polyethylene molecules were produced by the spinning method. The samples of low-density polyethylene (LDPE) contained $p \sim 0.56$ and 19.5 vol.% CNTs, which

corresponds to a weight content of 1 and 30%, while CNT loading in high-density polyethylene (HDPE) amounted to $p \sim 0.6$, 3, 6, and 20 vol.%, which corresponds to a weight content of 1, 5, 10, and 30%. Isotropic samples were prepared through recrystallization by means of a hot press. For the preparation of anisotropic samples on the basis of HDPE, the composites with the CNT content $p \sim 0.6$ and 1.2 vol.% (1 and 2 wt.%) were used. The electrical conductivity of the composites was measured by a standard two-contact method, while the conductivity of initial polyethylene was measured by the four-contact method.

The measured dependences of the electrical conductivity of composite samples prepared from LDPE and HDPE on the volume content of single-walled CNTs exhibit a percolation character. The percolation threshold position corresponds to the CNT content $p \sim 0.3$ vol.% for both types of a polymer matrix. At $p \sim 0.6$ vol.%, the composite conductivity reaches $\sigma \sim 10^{-4}$ S cm^{-1}, which exceeds that for a polymer matrix by 12 orders of magnitude. An important conclusion inferred from experiments [119, 210] relates an abrupt lowering of the composite electrical conductivity with the alignment of polymer filaments. Thus, the conductivity of a composite based on longitudinally aligned polyethylene filaments doped with 0.6 and 0.12 vol.% single-walled CNTs measured along the filament alignment amounts to $\sim 5 \times 10^{-10}$ S cm^{-1} [210], which is about 6 orders of magnitude lower than that for isotropic material of the same composition. This conclusion seems to be paradoxical at first glance, however, it is quite explainable in terms of the above-noted nonmonotone dependence of the composite conductivity on the degree of CNT alignment (see Fig. 11c).

3. Modeling of the conductivity of CNT-doped composites

3.1 Percolation model of the composite conductivity

While the main source of information on the electrical characteristics and percolation behavior of CNT-doped composites comprises experiments, many questions arising in the investigation of this problem can hardly be clarified by purely experimental means. This is due to difficulties in the experimental determination of nanotube geometry, the degree of their defectiveness, the degree of orientation ordering, the degree of homogeneity of the filler distribution over the polymer matrix volume, the character of the contact, etc. It seems more appropriate to find the answers to the above questions on the basis of numerical modeling, the results of which determine the further development of experimental studies and technological elaborations.

The percolation theory, based on the principles of statistical physics, was developed for describing the percolation behavior of heterogeneous systems, including CNT-doped polymer composites [6–10]. This theory has a general character and has resulted in analytical expressions like Eqn (5) interconnecting the values of the sample conductivity and the degree of deviation from the percolation threshold. However, the conclusions and results of the classical percolation theory are not always applicable for a detailed description of the behavior of CNT-doped composites, because this theory does not take into account such factors as possible aggregation of CNTs, bent and frequently waving nanotube structures, a spread in CNT conductivity caused by a spread in their diameter and (in the case of single-walled CNTs) chirality, and a variety of contact phenomena which are complicated by the possible formation of a thin polymer layer between the neighboring nanotubes in a polymer.

The above factors and some others can be taken into consideration within the framework of modern numerical approaches based on molecular dynamics and Monte Carlo methods. Nowadays, the active development of such approaches as applied to the description of transport characteristics of CNT-doped composites and much work performed in this field can be considered as a first approach to building an adequate percolation model of CNT-doped composites. A short review of this work, accompanied by an analysis of possible ways to further develop them, is given below.

Paper [212], where a 3D approach was guided by the ideas of the classical percolation theory [11], merits mentioning among early publications devoted to modeling the conductivity of polymer-based composites doped with CNTs. A trend of nanotubes in the aggregation was tried to take in account within the framework of this approach. In doing so, the possibility of forming bundles of single-walled nanotubes containing 3, 7, and 19 individual nanotubes was inserted artificially during computation of the percolation behavior of composites. In addition, the modeling of composites within the framework of the 3D approach included a possible bending of carbon nanotubes, and a spread in the values of contact resistivity of neighboring CNTs engaged in one or adjacent bundles was performed [213].

A series of recent publications [214, 215] is devoted to modeling the percolation behavior of composites doped with CNTs using the Monte Carlo method. The authors of these studies managed to take into account the influence of such factors as the aspect ratio of CNTs, degree of aggregation, structure and electrical properties of individual CNTs on the percolation threshold position and the character of the dependence of conductivity on the filler loading. The nanotubes were treated as soft-core cylinders l in length and D in diameter that are able to penetrate each other (for simplification of calculations). These cylinders are distributed randomly over the volume of a parallelogram.

Three types of contacts between neighboring CNTs are considered: (a) the coordinates of the ends coincide; (b) the coordinates of the end of one nanotube coincide with those of a point on the external wall of the second CNT, and (c) the points on the walls of both CNTs coincide. The relevant calculations imply that at the CNT parameters chosen most contacts (95%) correspond to case (c), when the adjacent nanotubes contact through the walls. The relative contribution from contacts of type (a) (through the ends of adjacent CNTs) amounts to 0.1–0.2%, while the contribution from contacts of type (b) (the end of one CNT contacts the wall of another one) ranges between 4.8–4.9%. Simulations also indicated that the relative calculational error relating to the usage of the assumption on the mutual penetration of CNTs is negligible at the low filler loadings considered.

Composites doped with bent CNTs were also treated in an effort to study the influence of distortion of the rectilinear CNT structure on the composite percolation behavior. According to the approach developed, a nanotube is divided into 10 rectilinear segments (elbows), so that each of those can be bent at some angle θ with respect to the adjacent one. The bending angle of each nanotube elbow is varied from 0 to θ_{max}. Moreover, the influence of the inhomogeneous distribution of CNTs over the volume of a polymer matrix on the

composite percolation behavior was also studied. To this end, aggregates whose parameters were characterized by the normal distribution were inserted into the composite material artificially. The degree of nanotube aggregation was characterized by the sole parameter

$$\delta = \frac{V_{\rm ag}}{V_{1/4}}\,, \tag{15}$$

where $V_{\rm ag}$ is the volume of the sphere, which includes 95% of CNTs involved in the aggregate, and $V_{1/4}$ is one quarter of the total volume of the 3D cube containing the composite. The homogeneous distribution of CNTs over the composite volume corresponds to $\delta = 1$, so that enhancement of the aggregation degree is accompanied by a lowering of the parameter δ. The Monte Carlo calculation procedure includes 100 independent runs for each specific CNT content with a subsequent averaging of the data obtained.

3.2 Influence of CNT parameters on the percolation threshold position

The above-considered approach [214, 215] has been applied to establish the dependence of the character of the composite percolation behavior on the CNT conductivity, their aspect ratio, degree of curving ($\theta_{\rm max}$), and the aggregation degree δ. Figure 12 presents the results of calculations performed for different values of the above-mentioned parameters. As follows from the dependences shown in Figs 12a and 12b, the electrical conductivity of a nanocomposite is proportional to the conductivity of CNTs and their aspect ratio. The enhancement of the aspect ratio is accompanied by a decrease in the percolation threshold position. Thus, the conductivity at a level of 10 S m^{-1} is reached at the volume content of CNTs with the aspect ratio of $l/D = 100$ and $l/D = 1000$ at the level of 1.3% and 0.3%, respectively. Therefore, CNTs possessing a higher aspect ratio are preferable for the usage as a filler to conducting composites. Along with this, as follows from the data in Fig. 12c, the bending of CNTs promotes some moderate lowering of the conductivity. The influence of CNT aggregation seems to be more essential (Fig. 12d). The conductivity declines as the parameter δ decreases, which corresponds to an increase in the aggregation degree.

Dependences of the composite conductivity on CNT loading calculated at various values of parameters have been treated in terms of the standard percolation formula (5). The results of the treatment indicate that the magnitude of the parameter t involved in Eqn (5) does not really depend on both the aspect ratio and the degree of CNT bending and is equal to $t = 1.8 \pm 0.05$. The value of this parameter decreases smoothly as the CNT aggregation degree increases.

The calculated dependence of the percolation threshold position $p_{\rm c}$ on the CNT aspect ratio is approximated by the power function

$$p_{\rm c} = \left(\frac{l}{D}\right)^{-1.1\pm0.03}\,, \tag{16}$$

which is applicable for quite high values of the aspect ratio, $l/D > 20$, and is in good agreement with analytical expression (7). The calculations also indicate that the parameter σ_0 involved in percolation formula (5) depends not only on the conductivity of CNTs but also on their aspect ratio. Taking into account this dependence, Eqn (5) can be represented in the form

$$\sigma_{\rm com} = \sigma_{\rm CNT} 10^{0.85[\lg(l/D)-1]}\,[p - p_{\rm c}]^t\,. \tag{17}$$

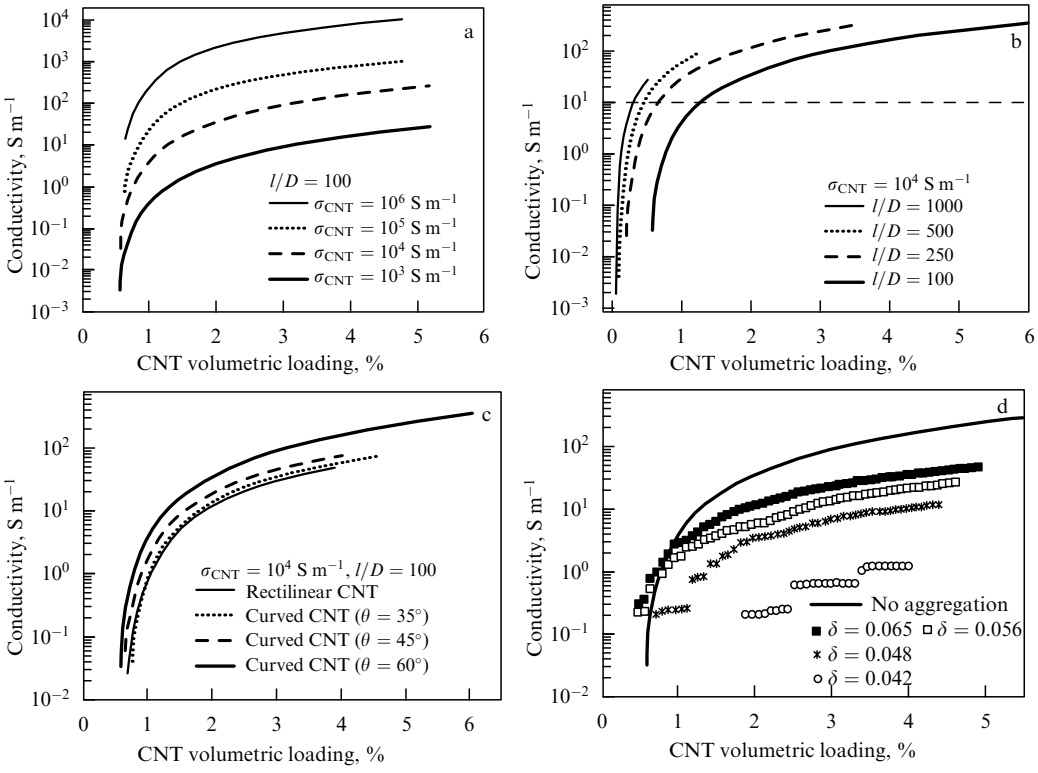

Figure 12. Dependences of the composite conductivity on CNT volumetric loading calculated for various magnitudes of the electrical conductivity of CNTs (a), aspect ratio of CNTs (b), parameter $\theta_{\rm max}$ characterizing the degree of CNT bending (c), and parameter δ characterizing the degree of their aggregation (d) [214, 215].

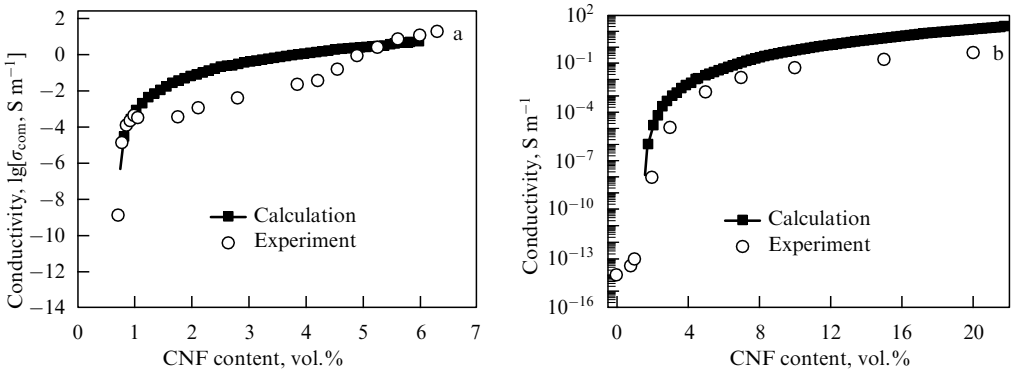

Figure 13. (a) Comparison of the dependence of the conductivity of a composite doped with short carbon nanofibers (aspect ratio $l/D = 428$, percolation threshold 0.7 wt.%, $t = 3$) on the filler loading (17) calculated in Refs [214, 215] with the measured data [213]; (b) comparison of the same dependence (17) calculated in Refs [214, 215] for a composite doped with carbon nanofibers (aspect ratio $l/D = 433$, percolation threshold 0.8 vol.%, $t = 3$) with the measurement data [216].

Therewith, the power index $t = 1.8$, and the percolation threshold position p_c depends on the aspect ratio in accordance with the expression $p_c = (l/D)^{-1.1}$.

The above approach is applicable to describing not only CNT-doped composites but also other composite types, such as carbon fiber-doped composites. This can be seen from a comparison of the dependences of the electrical conductivity of carbon nanofiber-doped composites calculated with the aid of Eqn (17) for various nanofiber aspect ratios with the measured results [216, 217] (see Fig. 13).

Experiments imply that in some cases the surface of nanotubes inserted into a polymer matrix is covered with a thin polymer layer that prevents the formation of an electric contact between adjacent nanotubes [218, 219]. In this circumstances, the charge transport is effected by way of electron tunneling through the polymer layer [220]. Due to the strong dependence of the tunneling probability on the intertube distance that is described by a statistical distribution, taking into account this effect complicates the percolation model. Furthermore, even in the absence of the insulating layer between neighboring nanotubes, the direct intertube contact is hampered by the van der Waals interaction, due to which the distance between the surfaces of neighboring nanotubes becomes quite large (≈ 0.34 nm). The authors of Ref. [221] have developed a 3D percolation model aimed at determining the influence of the electron tunneling effect on the percolation behavior of CNT-doped composites. This model was modified in subsequent work [222, 223]. A similar problem related to tunneling was stated by the authors of Ref. [4], who made a simplifying assumption about the possibility of the mutual penetration of CNTs.

To model bent CNTs, the authors of Refs [221–223] took advantage of the above approach (see Section 3.1), which was also applied in Refs [214, 215]. In accordance with this approach, a nanotube is divided into 10 segments, each of which is bent with respect to the neighboring segment at angle $0 < \theta < \theta_{max}$. The bending angle is chosen in a random manner. The authors dismissed as not justified the assumption about the mutual penetration of CNTs, as opposed to the models applied earlier. Adjacent nanotubes are separated from each other by a distance determined by the van der Waals interaction potential. The minimum intertube distance d_V corresponds to the critical spacing at which the electron tunneling is still possible. This spacing depends on the properties of the polymer film covering the nanotube surface.

In the course of modeling, the nanotubes are inserted sequentially in a random manner into a 3D cubic cell L_{cell} in size. Thus, the minimum distance is calculated between the newly inserted CNT and all the CNTs inserted before. If the minimum distance D_{min} is less than the sum of the CNT diameter D and van der Waals spacing d_V, the inserted nanotube is removed and a new CNT is inserted inside the cell instead. The process is repeated until the shortest distance between the newly inserted CNT and all the CNTs inserted before exceeds D_{min}. If the shortest distance between two nanotubes is less than or equal to the maximum value $D_{max} = D + d_t$ at which electron tunneling is still possible, it is believed that this pair of nanotubes is coming into electrical contact. Periodic boundary conditions are introduced for all directions. Simulations have shown that the usage of a cell with the ratio of $L_{cell}/l_{CNT} = 5$ is enough for good convergence of calculated results. One hundred Monte Carlo runs were performed for each pair of l_{CNT} and D values; afterward, the calculated results were averaged.

At the first stage of calculations performed in Refs [221–223] for the verification of the model, a network of mutually penetrating CNTs was considered without taking into account the electron tunneling and van der Waals intertube interaction. This corresponds to the conditions of $D_{max} = D$ and $D_{min} = 0$ accepted in the above-described model [214, 215]. Following Hu et al. [214, 215], the nanotube length and diameter were chosen to be equal to 5 μm and 50 nm, respectively while the cubic cell size equaled 25 μm. The calculations performed in accordance with the above procedure resulted in the percolation threshold position of 0.6107%, which is in good agreement with the value of 0.6165% computed earlier [214, 215].

In order to simplify the calculations, the fixed value of $d_V = 0.34$ nm was chosen as the van der Waals intertube spacing. This value corresponds to the equilibrium spacing between hexagonal planes in graphite. The value of $d_t = 1.8$ nm calculated in Ref. [221] was chosen as the maximum tunneling spacing. The ratio D_{min}/D_{max} was fixed at 0.4786, which shortens the calculation time as well. The simulations were performed for CNT lengths of $l_{CNT} = 10$, 20, 50, 100, 150, and 200 nm, and in each case the cubic cell size was set to $5l_{CNT}$.

Figure 14 exhibits the dependences of the electric percolation threshold (EPT) position on the CNT aspect ratio (l_{CNT}/D) calculated on the basis of the above approach. As

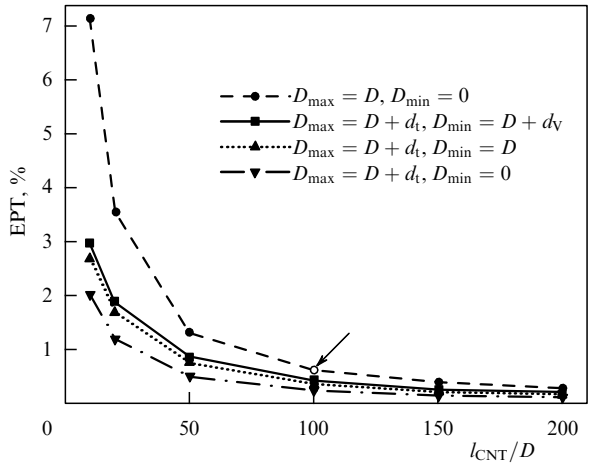

Figure 14. Dependence of the electric percolation threshold (EPT) position on the CNT aspect ratio calculated for a composite doped with rectilinear CNTs [221– 223]. The result of Refs [217, 218] is shown by the arrow.

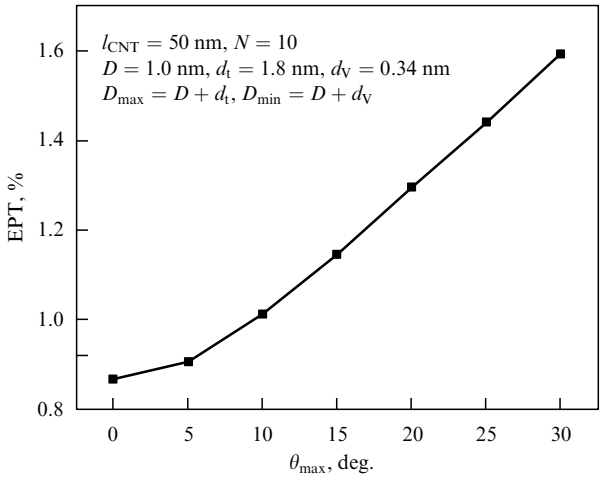

Figure 15. Dependence of the electric percolation threshold (EPT) position on the maximum bending angle calculated for a composite doped with bent CNTs [221–223]. N is the number of segments.

is seen, an increase in the aspect ratio is accompanied by an abrupt lowering of the percolation threshold, especially in the region of low aspect ratios. The calculated results obtained for a cell $5l_{CNT}$ in size were compared with those for the cell size of $8l_{CNT}$ to test the character of convergence of the computational procedure. The distinction in the threshold position does not exceed 1.4% for CNTs with the aspect ratio of 20. This justifies the usage of the cell size of $5l_{CNT}$ for providing a reliable result.

A comparison of the calculated dependences with those obtained within the framework of the standard percolation model [214, 215] ($D_{min} = 0$ and $D_{max} = D$) indicates that the utilization of the standard model results in an overestimation of the percolation threshold position, especially in a low-threshold region. Thus, the degree of overestimation amounts to 110% in the case of the aspect ratio equal to 10. Two other models ($D_{max} = D + d_t$, $D_{min} = D$ and $D_{max} = D + d_t$, $D_{min} = 0$) underestimate the threshold position. However, the distinction between the predictions of those models vanishes as the aspect ratio increases. Thus, the usage of the standard percolation model neglecting CNT bending and tunneling effects at an aspect ratio exceeding 200 permits obtaining a reasonable accuracy at a notable shortening of the computing time.

In order to study the influence of disruption of the rectilinear CNT structure on the percolation behavior of composites, each nanotube was divided into 10 segments bent in respect to the neighboring one at an arbitrary angle $0 < \theta < \theta_{max}$. Therewith, θ_{max} was limited by the value of 30° to shorten the computing time. Figure 15 represents the calculated dependence of the electric percolation threshold (EPT) position on the maximum bending angle. This dependence corresponds to the trend noted in Refs [213–215], in accordance to which an increase in the degree of deviation from the rectangular CNT structure is accompanied by an increase of the percolation threshold.

3.3 Influence of the degree of alignment

The dependence of the electrical conductivity on the interrelation between sample thickness and nanotube length is one of the important peculiarities of the conduction in CNT-doped composites. In particular, it follows from the results of experiments [224, 225], where it was established that the resistivity of CNT films near the percolation threshold varies inversely proportional to the sample thickness. Another peculiarity of this phenomenon relates to the possible orientation ordering of CNTs inside a composite. The dependence of the composite resistivity on the degree of nanotube's orientation was first noted by the authors of experiments [119, 120]. This dependence was studied numerically for a 3D CNT network in Refs [226–228].

The electrical conductivity of CNT-doped materials can depend not only on the degree of CNT alignment but also on the direction of measurement. The above-mentioned experimental data [119, 120] on the percolation conduction of composites in the conditions of partially aligned CNT filler were analyzed in Refs [226–228] using a numerical simulation on the basis of the Monte Carlo method. Such an approach to the simulation of the percolation conduction was first applied in Ref. [227], well before the discovery of carbon nanotubes. In accordance with this relatively simple approach, a 2D square unit cell is filled with rods of zero diameter and of a fixed length l, which amounts to some fraction of the cell size. The rod centers are distributed in a random manner over the cell space.

To simulate the rod alignment, the angle of orientation θ of a rod in respect to some prescribed direction is chosen in a random manner within the interval $-\theta_\mu > \theta > \theta_\mu$, so that the maximum angle $0 < \theta_\mu < 90°$ determines the degree of alignment of rods inside the material. At $\theta_\mu = 90°$, the rods are distributed isotropically, while lesser values of θ_μ correspond to some orientation ordering. The electrical contact of the rods occurs at their crossing. Percolation takes place when a network of contacting rods penetrates through the cell. The percolation probability P is defined as a fraction of the 1000 configurations for which the percolation occurred. This indicator can be considered as the conductivity of a cell in relative units, since the higher the magnitude of the parameter P, the greater the number of percolation paths.

Figure 16 displays the dependences of the percolation probability P on the degree of alignment calculated for rods with $l = 0.108\, L_{cell}$ [119]. The abrupt character of the percolation transition at some critical value of the alignment angle θ_c corresponds qualitatively to the experimental results

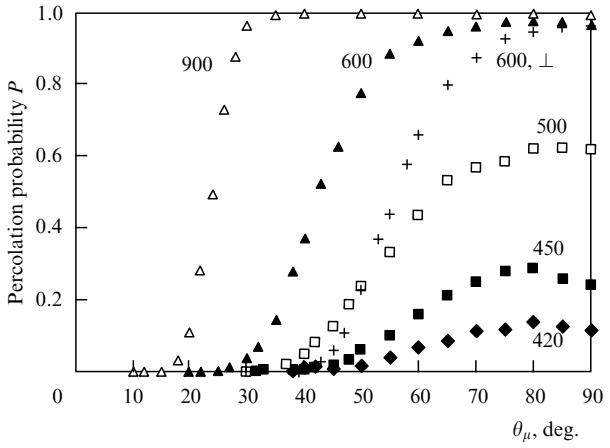

Figure 16. Dependence of the probability of percolation on the degree of alignment calculated on the basis of 1000 trials for various quantities of rods $l = 0.108L_{cell}$ in size [119]. The number of rods is marked alongside the relevant dependences. The critical angle θ_c corresponding to the percolation threshold is equal to: 11° (△); 21° (▲); 31° (□); 33° (■), and 37° (◆). The symbol (+) corresponds to the percolation probability for the direction perpendicular to that of alignment. In this case, one has $\theta_c = 31°$.

[119] given above in Fig. 11. Processing the calculated results represented in Fig. 16 implies that the dependence of the percolation probability on the degree of alignment near the percolation transition point is described approximately by the power function $P \sim (\theta_\mu - \theta_c)^{\beta_\theta}$, where β_θ is the power index. The calculations indicate an increase in the percolation probability with a rise in θ_c, which implies the effect of the displacement of the alignment threshold to a higher anisotropy according to experiment [119].

The calculated results depicted in Fig. 16 suggest a nonmonotone character of the dependence of the conductivity on the degree of alignment of rods that occurs at a relatively low filler loading (the number of rods is less than 600). Therewith, the maximum percolation probability (conductivity) is reached at $\theta_\mu = 70°-90°$, i.e. when the degree of alignment is rather low. In other words, at low filler loadings a minor alignment corresponds to a higher conductivity than in the case of filler isotropic distribution. This conclusion is in qualitative agreement with the experimental data [119].

The influence of the CNT alignment on the percolation behavior of composites can be illustrated through the ratio of the maximum percolation probability P_{max} to the relevant value P_{iso} for filler isotropic distribution. For a cell containing 600 or more rods, one has $P_{max}/P_{iso} = 1$. Therefore, the alignment does not affect the number of percolation paths at a high degree of alignment ($\theta_\mu < 50°$). However, this ratio increases as the number of rods decreases, amounting to 1.01, 1.19, and 1.22 for 500, 450, and 420 rods, respectively. Hence, even weak anisotropy promotes at low filler loading an increase in the number of percolation paths. This conclusion is in qualitative agreement with the experimental data on the electrical conductivity of composites PMMA/SWNT [119, 120].

The percolation behavior of CNT-doped composites was studied in detail in Ref. [229], taking into account the above effects and falling back on the Monte Carlo simulation as well. This work is the development of earlier publication [230] devoted to the calculation of the influence of various CNT parameters on the electrical properties of composites.

As follows from the calculations [229], the maximum value of the composite conductivity is not reached at a full but at a partial alignment of CNTs. At first glance, such an important conclusion seems to be paradoxical; however, it is confirmed by the results of experiments [119, 231], reporting a nonmonotone dependence of the composite conductivity on the degree of filler alignment. At a high alignment of CNTs, the composite demonstrates the anisotropy that manifests itself in a dependence of the conductivity on the direction of measurement.

According to the model developed by the authors of Ref. [228], the nanotube is represented as a rod l_{CNT} in length possessing two degrees of freedom (the position of one end and the orientation angles). The nanotubes are inserted into a composite at an arbitrary angle θ with respect to the horizontal axis, following the conditions: $\theta_m - \theta_a \leqslant \theta \leqslant \theta_m + \theta_a$, and $180° + \theta_m - \theta_a \leqslant \theta \leqslant 180° + \theta_m + \theta_a$. The first of the angles (θ_a) is defined as the nanotube's orientation angle that determines the degree of alignment of the nanotube in the material. At $\theta_a = 90°$, the orientation is fully random, while at $\theta_a = 0°$ the nanotubes are fully ordered in some direction. The second angle (θ_m) defines the direction of measuring the conductivity, i.e., the direction connecting the electrodes. If $\theta_m = 0°$, then the resistance is measured in parallel to the direction of the CNT alignment, while if $\theta_m = 90°$, the measurement is performed in the perpendicular direction.

CNTs are applied onto a 2D grid until the desired surface density n is reached. Subsequent surface layers are formed in the same manner, so that a 3D film is produced as a result of this procedure. It is assumed that only nanotubes belonging to adjacent 2D layers can contact, so that the position of the contact points is determined through the calculation. The resulting effective integral density of the 3D film consisted of l layers, each of which is characterized by the surface density n, which is always less than ln because only CNTs belonging to the nearest layer are connected by the electrical contact. After completing the film formation, the positions of the intertube contact points are determined. Following Ref. [230], the intertube contacts are characterized by a joint contact resistance R_{JCT} (neglecting a spread in the electron properties of CNTs). The electric network obtained is simulated conventionally on the basis of Kirchhoff's laws. The interconnection between the applied voltage and the total current through the film calculated on the basis of such an approach permits the determination of the composite resistivity ρ.

Each point is obtained as a result of averaging at least 200 independent configurations of CNTs inside the composite generated in a random manner. The main calculations were performed for a composite film sample $L = 7$ μm in length, $W = 2$ μm in width, CNT surface density in a layer $n = 2$ μm^{-2}, nanotube length $l_{CNT} = 2$ μm, and the number of layers in the film equal to 5, which corresponds to a film thickness $t = 15$ nm. The contact resistance was set to the ballistic one (~ 6.5 kΩ) multiplied by 100.

Figure 17a displays the dependences of the normalized composite resistance on the CNT alignment angle, calculated for three different directions of measurement ($\theta_m = 0°$, 45°, and 90°). It is seen that at $\theta_m = 0°$ the resistance decreases smoothly as θ_a decreases, reaching the minimum value at $\theta_a^{min} = 45°$. Such a behavior of the resistance can be described by decreasing the number of electrical contacts necessary for formation of percolation paths with the enhancement of the alignment degree. However, further lowering θ_a results in a notable rise in the resistance, because it is accompanied by a

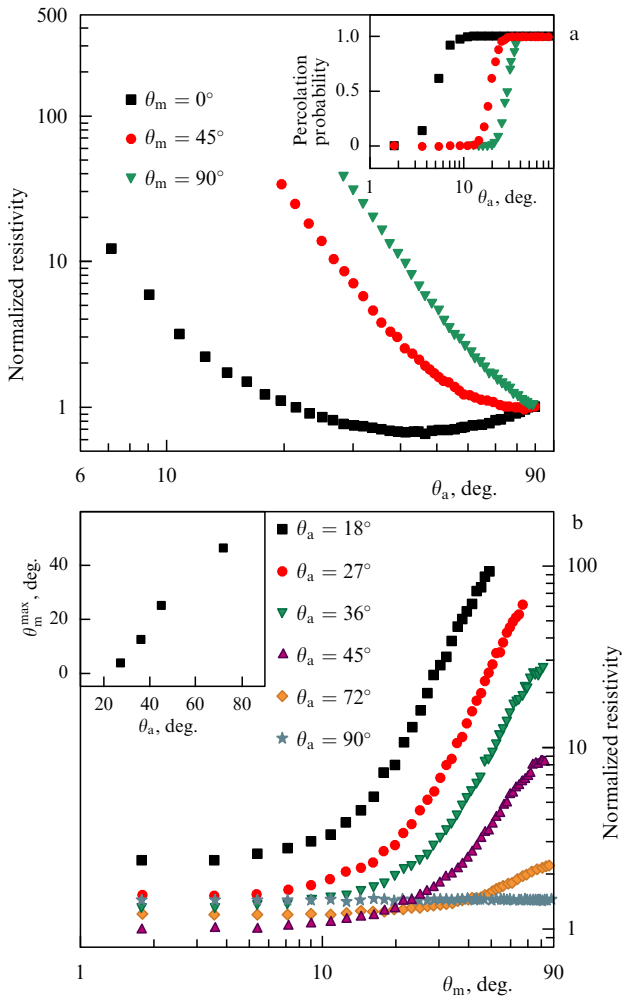

Figure 17. (a) Dependences of the normalized composite resistivity on the angle of CNT alignment, calculated for different measurement directions θ_m. The film sample was $l = 7$ μm in length, $W = 2$ μm in width, $n = 2$ μm^{-1}, $l_{CNT} = 2$ μm, and $t = 15$ nm. The inset represents the dependences of the percolation probability on the alignment angle θ_a, calculated for the same values of θ_m. (b) Dependences of the normalized composite resistivity on the measurement direction, calculated for various alignment angles. The values of the power index β in Eqn (18) approximating the dependences $\rho(\theta_m)$ near the percolation threshold are equal to $\beta = 2.9$, 2.9, 2.7, 1.85, 0.65, and 0 for $\theta_a = 18°$, 27°, 36°, 45°, 72°, and 90°, respectively. Upon approaching $\theta_m = 90°$, the highly aligned films (at $\theta_a = 18°$ and 27°) cease to conduct the current completely. The dependence $\theta_m^{max}(\theta_a)$ is shown in the inset [229].

decrease in the number of conducting paths. For example, in the case of almost full orientation ordering, the nanotubes are oriented almost in parallel to each other, so that the number of contacts turns out to be practically negligible.

Therefore, the occurrence of the resistivity minimum at the alignment angle of θ_a^{min} is a result of competition between the decreasing number of electrical contacts and shortening of the percolation path length (enhancing the resistivity). In the model considered, the sample length always exceeds the CNT length. Under such conditions, the electrical conduction is never accomplished through one nanotube. In this case, the conductivity decreases at a high alignment degree.

Figure 17a also illustrates the influence of the measurement direction on the results of measuring the resistance for composites with different alignment degrees. At $\theta_a = 90°$, the alignment is absent, so the resistance does not depend on the measurement direction θ_m. In contrast, at $\theta_m = 45°$ and 90°, the resistance increases monotonically with decreasing θ_a. In those cases, since the measurement direction does not coincide with that of the alignment, an increase in the alignment degree does not lead to a notable decrease in the number of electrical contacts or a shortening of the percolation path length. Therefore, the change in the resistance relates in these conditions to decreasing the number of percolation paths.

The dependences of the resistivity on the alignment angle shown in Fig. 17a are approximated by the inverse power function

$$\rho \sim (\theta_a)^{-\alpha}, \tag{18}$$

where $\alpha = 2.9$, 3.6, and 3.9 are the values of the power index evaluated on the basis of these dependences at $\theta_m = 0°$, 45°, and 90°, respectively. The value of the parameter α increases with θ_m due to the influence of the effect of decreasing the number of conducting paths on the change in the resistance. The calculated results given in Fig. 17 are in qualitative agreement with those obtained in the experimental study of the influence of the CNT alignment on the percolation conduction of CNT-doped polymers [119, 120].

The inset to Fig. 17a presents the dependences of the percolation probability P (i.e., probability of the occurrence of at least one conducting path) on the CNT alignment angle, calculated for various measurement directions θ_m. If the measurement direction does not coincide with that of the alignment, the percolation threshold is observed at higher values of θ_a than those specifying the coincidence of these directions. Thus, at $\theta_m = 0°$, the transition from $P = 1$ to $P = 0$ occurs for $\theta_a < 10°$, while at $\theta_m = 90°$, this transition proceeds already for $\theta_a < 40°$.

3.4 Role of the measurement direction

The influence of the angle between the direction of the conductivity measurement and the direction of CNT alignment in the composite is illustrated by Fig. 17b, where the dependences of the normalized composite resistance on the angle θ_m measured for various values of θ_a are shown. As is seen, in the absence of alignment ($\theta_a = 90°$), the resistance does not really depend on θ_m. However, even at a minor degree of alignment (such as $\theta_a = 72°$), an increasing dependence of the resistance on θ_m is observed, and at a higher degree of alignment (such as $\theta_a = 18°$), this dependence takes on a rather strong character. At high values of the measurement angle, the calculated dependences near the percolation threshold adhere to a power-like law:

$$\rho \sim (90 - \theta_m)^{-\beta}, \tag{19}$$

where β is the power index. This parameter, retrieved on the basis of calculations (see Fig. 17b), increases from $\beta = 0.65$ to $\beta = 2.9$ as θ_a decreases from 72° to 18°. This implies an influence of the alignment degree upon the character of the resistance dependence on the angle θ_m.

The sensitivity of the film resistance to the measurement direction is characterized by the parameter θ_m^{max}, defined as the maximum value of the angle θ_m, whose exceeding leads to the resistance of the ordered film becoming more than that for a fully disordered CNT film. In other words, the parameter θ_m^{max} represents the measure of disordering in the direction of measurement that is acceptable without increasing the film

resistance, in contrast to that of a fully disordered film. In accordance with this definition, the parameter θ_m^{max} is meaningful only for such alignment angles θ_a at which the film resistance at $\theta_m = 0°$ is lower compared with that for a fully disordered film. This corresponds to $\theta_a = 22°$ for the case presented in Fig. 17a. The dependence $\theta_m^{max}(\theta_a)$ is depicted in the inset to Fig. 17b. As is seen, the parameter θ_m^{max} increases as the alignment degree decreases. This implies a sensitivity of the results of measuring the ordered film resistance to the measurement direction.

3.5 Role of CNT parameters and the sample sizes

Calculations performed by the authors of Ref. [229] demonstrate that both the position of the resistance minimum and the values of fitting parameters α and β involved in Eqns (18) and (19) exhibit dependences on the sample size and CNT geometry. Figure 18a represents the dependences of the normalized resistance of composites on the alignment angle calculated at $\theta_m = 0°$ for three CNT lengths. As may be seen, increasing the value of l_{CNT} from 1.5 to 3.0 μm is accompanied by a decrease in the parameter θ_a^{min} from 55° to 30°, and the power index α from 2.9 to 1.6. The character of the dependences obtained is consistent with the longer CNTs forming more contacts with each other, so the number of conducting paths decreases with an increase in the alignment degree not so strongly as in the case of shorter CNTs. This explains the lowering of values of θ_a^{min} and α with a rise in l_{CNT}.

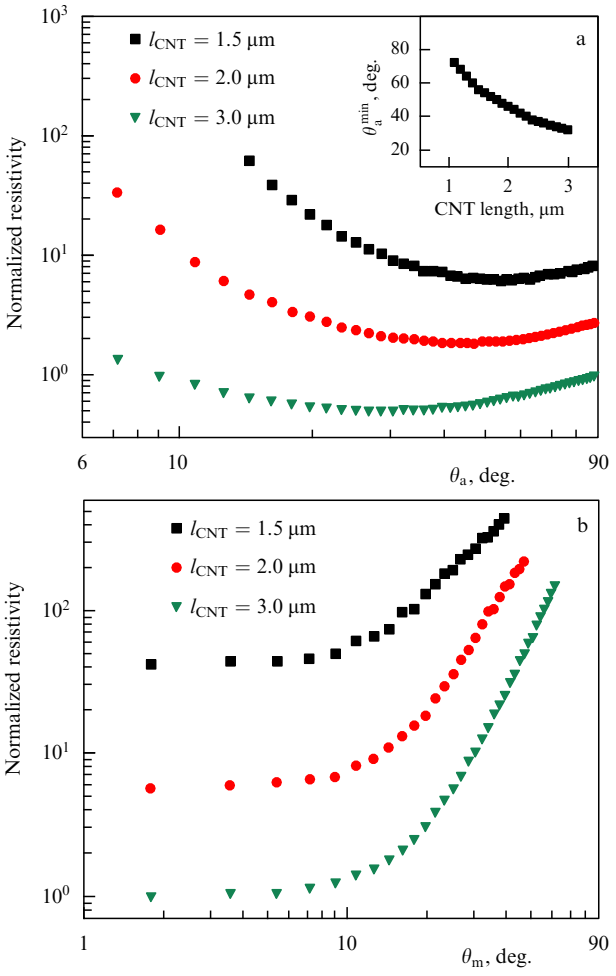

Figure 18. (a) Dependences of the normalized composite resistivity on the angle between the measurement direction and the CNT alignment angle, calculated for nanotubes of various lengths at $\theta_m = 0°$ (total alignment). The positions of the minimum resistivity $\theta_a^{min} = 55°$, 45°, and 30° and the values of the power index $\alpha = 2.9$, 2.9, and 1.6 correspond to $l_{CNT} = 1.5$, 2, and 3 μm, respectively. The inset presents the dependence of θ_a^{min} on the CNT length. (b) Dependences of the normalized composite resistivity on the angle between the measurement direction and the CNT alignment angle, calculated for nanotubes of various length at $\theta_a = 18°$ [229].

The dependence of θ_a^{min} on the nanotube length is shown in the inset to Fig. 18a. It is seen that the rate of changing θ_a^{min} increases as the CNT shortens. A film consisting of shorter CNTs is closer to the percolation threshold; therefore, even a minor increase in the alignment degree can result in the removal of a considerable number of conducting paths. For this reason, the value of the parameter θ_a^{min} approaches 90° in the case of very short CNTs.

Figure 18b plots the dependences of the normalized resistance of composites on the angle θ_m calculated at $\theta_a = 18°$ for three CNT lengths l. The value of $\theta_a = 18°$ was chosen for calculations, because the influence of θ_m on the resistance is most prominent at a high alignment degree (see Fig. 17b). At lower values of θ_a, the percolation threshold is not reached even in the case of low θ_m. The power index β involved in Eqn (19) and evaluated on the basis of the calculated results of Fig. 18b increases with the nanotube length ($\beta = 1.7$, 2.9, and 3.75 for $l = 1.5$, 2, and 3 μm, respectively). This dependence differs qualitatively from that evaluated from the data in Fig. 18a. Since the number of conducting paths is higher from the outset for films with longer CNTs, a change in the direction of measuring the conductivity with respect to the alignment direction decreases the number of conducting paths to a higher degree (and therefore increases the resistivity) in the case of films with longer CNTs. This is reflected in the enhancement of the parameter β.

The dependences of the normalized film resistivity on the CNT alignment angle, calculated for films of various CNT densities at $\theta_m = 0°$ [229], are exhibited in Fig. 19a. As can be seen, the influence of CNT density on the values of parameters θ_a^{min} and α is not as prominent as the influence of the nanotube length. The dependence of the percolation probability P on the alignment angle, calculated for various values of CNT density and presented in the inset to Fig. 19a, indicates a notable dependence of the percolation threshold position on the CNT density. Thus, at $n = 1$ μm^{-2}, the transition from $P = 1$ to $P = 0$ occurs for $\theta_a \lesssim 30°$, while at $n = 3$ μm^{-2} this transition begins for $\theta_a \lesssim 5°$.

The dependences of the normalized film resistivity on the CNT alignment angle, calculated for films of various CNT densities at $\theta_a = 18°$ [229], are shown in Fig. 19b. The magnitudes of the parameter $\theta_a^{min} \sim 50°$, 45°, 45°, and 40° and the power index $\alpha = 2.8$, 3.0, 2.9, and 2.9 correspond to the values of $n = 1$, 1.5, 2, and 3 μm^{-2}, respectively. The influence of the CNT density on the power index β is less prominent than the above-noted influence of the CNT length. The dependences of the percolation probability P on the measurement angle, calculated for the same values of the CNT density, are shown in the inset. As is seen, the influence of the CNT density on the percolation threshold position is quite essential. Thus, in the case of $n = 1$ μm^{-2} the transition from $P = 1$ to $P = 0$ occurs for $\theta_m \gtrsim 7°$, while for $n = 3$ μm^{-2} this transition begins for $\theta_m \gtrsim 50°$.

Dependences of the resistivity of CNT films of various sizes l on the alignment angle were calculated in Ref. [229]

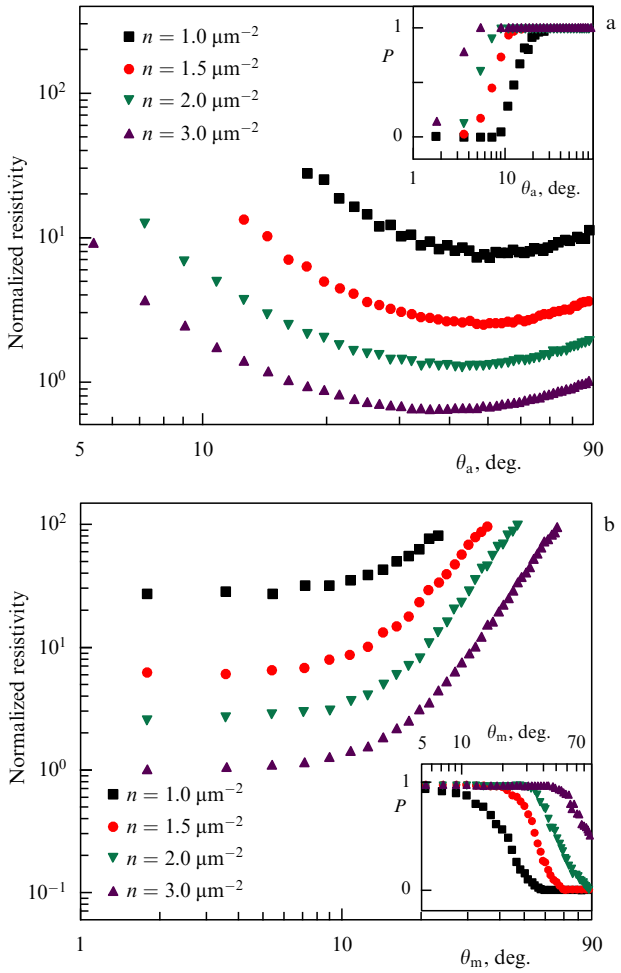

Figure 19. (a) Dependences of the normalized composite resistivity on the CNT alignment angle, calculated for films of different densities at $\theta_m = 0°$. The positions of the parameter $\theta_a^{min} \sim 50°, 45°, 45°$, and 40° and the values of the power index $\alpha = 2.8$, 3.0, 2.9, and 2.9 correspond to $n = 1$, 1.5, 2, and 3 μm^{-2}, respectively. (b) The dependence of the percolation probability on the alignment angle θ_a, calculated for films of different densities at $\theta_a = 18°$. The dependence of the percolation probability on θ_m calculated for the same n values is plotted in the inset [229].

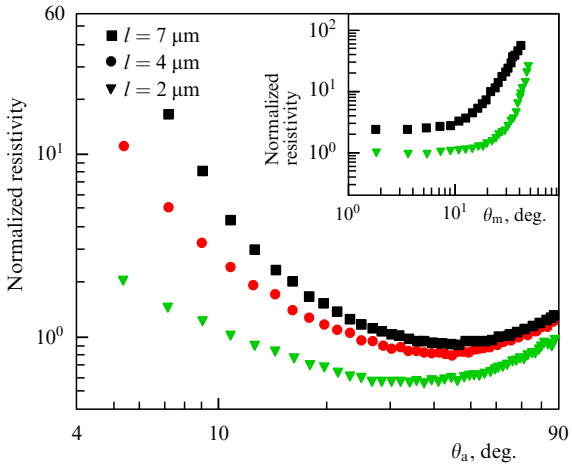

Figure 20. Dependences of the normalized composite resistivity on the CNT alignment angle, calculated for samples of different lengths at $\theta_m = 0$. The inset shows the dependences of the normalized resistivity on the CNT measurement angle, calculated for samples $l = 2$ and 7 μm in length at $\theta_a = 18°$ [229].

with a view to establish the influence of the sample size on the percolation behavior of composites. Results of these calculations performed at $\theta_m = 0°$ are given in Fig. 20. The magnitudes of the parameter $\theta_a^{min} = 35°$, 45°, and 45° and the power index $\alpha = 0.9$, 2.2, and 2.9 correspond to the values of $l = 2$, 4, and 7 μm, respectively. In shorter samples, the circuit can be closed by one nanotube. The longer the sample, the greater the number of nanotubes necessary to close the circuit, and this quantity increases as the alignment degree increases. This fact explains the increasing dependence of the parameter α on the sample longitudinal size.

The character of the θ_a^{min} dependence on the longitudinal sample size is explained in a similar manner. The dependences of the normalized resistivity on the measurement angle, calculated for the longitudinal sample sizes $l = 2$ and 7 μm at $\theta_a = 18°$, are shown in the inset. The relevant values of the power index β are 4.9 and 2.9. As in the above-considered example, even a minor increase in the measurement angle in the case of short samples results in elimination of a notable number of percolation paths, which causes a stronger dependence of the conductivity on the measurement angle for shorter samples. Therefore, the shorter the sample, the higher the power index β.

3.6 Composite in an alternating field

The main peculiarity of the AC electrical conduction in CNT-doped composites relates to the displacement current, due to which the formation of percolation conducting paths is not required to provide nonzero conduction. In this case, the percolation threshold position depends not only on the conducting filler loading but also on the frequency. In principle, the percolation threshold notion at quite high frequencies is entirely absent, because the main contribution to the conduction is due to the displacement current that occurs at any filler loading. The behavior of CNT-doped composites in an alternating field was simulated by the authors of Ref. [232], who applied the inverse matrix method [233, 234] to calculate the complex impedance.

In accordance with this approach, CNTs form a ramified electrical network whose total resistance is evaluated through a numerical method on the basis of the standard Kirchhoff laws. Therewith, two limiting case are considered, for one of which (NT-limited case) the total resistance of the network is determined by the resistance of individual CNTs involved in its structure, while for the other one (CR-limited case) the total resistance of the network is determined by the magnitude of the contact resistance between neighboring nanotubes.

A composite polymer/CNT was modelled by a 2D film for which the frequency dependence of the complex permittivity and the spatial distribution of the current over the material were calculated. Nanotubes l in length are characterized by the resistance R. The specific capacity accounted by the unit area is C. According to the procedure developed in Refs [233, 234], the composite is represented in the form of an RC circuit, so that the resistance $r = R/N$ is ascribed to each part of a CNT between the contacts, where N is the total number of contacts inherent in the nanotube under consideration, which depends on the alignment degree. The angle between the CNT axis and the vertical axis corresponding to the electrical field direction is θ. The degree of alignment of CNTs in a composite is determined by the maximum orientation angle

(cutoff angle) θ_μ. The homogeneous distribution of CNTs by angles θ within the interval

$$-\theta_\mu \leqslant \theta \leqslant \theta_\mu \tag{20}$$

is assumed. The CNT concentration n is defined as the number of nanotubes positioned in a square l^2 in area. It is believed that the nanotube centers are spread in an arbitrary manner inside this square. The intertube contact resistance is set to R_c.

The electrical properties of a material in an alternating electric field are characterized by the complex conductivity Y, which is expressed through the effective conductivity tensor σ^{eff} and the effective capacity tensor C^{eff} by the standard relationship

$$Y = \sigma^{\text{eff}} + \mathrm{i}\omega C^{\text{eff}}, \tag{21}$$

where ω is the AC frequency. The complex conductivity is expressed through the frequency-dependent complex dielectric constant $\varepsilon(\omega)$ by the relation $Y = |Y| \exp(\mathrm{i}\Phi)$, where $\mathrm{Im}\,(\varepsilon)/\mathrm{Re}\,(\varepsilon) = 1/\tan\Phi$.

In numerical calculations, the sample size L was set to $L = 10l$, and the mesh size was set to $\Delta = L/20$. The calculations were performed for three values of CNT concentration in the composite: $nl^2 = 6, 7$, and 10. The finite mesh size effect manifests itself as the concentration decreases, approaching the percolation threshold, which results in an overestimation of the conductivity. As Δ decreases, the finite mesh size effect weakens and becomes negligible at $\Delta = L/30$. However, the mesh size was chosen to be $\Delta = L/10$ in order to shorten the computational time. Calculations imply that at such a mesh size the error caused by the finite mesh size effect does not exceed 10%. Each point was obtained as a result of averaging over 100 runs for various samples. The magnitude of $1/R$ or $1/R_c$ in the CR-limited case was accepted as the effective conductance σ^{eff}. As the effective capacitance, the C value was taken. The ω frequency was expressed in units of $1/RC$.

Figure 21 demonstrates the dependences of the vertical (longitudinal) σ_v^{eff} (a) and horizontal (transverse) σ_h^{eff} (b) components of the effective conductivity on the CNT content, calculated for the NT-limited case at various values of θ_μ [232]. As is evident, an increase in the CNT alignment degree is accompanied by an increase in the difference between the vertical and horizontal conductivities. The relevant positions of the percolation threshold, calculated within the framework of the continuous stick model [188, 189,

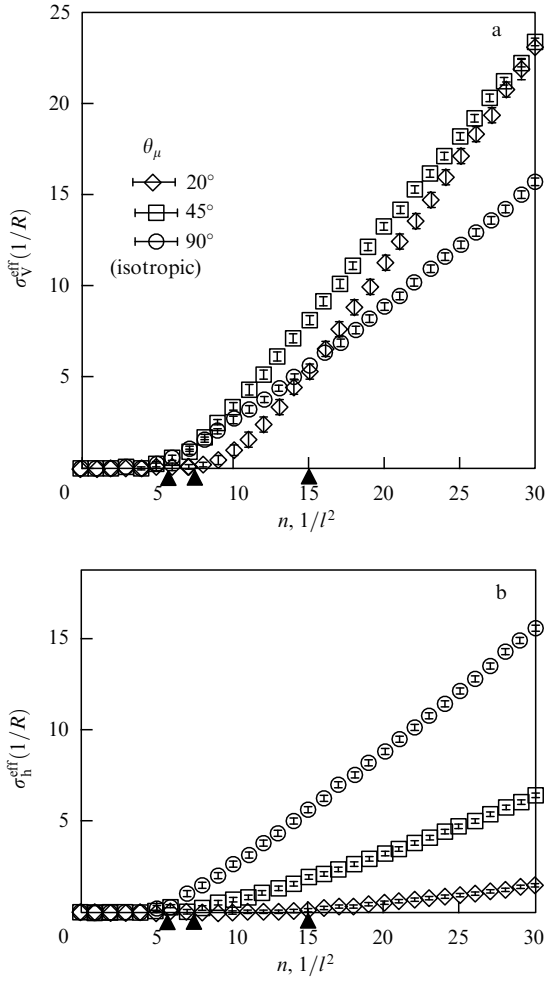

Figure 21. Dependences of the vertical σ_v^{eff} (a) and horizontal σ_h^{eff} (b) components of the effective conductivity on the CNT concentration, calculated for different values of θ_μ [69]. The percolation threshold positions calculated within the framework of the continuous rod model are marked by the arrows [188, 189, 227]. The concentration is expressed in units of $1/l^2$, and the conductivity in $1/R$.

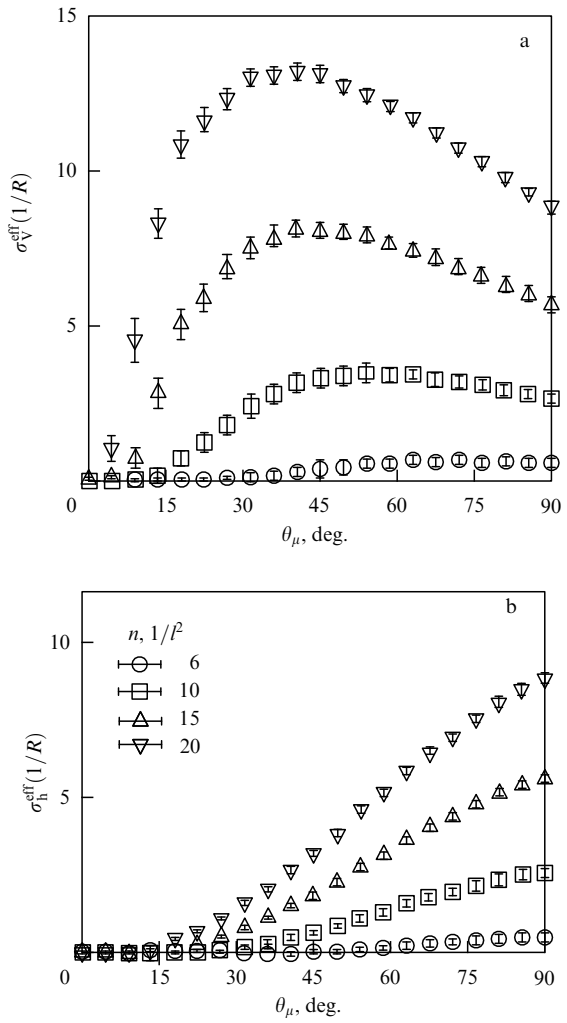

Figure 22. Dependences of the vertical σ_v^{eff} (a) and horizontal σ_h^{eff} (b) components of the effective conductivity on the alignment angle, calculated for various values of CNT loading n [232].

227], are marked by the arrows. As indicated by the calculated data, decreasing the θ_μ value results in an increase in the percolation threshold position. It should be noted that the percolation threshold positions depicted in Fig. 21 coincide within a 2% accuracy with the results of more comprehensive calculations [235] performed with the usage of a finite element method.

Components of the DC composite effective conductivity vs alignment angle are presented in Fig. 22. While the horizontal component of the conductance increases monotonically with θ_μ, the vertical one reaches the maximum value at $\theta_\mu^{\max}$, which decreases with increasing the CNT content n. Such a behavior of the conductance has been considered above and observed experimentally [119].

Figure 23 exhibits the frequency dependences of the effective conductivity, effective capacity, complex permittivity angle, and dielectric loss factor, calculated for the isotropic case at various CNT contents. When the CNT loading exceeds the percolation threshold in a low frequency region, $\omega \ll 1/RC$, the effective conductance does not depend on the frequency, while in a high frequency region the monotone rise of the conductance with the frequency is observed. At a filler loading below the percolation threshold, lowering of the frequency is accompanied by a decrease in the conductance to the zero level. As to the effective capacitance, its value demonstrates a monotonic decrease with the rise in the frequency independent of CNT loading; however, this parameter saturates in the high-frequency region.

The argument Φ of the complex permittivity increases monotonically from 0 to $\pi/2$ for conducting composites, while for nonconducting composites its value is close to $\pi/2$ at all frequencies excluding the vicinity of $1/RC$. The dielectric loss factor for conducting composites decreases monotonically with the rise in the frequency, while for nonconducting composites it shows a small peak at a frequency close to $1/RC$. Such a behavior is in agreement with the experimental results [172].

The concentration dependences of the composite conductivity calculated for NT-limited composite resistivity are compared in Fig. 24 with those for the CR-limited

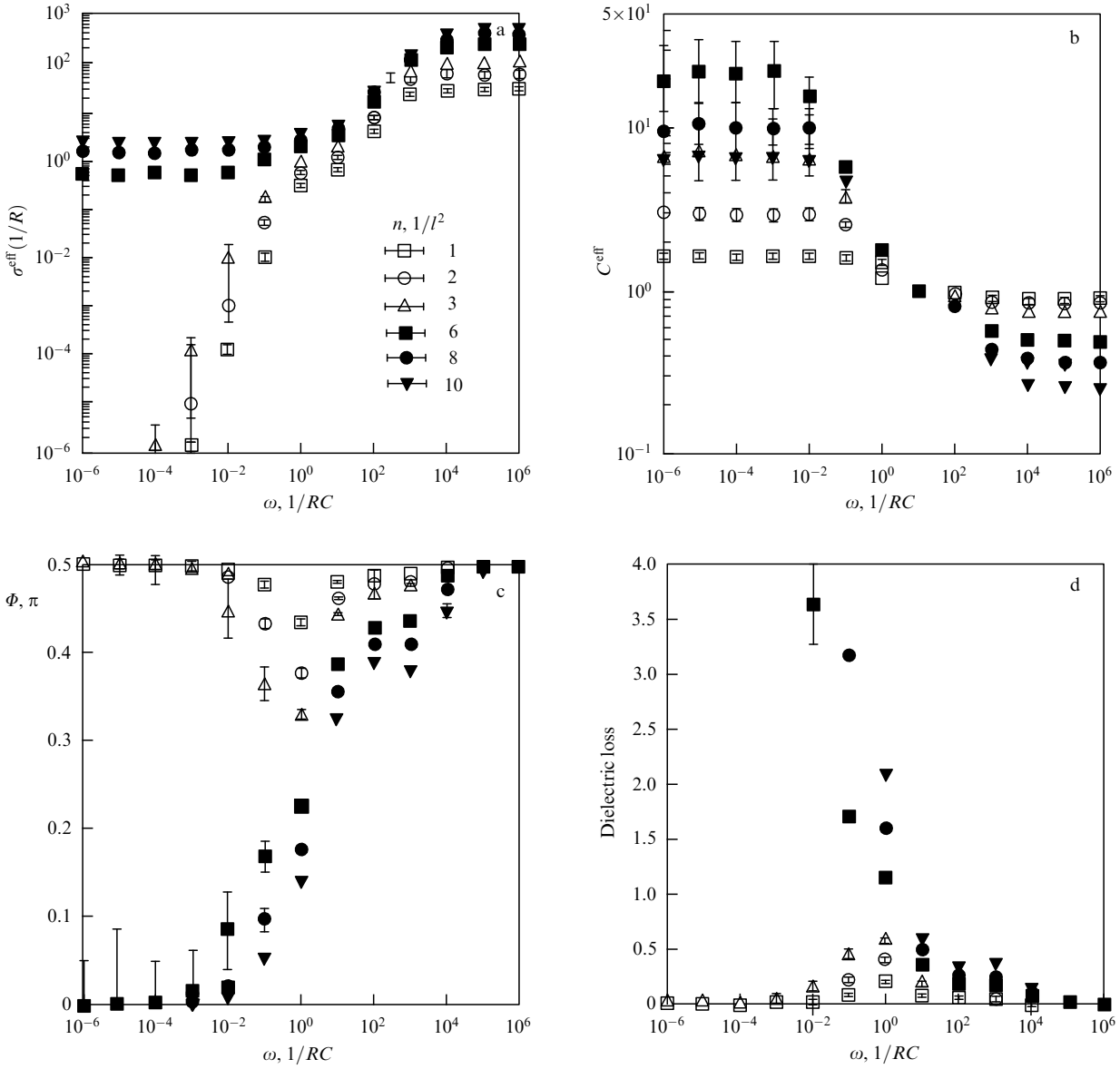

Figure 23. Frequency dependences of the effective conductivity σ^{eff} (a), effective capacity C^{eff} (b), argument of the comlex dielectric constant Φ^{eff} (c), and the dielectric loss factor $\text{Im}\,(\varepsilon^{\text{eff}})/\text{Re}\,(\varepsilon^{\text{eff}}) = 1/\tan(\Phi^{\text{eff}})$ (d), calculated at different CNT loadings for an isotropic case [232].

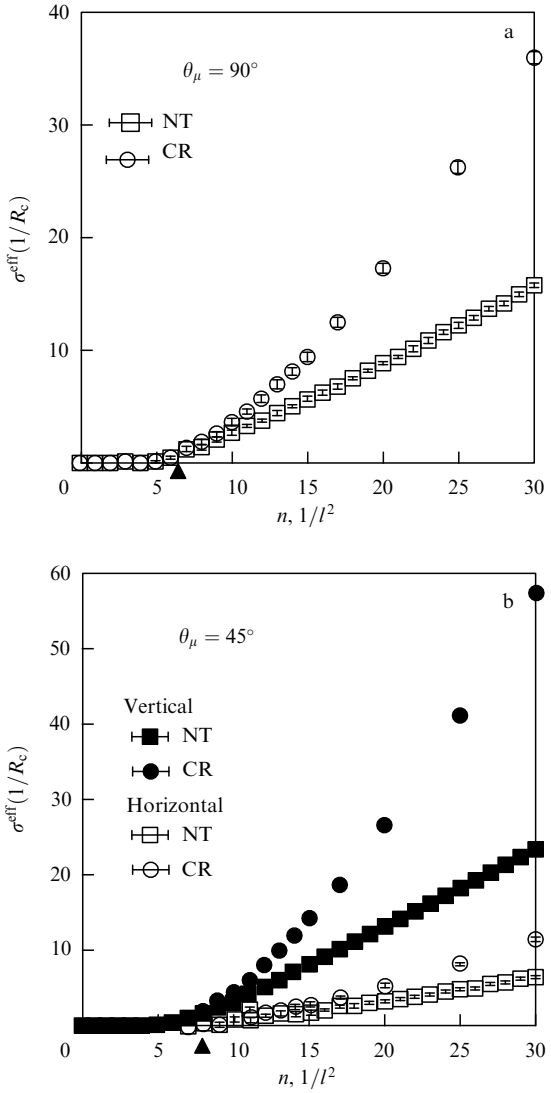

Figure 24. Comparison of concentration dependences of electrical conductivities for composites with nanotube-resistance-limited (NT) and contact-resistance-limited (CR) resistivities. These dependences have been calculated for an isotropic case, $\theta_\mu = 90°$ (a), and for the case of CNT alignment with $\theta_\mu = 45°$ (b). The percolation threshold positions calculated within the framework of the continuous rod model are marked by the arrows [232].

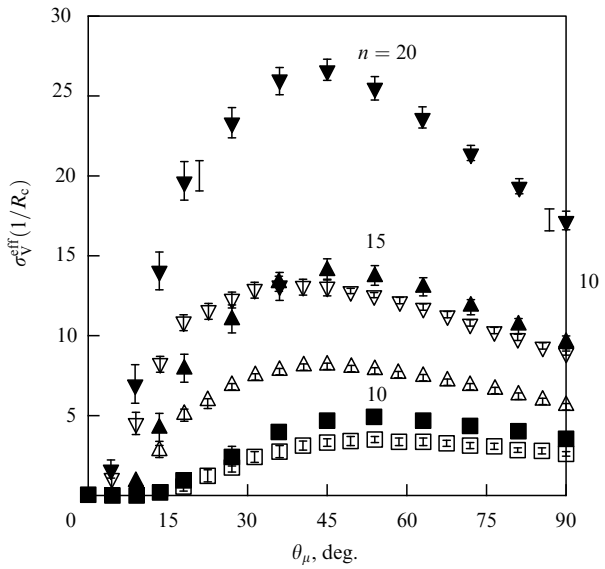

Figure 25. Comparison of the dependences of the vertical (longitudinal) conductivity σ_v^{eff} on the alignment degree calculated for composites with CR-limited (dark symbols) and NT-limited conductances (light symbols) at various CNT loadings [232].

case. CR-limited conduction demonstrates a sharp concentration dependence at a filler loading exceeding $2n_c$ (n_c is the percolation threshold position) both in the case of an isotropic conductor and in the case of CNT alignment. At the same time, the behavior of both types of conductors is similar in the region below $2n_c$. The dependences of the vertical conductivities on the alignment angle θ_μ were calculated for the purpose of establishing the influence of the alignment on the effective composite conductance. The dependences of the vertical conductivity of samples on the alignment degree, calculated for the CR- and NT-limited cases, are compared in Fig. 25. As is evident, the CR-limited conductance is characterized in this case by a smoother lowering when exceeding the peak value $\theta_\mu^{\max}$ of the angle than in the case of NT-limited conductance.

The physical origin of the nonmonotone behavior of the CNT alignment dependence of the vertical (longitudinal) conductance component has been considered above (see text in Section 3.3 to Fig. 17). At the same time, the horizontal (transverse) conductance component increases in a monotone manner as the angle θ_μ increases, i.e., the alignment degree decreases. Therewith, the growth of the angle θ_μ is accompanied by an increase in the number of percolation paths in parallel with a decrease in the degree of their meandering. Both these factors promote an increase in the horizontal conductance.

Calculations indicate that the dependences of the composite conductance on CNT loading in the case of CR- and NT-limited conduction mechanisms are somewhat different. This can be seen from a comparison of data presented in Fig. 26. The power index t characterizing these dependences has the same value for both vertical and horizontal conductance components; however, it depends on the conduction mechanism. In the case of CR-limited conduction upon CNT loading above $2n_c$, this parameter is $t \approx 1.3$. This value corresponds to the classical 2D percolation model [7–10]. However, in the case of CN-limited conduction, this value declines to ≈ 1.0. Such a distinction contradicts the conclusion of the classical study [227]. This distinction can be explained through the argument [236], in accordance with which upon redoubling the number of intersections of nanotubes at a parallel connection, the conductance increases twofold in the NT-limited case and fourfold in the CR-limited case. This results in a less strong concentration dependence of the conductance ($t \approx 1.0$) in the CN-limited case.

An important problem arising when simulating the electrical properties of CNT-doped nanocomposites relates to establishing the mechanism of current passage through the contacts between adjacent nanotubes. The authors of many known studies use an arbitrary assumption about the value of the contact resistance instead of the comprehensive solution to this problem. Reference [237] whose authors paid special attention to the contact problem can be considered an exception. In this work, the percolation conduction of CNT-doped composites is simulated making use of the standard Monte Carlo method, in accordance with which nanotubes are assumed to be spread in a random manner inside a cube of

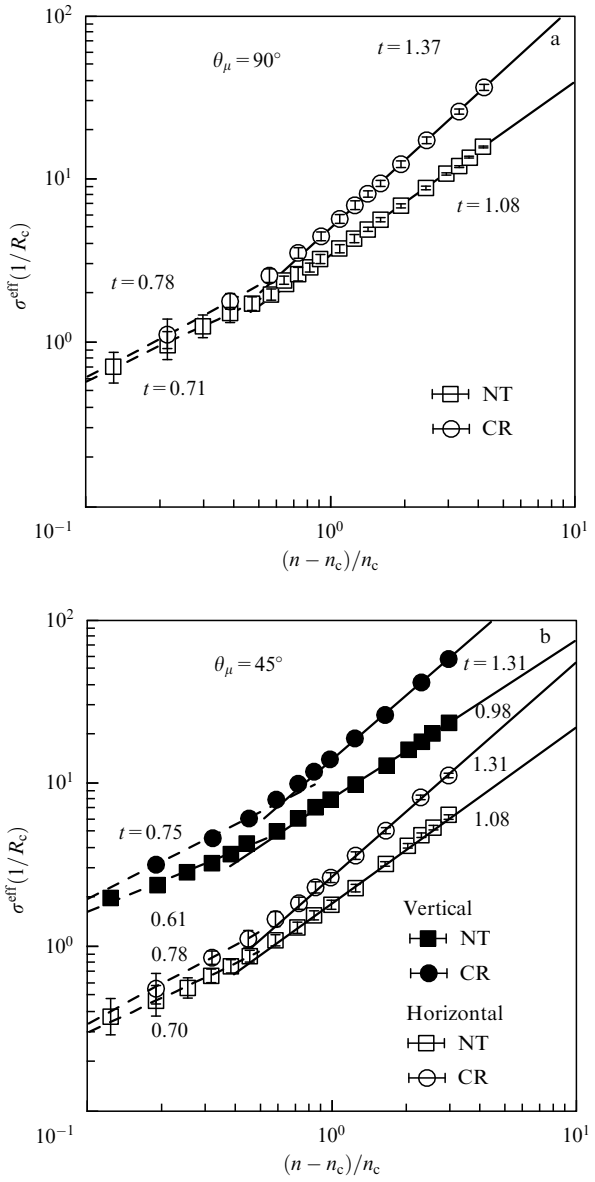

Figure 26. Comparison of the dependences of composite conductivity on the relative CNT loading, calculated for NT- and CR-limited charge transport mechanisms: (a) isotropic composite ($\theta_\mu = 90°$); (b) composite with the alignment angle of $\theta_\mu = 45°$. The values of the power index t providing the best fitting for these dependences are marked alongside the curves [232].

unit size filled with a polymer matrix. An allowance for the deviation of the CNT structure from the rectilinear one is also made.

According to the approach developed, the total electrical resistance $R_{\rm tot}$ of the percolation network formed by nanotubes is fully determined by nanotube's ($R_{\rm t}$) and contact ($R_{\rm c}$) resistances:

$$R_{\rm tot} = R_{\rm t} + n_{\rm c} R_{\rm c} \,, \tag{22}$$

where $n_{\rm c}$ is the number of contacts. The equivalent electrical scheme of the nanocomposite is represented through the CNT resistance $R_{\rm tot}$ and polymer matrix resistance $R_{\rm polym}$ put in parallel, so that the effective resistance of the nanocomposite is expressed as

$$\frac{1}{R_{\rm com}} = \frac{1}{R_{\rm tot}} + \frac{1}{R_{\rm polym}} \,. \tag{23}$$

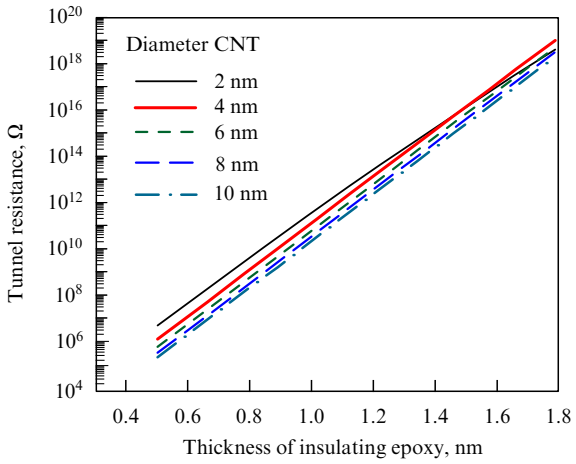

Figure 27. Dependence of the tunnel resistance on the thickness of the intertube epoxy resin layer, calculated for CNTs of different diameters by the authors of Ref. [239] on the basis of the approach developed in Ref. [238].

Usually, one has $R_{\rm polym} \gg R_{\rm tot}$, so that $R_{\rm com} \sim R_{\rm tot}$. The effective electrical conductivity σ of the sample is also expressed in a standard manner through its resistance and dimensions:

$$\sigma = \frac{l_{\rm com}}{R_{\rm com} A_{\rm com}} \,, \tag{24}$$

where $l_{\rm com}$ and $A_{\rm com}$ are the length and cross section area of the sample.

3.7 Modeling contact phenomena

A comparison of the results of measuring the conductance of CNT-doped composites with calculated data obtained in the framework of the percolation theory indicates that the absolute value of the conductance is several orders of magnitude lower than that obtained supposing a good intertube electrical contact. In real situations, as was noted above, the contact resistance as a rule exceeds notably a typical nanotube's resistance. For this reason, the absolute value of the composite conductance near the percolation threshold is virtually completely determined by the contact resistance. In this connection, the main effects determining the contact resistance of intersecting nanotubes will be considered below.

The simplest approach to describe the intertube surface contact resistance is based on the model of electron tunneling through a potential barrier. Detailed calculations of the contact resistance with the aid of this model were performed in Ref. [238] within the framework of the perturbation theory. According to these calculations, the resistance of the contact between flat conductors separated by a dielectric layer is expressed through the height of the potential barrier, applied voltage, area of the contact, and permittivity of the dielectric. Figure 27 presents the dependences of the intertube contact resistance on the thickness of the epoxy resin layer separating the nanotubes, as calculated in Ref. [239] on the basis of the above-described approach [238]. The exponential dependence of the contact resistance on the thickness of an isolating layer is a characteristic feature of the tunnel conduction mechanism. Some departure from this dependence observable at large thicknesses of the dielectric layer is caused by the influence of the applied voltage on the potential barrier parameters. For

comparison, notice that the typical conductivity of nanotubes amounts to about 10^6 S m^{-1}, so that the resistance of a nanotube several microns in length and about 1 nm in radius amounts to about 10^6 Ω. Therefore, the contact resistance limits the nanocomposite conductance if the thickness of the dielectric layer exceeds 0.5 nm.

The model approach in Ref. [238] has resulted in the following approximate dependence of the barrier tunneling probability on the thickness of the dielectric layer d [240]:

$$T \propto \exp\left(-\frac{d-D}{d_{\text{tun}}}\right), \tag{25}$$

where $d_{\text{tun}} = \hbar/\sqrt{8m_e\Delta E}$ is the characteristic tunneling length, ΔE is the height of the barrier between CNTs and the polymer, d is the minimum distance between the nanotube axes, and D is the nanotube diameter. This formula permits easily estimating that the tunneling probability for $\Delta E = 1$ eV and $d - D = 20$ Å is less than 10^{-10}, and the resulting contact resistance exceeds 10^{13} Ω. Such a high contact resistance is virtually equivalent to the absence of intertube electrical contact; therefore, the nanotubes separated by a polymer layer > 20 Å thick can be considered to be electrically isolated.

If the nanocomposite conductance is determined by the intertube contact resistance, the statistical spread of contact resistances in the material plays an essential role. According to the above-mentioned semiclassical tunneling model, this distribution relates to the distribution of the intertube distances in contact points. The conductance of CNT-doped nanocomposites, taking into account the statistical spread of intertube contacts, is usually calculated using the Monte Carlo method. In doing so, most authors assume that the intertube distances are spread homogeneously within the interval ($d_{\min}$, $d_{\max}$), where the lower limit stands for the van der Waals distance between pure nanotubes, and the upper one is determined by the maximum acceptable resistance.

However, the distribution of the intertube distances in contact points is not homogeneous in reality, as was noted by Grimaldi et al. [241]. Specifically, there is some fraction of contacts not containing polymer molecules. In this case, the average intertube distance is close to the equilibrium van der Waals distance between graphene layers: 3.4 Å. For the second group of contacts, containing matrix molecules, the minimum intertube distance is also limited by the van der Waals interaction between the intercalated molecules and the nanotubes, thus amounting to about 6 Å. Therefore, the distribution function for the distances between the filler particles and, correspondingly, the contact resistance distribution function should possess two peaks relating to contacts containing and not containing intercalated polymer molecules. Therewith, since the minimum intertube distance cannot be less than 6 Å in the presence of polymer molecules within the contact, the value of the contact resistance substantially exceeds that of a nanotube.

However, the contact resistance can be rather high even in the absence of a polymer layer between nanotubes in the contact point. To analyze the physical origin of such an effect, it is appropriate to consider the resistance of model intertube nanocontacts and its dependence on contact parameters. Taking into account quantum mechanical effects, the contact resistance can be conveniently described through the Landauer–Buttiker formalism developed for modeling the charge transport. According to this formalism, the contact resistance can be represented as follows:

$$R_c = \frac{1}{G_0}\frac{1}{MT}, \tag{26}$$

where M is the number of conducting paths, T is the transmission coefficient, and $G_0 = 1/12.9$ kΩ is the ballistic conductance quantum. The transmission coefficient can be evaluated at the atomic level applying the Green's function method.

The simplest configuration of the intertube contact corresponds to the case of parallel arrangement of nanotubes, which is characterized by the intertube distance and the length of the overlapping region. Atomic calculations of the contact resistance have stated that the conductance of the contact between parallel nanotubes depends weakly on a tube's size. However, this parameter depends critically (in a nonmonotonic manner) on the overlapping region length and the nanotube chirality [242]. The dependence of the conductance on the overlapping region length is characterized by oscillations relating to both the periodic structure of nanotubes and the Fermi wavelength of the electron and the relevant quantum interference in the contact region. For contacting nanotubes possessing a similar chirality (for example, armchair/armchair or zigzag/zigzag), the contact conductance can reach $4G_0$ (the conductance of an ideal nanotube) at a contact length of about 10 nm (see Fig. 28). However, the contact conductance is about an order of magnitude lower at the overlapping region length of about 1 nm.

Calculations indicate the occurrence of minima in the dependence of the conductance on the electron energy, which are caused by the existence of quasibound states in the contact region, promoting the resonance scattering of charge carriers. Computations [242] performed for contacting single-walled nanotubes of different chiralities indicate that the intertube contact conductance is considerably lower in this case (on the order of $0.01G_0$) even at the overlapping region length of 10 nm. This is caused by the violation of the electron momentum conservation law or the charge transport between the nanotubes having a different chirality and therefore possessing a different electron structure. Such a difference essentially lowers the electron tunneling probability between different nanotubes.

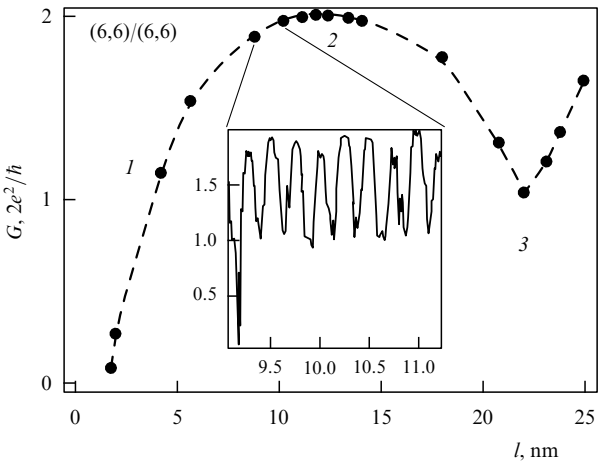

Figure 28. Dependence of the conductance envelope for two parallel (6,6) nanotubes on the length of the overlapping region [242].

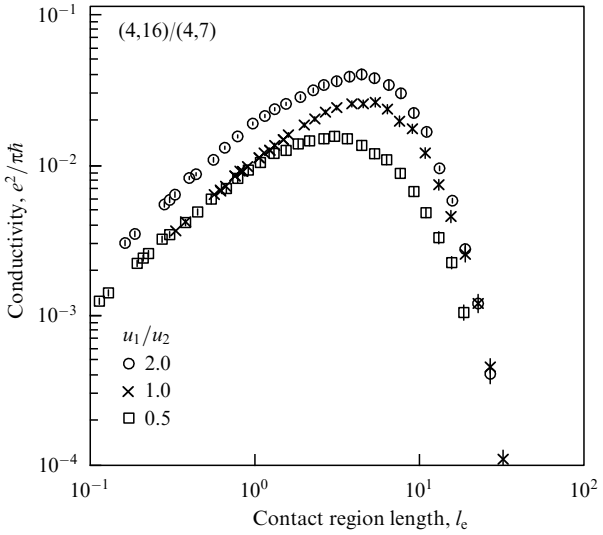

Figure 29. Dependence of the interlayer conductance on the length of the contact between nanotubes with chirality indices (4,16)/(4,7) [244]. Contact region length is expressed in units of electron scattering length l_e, and conductivity in $e^2/\pi\hbar$; u_1/u_2 stands for the ratio between electron mean free paths, where u_1 deals with an outer tube, and u_2 with an inner tube.

In other words, the electron conductance of the contact between defectless nanotubes with different chiralities is relatively low due to a disparity between the longitudinal components of the electron wave vector in adjacent nanotubes. In this case, the parallel nanotubes behave like independent conductors. The results of calculations [243] imply that the occurrence of structural defects in nanotubes (such as vacancies) can promote electron tunneling between non-commensurate nanotubes. Thus, a single vacancy in the region of contact between CNTs with a chirality of (10,10) and (18,0) and with an overlapping region about 10 nm in length raises the conductance to $0.01G_0$. In the presence of several noncoherent defects, the conductance is proportional to the number of defects. The maximum conductance is reached at the overlapping region length which is on the order of the electron scattering length l_e in a defective nanotube [244]; however, the maximum conductance is still much lower than the conductance quantum G_0 (Fig. 29).

The dependence of the contact conductance for intersecting metal nanotubes on the contact geometry has been studied in Refs [245, 246] with the use of the Landauer–Buttiker formalism and the Hamiltonian of a tight binding method. The value of the conductance is dictated by the intertube distance and depends in a nonmonotonic manner on the angle between the intersecting nanotubes, which determines the contact area (Fig. 30). It was found that the dependence of the contact conductance on the intersection angle usually exhibits three peaks. These peaks correspond to the angle for which the consistency between the nanotube's structures in the contact point is maximum. Therefore, the key parameters determining the contact conductance are the nanotube chirality and the intersection angle; in most cases, however, the maximum conductance is considerably less than the conductance quantum G_0.

The mechanism of electron transport between nanotubes of different chiralities has been studied in detail in Ref. [247] with the use of the Landauer–Buttiker formalism. It has been revealed that an elongated weak potential providing electron

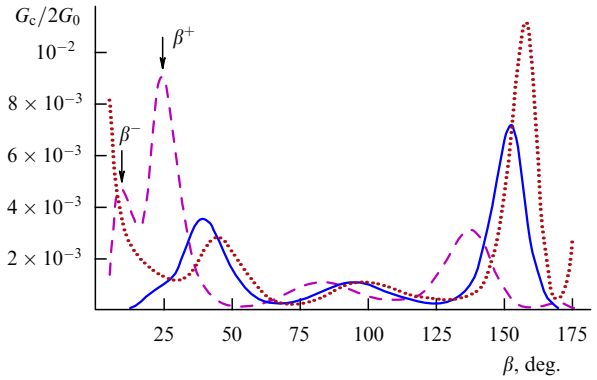

Figure 30. Dependence of the contact conductance for intersecting nanotubes on the intersection angle [246].

scattering with a change in the momentum is sufficient for an enhancement of the transmission coefficient. Such a potential can be formed by adsorbed molecules, polymer chains, and phonons propagating in nanotubes. Therefore, this investigation predicts that the presence of polymer molecules in the contact region can facilitate electron transport through contacts in CNT-doped nanocomposites.

The dependence of the contact resistance between nanotubes connected by the ends and separated by a polymer layer on the intertube distance has been studied in Ref. [248] taking advantage of the atomic modeling method. The polymer structure at a fixed arrangement of nanotubes was calculated by the molecular dynamics method with the utilization of empirical potentials. The contact resistance for a given atomic polymer structure was calculated on the basis of the density functional theory (DFTB) with the use of the Green's function and tight binding Hamiltonian. In doing so, the contact resistance was evaluated as a result of averaging over many configurations found from the molecular dynamic trajectory. Therefore, this approach permits taking into account the influence of thermal fluctuations on the composite conductance.

Calculations have shown (see Fig. 31) that the dependences of the contact resistance on the intertube distance at small distances (< 6 Å) and at large distances (> 6 Å) are different, which may be attributable to the absence of polymer molecules between nanotubes at small intertube

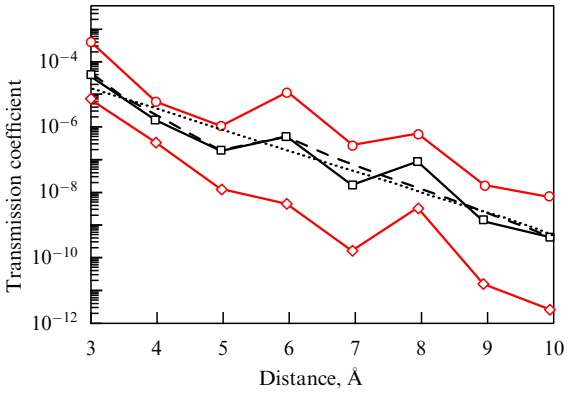

Figure 31. Dependences of the mean (□), minimum (◇), and maximum (○) transmission coefficients through the CNT contact on the intertube distance calculated for nanotubes contacting in a polymer matrix [248]. Dashed and dotted lines depict the calculated results for simplified models.

distances. Indeed, as is seen from the picture, the transmission coefficient at large distances (> 6 Å) can exceed that at small distances, which can be explained, on the one hand, by the lowering of the potential barrier for tunneling at the intercalation of a polymer molecule and, on the other hand, by an enhancement of the electron tunneling probability under the action of the perturbing potential of the intercalated molecule. At small intertube distances, there is direct tunneling of electrons through a vacuum with the barrier about 5 eV in height, while the existence of a polymer layer between the nanotubes results in lowering the barrier height to about 3 eV.

The calculated results obtained in Ref. [248] are in qualitative agreement with the results of atomistic simulations of the contact resistance for two nanotubes intersecting at a right angle. These simulations imply that the penetration of one polymer layer between filler particles causes a decrease in the contact resistance almost to the intertube resistance at the van der Waals distance (3.4 Å). Therefore, the dependence of the contact resistance on the distance between filler particles in a polymer matrix is not a monotonically increasing function having an intermediate minimum at the penetration of the first molecular polymer layer, which occurs at the intertube distance of about 6 Å.

Lowering of the contact resistance and improving the conductance can be reached using nanotube decoration with transition metal atoms [249]. Atomistic calculations of the intertube contact conductance, performed with application of the Green's function method, have shown that the hybridization of d-orbitals of a transition metal atom with π-orbitals of carbon atoms belonging to CNTs offers an opportunity to enhance considerably the electron tunneling probability and to reach the conductance of $0.8G_0$. The best results for the contact conductance were obtained for Ti, V, and Cr atoms. It has been proposed to dope the carbon nanotubes with nitrogen that is bound firmly with transition metal atoms, enhancing the adsorption energy for nanotubes. The experimental findings [250] have clearly demonstrated that the decoration of CNTs with metal clusters results in an increase in the nanocomposite conductivity to magnitudes on the order of 1 S cm^{-1}.

Experimental values of the contact resistance in CNT-doped composites are usually evaluated by comparing the calculation magnitudes of the composite conductivity obtained by the Monte Carlo method with the relevant experimental data. Thus, the conductivity of a composite based on an epoxy matrix doped with single-walled and multiwalled nanotubes, measured in Ref. [251], fell in the range 10^{-8} to 10^{-9} S cm^{-1}, which resulted in the estimate of the contact tunneling resistance of $10^{12}-10^{13}$ Ω. This value of the contact resistance corresponds to a polymer layer about 1.0–1.1 nm thick. A similar estimation of the contact resistance (10^{13} Ω) was made in Ref. [226], being guided by a comparison between the results of 3D Monte Carlo simulations and the relevant experimental data [252]. An estimation of the tunneling resistance between aligned nanotubes ($10^{7}-10^{10}$ Ω) was performed in Refs [253, 254] on the basis of measurements of the longitudinal conductivity of thin-film nanocomposites doped with vertically aligned nanotubes. This estimate corresponds to a polymer layer thickness of about 0.6–1.0 nm. Therefore, a comparison of simulation results with experimental data confirms indirectly the existence of a thin polymer layer between filler particles in the contact point, which enhances considerably the contact resistance.

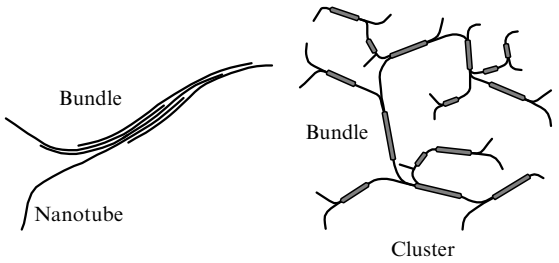

Figure 32. Multiscale structures of aggregated CNTs in a polymer matrix, considered in Ref. [256].

It should be noted that the assumption of a random distribution of nanotubes over the polymer matrix is not always obeyed. The experimental data [255] indicate that the CNT aggregation in a viscous matrix occurs in the course of time and is usually accompanied by an increase in electrical conductivity. The main mechanisms of the aggregation relate to either hydrodynamic phenomena and the attendant emergence of shear stresses or electrostatic effects caused by the action of external electric fields. Thus, it was shown in Ref. [207] that the formation of conducting networks from nanotubes occurs under the action of an alternating electric field applied during the polymerization of the matrix. Such a self-organization of nanotubes in a polymer matrix may influence the properties of intertube contacts. Some structures that can form particularly in a CNT-doped polymer matrix are illustrated in Fig. 32 [256]. The contacts in such a structure are characterized by a long length and therefore should possess a high conductance.

Therefore, the analysis of the electrical properties of nanotube contacts in a polymer material demonstrates that the nanocomposite conductivity is limited, as a rule, by the intertube contact resistance. Therewith, the contact resistance substantially depends on the nanotube's structure and contact geometry (intertube distance, transection angle). A high magnitude of contact resistance in a nanocomposite can be caused both by a large intertube gap due to the penetration of polymer molecules between the nanotubes, which lowers the tunneling probability and by a difference in the electron structures of contacting nanotubes. Specifically, the incompatibility of longitudinal electron wave vectors in adjacent nanotubes results in a rather low probability of electron transport between nanotubes with different chiralities. In this case, the contact conductance is considerably lower than the conductance quantum limit.

While the percolation threshold is mainly determined by the geometric parameters of nanotubes (such as the aspect ratio and the curvature) and the structural properties of the nanotube assembly (degree of dispersion, distribution homogeneity, orientation and ordering of nanotubes), the absolute value of nanocomposite conductivity after reaching the percolation threshold is mainly determined by the properties of intertube contacts which depend on the functionalization of nanotubes, properties of the polymer matrix, and conditions of nanocomposite production. Specifically, a strong interaction between a filler and a polymer matrix (for example, due to functionalization of the filler surface) improves the dispersion of the filler in the matrix; however, it can promote an enhancement of the contact resistance because of the sharp decrease in the tunneling probability.

Properties of the intertube contacts can be changed, controling the interaction energy between CNTs and the

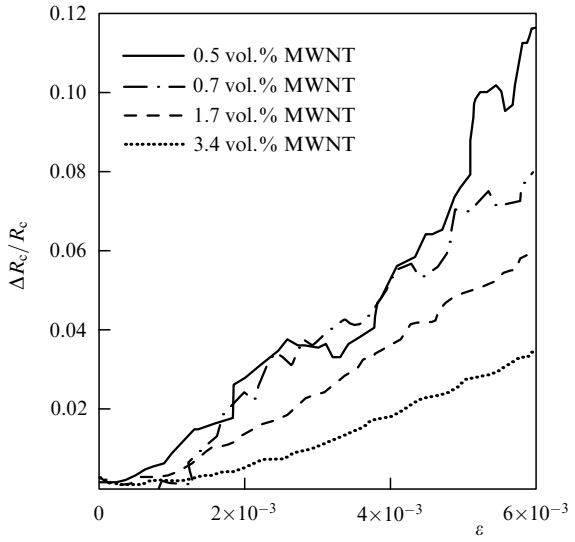

Figure 33. Dependences of the relative resistance of polycarbonate/CNT composite on weak mechanical stresses, measured at various filler loadings [258].

polymer matrix. It was shown by Zeng et al. [257] that the usage of annealed CNTs having a reduced number of polar groups on their surface permits lowering the surface energy of nanotubes and the energy of adhesion of a polyoxymethylene matrix, which should result in a less coverage of nanotubes with polymer molecules in accordance with the high electrical conductivity of the nanocomposite obtained.

A strong dependence of the conductivity of CNT-doped nanocomposites on their structure can be used to measure mechanical stresses by means of these materials and develop sensors built around them [258]. A mechanical deformation of a nanocomposite causes a change in the filler structure that can be described in the framework of the fiber reorientation model through the rotation, displacement, and tension of filler particles [259, 260]. Such a structural modification causes a change in the thickness of the interfiller polymer layer, which is reflected in the change of the contact resistance. The decrease in the polymer layer thickness due to the deformation of the polymer matrix along the filler particle is determined by the Poisson ratio ν_m of the matrix. The sensitivity of the contact resistance R_c to small strains ε can be estimated through the following expression

$$\frac{\Delta R_c/R_c}{\varepsilon} \approx \nu_m \frac{d-D}{d_{tun}} \gg 1\,. \qquad (27)$$

The results of the above analysis are in agreement with the available experimental data on the dependence of the composite conductivity on small mechanical stresses. The dependences of $\Delta R_c/R_c$ on the relative strain ε measured in Ref. [258] for composite polycarbonate/MWCNT (see Fig. 33) demonstrate that the ratio $(\Delta R_c/R_c)/\varepsilon$ can reach 20 at low CNT loadings.

4. Conclusions

The analysis of extensive experimental data reveals that the addition of CNTs to a polymer matrix results in a nonproportional increase in the electrical conductivity of the composite produced. The composite conductivity can increase by 8–10 orders of magnitude, transforming the material from an insulator into a conductor as a result of CNT loading at the level of 0.1 wt.%. Such a transformation has a percolation character, in accordance with which, upon exceeding some loading (the percolation threshold), nanotubes in the polymer matrix form conducting paths providing the charge transport. The data related to the percolation threshold and the maximum magnitude of the conductivity measured for materials of the same composition are characterized by a considerable spread, which is caused by a spread in the properties of CNTs, their possible aggregation and alignment, various degrees of homogeneity of the composite, and other factors that are determined by conditions of sample preparation.

In such a situation, efforts addressed at modeling the electrical properties of CNT-doped composites play a special role. Execution of model calculations permits establishing the dependences of the electrical characteristics of composites on such factors as the length and aspect ratio of CNTs, their conductance, the intertube contact resistance, the possibility of formation of a thin polymer film surrounding CNT surface and inhibiting the electrical contact formation, violation of the rectilinear CNT structure, degrees of their aggregation and the alignment, etc.

Modeling the electrical properties of CNT-doped composites is based mainly on the Monte Carlo method, which permits a description and analysis of percolation circuits of arbitrary structure with any physical and chemical properties. In spite of a large number of studies devoted to the numerical modeling of the electrical properties of CNT-doped composites using the Monte Carlo method, many issues related to this problem still remain unclear. Thus, the authors of most publications usually proceed from the belief that all the nanotubes involved in the composite possess similar characteristics (length, aspect ratio, and conductance). Moreover, the resistance of the intertube electrical contact is assumed to be fixed.

The above assumptions are inspired by shortening the computing time and do not correspond to the real physical situation. One can believe that the further development of computer techniques and supercomputers will permit the creation of models free from the above and other simplifying assumptions. Such models will form the basis for the wide development and utilization of new composite materials combining the mechanical and optical properties of polymers with the electrical properties of CNTs.

However, in order to ensure the production of composites with predictable characteristics, it is necessary to modify the technology used to prepare such composites, in parallel with the development of methods of their modeling. An analysis of the situation performed on the basis of the available experimental data and simulation results indicate that the intertube contact resistance depends on such factors as the occurrence of polymer molecules within the contact region, which hinders electron tunneling through the contact, and the interrelation between the chiralities of contacting nanotubes. These factors are hardly controllable by experimenterlists, which is why the data on the conductivity of CNT-doped composites are characterized by a considerable spread, as seen in Table 1. The approaches demonstrated recently and directed to the improvement of the intertube contact conditions include the functionalization of nanotubes with radicals or metal atoms, as well as the usage of nanotubes doped with, for example, nitrogen. The problem of conjugation of

nanotubes of different chiralities is resolved through the utilization of defective nanotubes, which permits partially overcoming the difficulty of their contact related to non-conservation of the electron momentum.

The practical importance of the problems of the development and usage of CNT-doped polymer composites is connected directly with the issue of the stability of such composites and the stability of their physical and chemical properties. The stability of such systems is mainly determined by the stability of the polymer matrix which is prone to thermal degradation. It has been found [123, 261, 262] that doping a polymer matrix with CNTs, as well as with clay particles, results in an enhancement of the stability of the material in relation to thermal degradation. Therewith, the temperature of the maximum rate of the weight loss increases by about 10%, and the absolute value of the weight loss can decrease by more than 50%. This permits the usage of this material as a flame retardant and fire proofing.

Considering the thermal stability of a polymer material, it should be realized that the thermal stability relates to rheological characteristics of the material and inserting nanoparticles allows a considerable enhancement of the nanocomposite viscosity. The rheological properties of nanocomposites also demonstrate the threshold dependence on nanotube content. However, the percolation threshold in this case is lower than that for electrical conduction [112].

It should be noted that the development of investigations of CNT-doped polymer composites has an impact on the general methodology of the approach to the theoretical description of such systems. In particular, in the usage as a filler of nanotubes having a high aspect ratio, the problem of anisotropy of physical, chemical, and specifically electrical properties comes to the forefront. Brief mention has already been made of this problem at the end of the present article; however, in spite of its practical importance, it has received rather little attention in most theoretical work. The origin of the occurrence of anisotropy in the physical and chemical properties of a CNT-doped composite can be related to both the fabrication procedure and the action of an external electric field promoting the alignment of nanotubes in a polymer matrix and corresponding spatial anisotropy in composite properties. As far as we know there has never been a theory describing the process of the orientation ordering of CNTs in a liquid polymer matrix under the action of an electric field. Building and developing such a theory could promote further advances in the field of composite materials with conducting fillers.

Acknowledgments

This study was supported by the Russian Federation Ministry of Education and Science within the framework of Megagrant No. 14.Z50.31.0002 and the State Program 'Organization of Scientific Research' (project 1001140) as well as the RFBR (grants Nos 14-29-04071 and 13-08-00404a).

References

1. Eletskii A V *Phys. Usp.* **50** 225 (2007); *Usp. Fiz. Nauk* **177** 233 (2007)
2. Ngabonziza Y, Li J, Barry C F *Acta Mech.* **220** 289 (2011)
3. Eletskii A V *Phys. Usp.* **52** 209 (2009); *Usp. Fiz. Nauk* **179** 225 (2009)
4. Charlier J-C, Blase X, Roche S *Rev. Mod. Phys.* **79** 677 (2007)
5. Grigoriev I S, Meilikhov E Z (Eds) *Handbook of Physical Quantities* (Boca Raton, NY: CRC Press, 1996); Translated from Russian: *Fizicheskie Velichiny* (Moscow: Energoatomizdat, 1991) p. 543
6. Sarychev A K, Shalaev V M *Electrodynamics of Metamaterials* (Singapore: World Scientific, 2007); *Elektrodinamika Metamaterialov* (Moscow: Nauchnyi Mir, 2011)
7. Shklovskii B I, Éfros A L *Sov. Phys. Usp.* **18** 845 (1975); *Usp. Fiz. Nauk* **117** 401 (1975)
8. Stauffer D, Aharony A *Introduction to Percolation Theory* (London: Taylor and Francis, 1992)
9. Sahimi M *Applications of Percolation Theory* (London: Taylor and Francis, 1994)
10. Kirkpatrick S *Rev. Mod. Phys.* **45** 574 (1973)
11. Coleman J N et al. *Phys. Rev. B* **58** R7492 (1998)
12. Bauhofer W, Kovas J *Compos. Sci. Technol.* **69** 1486 (2009)
13. Spitalsky Z et al. *Prog. Polymer Sci.* **35** 357 (2010)
14. Smith J G (Jr.) et al. *Polymer* **45** 825 (2004)
15. Chen Q, Bin Y, Matsuo M *Macromolecules* **39** 6528 (2006)
16. Bokobza L *Vib. Spectrosc.* **51** 52 (2009)
17. Landi B J et al. *Nano Lett.* **2** 1329 (2002)
18. Martin C A et al. *Compos. Sci. Technol.* **64** 1236 (2004)
19. Sandler J K W et al. *Polymer* **44** 5893 (2003)
20. Moisala A et al. *Compos. Sci. Technol.* **66** 1285 (2006)
21. Bryning M B et al. *Adv. Mater.* **17** 1186 (2005)
22. Kovacs J Z et al. *Compos. Sci. Technol.* **67** 922 (2007)
23. Sandler J et al. *Polymer* **40** 5967 (1999)
24. Gojny F H et al. *Polymer* **47** 2036 (2006)
25. Kim Y J et al. *Carbon* **43** 23 (2005)
26. Yu A P et al. *Appl. Phys. Lett.* **89** 133102 (2006)
27. Kim B, Lee J, Yu I *J. Appl. Phys.* **94** 6724 (2003)
28. Barrau S et al. *Macromol. Rapid Commun.* **26** 390 (2005)
29. Sun L-H et al. *J. Nanomater.* **2011** 307589 (2011)
30. Brown J M et al. *Polymer* **46** 10854 (2005)
31. Li J et al. *Adv. Funct. Mater.* **17** 3207 (2007)
32. Hu N, Masuda Z, Fukunaga H, in *Proc. 16th Intern. Conf. on Composite Materials, Kyoto, Japan, 2007*
33. Du F M et al. *J. Polym. Sci. B* **44** 1513 (2006)
34. Bai J B, Allaoui A *Composites A* **34** 689 (2003)
35. Liu L *J. Appl. Phys.* **101** 94106 (2007)
36. Yuen S M et al. *J. Appl. Polym. Sci.* **103** 1272 (2007)
37. Allaoui A et al. *Compos. Sci. Technol.* **62** 1993 (2002)
38. Cui S et al. *Carbon* **41** 797 (2003)
39. Barrau S et al. *Macromolecules* **36** 9678 (2003)
40. Song Y S, Youn J R *Carbon* **43** 1378 (2005)
41. Li N et al. *Nano Lett.* **6** 1141 (2006)
42. Thostenson E T, Chou T W *Carbon* **44** 3022 (2006)
43. Santos A S et al. *J. Appl. Polym. Sci.* **108** 979 (2008)
44. Spitalsky Z et al. *Composites A* **40** 778 (2009)
45. Liu L et al. *Macromol. Rapid Commun.* **30** 627 (2009)
46. Pecastaings G et al. *J. Nanosci. Nanotechnol.* **4** 838 (2004)
47. Wichmann M H G et al. *Mech. Compos. Mater.* **42** 395 (2006)
48. Kodgire P V et al. *Chem. Phys. Lett.* **432** 480 (2006)
49. Krause B, Potschke P, Hauser L *Compos. Sci. Technol.* **69** 1505 (2009)
50. Kim H S et al. *Mater. Lett.* **61** 2251 (2007)
51. Wang T et al. *Adv. Mater.* **18** 2730 (2006)
52. Musumeci A W et al. *Polymer* **48** 1667 (2007)
53. Kuila B et al. *Macromolecules* **40** 278 (2007)
54. Singh I et al. *Carbon* **46** 1141 (2008)
55. Yoshino K et al. *Fullerene Sci. Technol.* **7** 695 (1999)
56. Kymakis E, Amaratunga G A J *J. Appl. Phys.* **99** 84302 (2006)
57. Tchmutin I A et al. *Carbon* **41** 1391 (2003)
58. Logakis E et al. *Polymer* **50** 5103 (2009)
59. Meincke O et al. *Polymer* **45** 739 (2004)
60. Han S J, Kim B, Suh K D *Macromol. Chem. Phys.* **208** 377 (2007)
61. Blanchet G B, Fincher C R, Gao F *Appl. Phys. Lett.* **82** 1290 (2003)
62. Konyushenko E N et al. *Polymer* **47** 5715 (2006)
63. Nogales A et al. *Macromolecules* **37** 7669 (2004)
64. Deng J et al. *Eur. Polym. J.* **38** 2497 (2002)
65. Huang J E et al. *Carbon* **41** 2731 (2003)
66. Sainz R et al. *Nanotechnology* **16** S150 (2005)
67. Ramasubramaniam R, Chen J, Liu H *Appl. Phys. Lett.* **83** 2928 (2003)
68. Takeda T et al. *Polymer* **52** 3852 (2011)
69. Pötschke P et al. *AIP Conf. Proc.* **786** 596 (2005)
70. Hornbostel B et al. *Phys. Status Solidi B* **243** 3445 (2006)

71. Pötschke P et al. *Polymer* **45** 8863 (2004)
72. Pötschke P, Dudkin S M, Alig I *Polymer* **44** 5023 (2003)
73. Chen L, Pang X J, Yu Z L *Mater. Sci. Eng. A* **457** 287 (2007)
74. Pötschke P, Fornes T D, Paul D R *Polymer* **43** 3247 (2002)
75. Pötschke P, Bhattacharyya A R, Janke A *Carbon* **42** 965 (2004)
76. Pötschke P, Bhattacharyya A R, Janke A *Eur. Polym. J.* **40** 137 (2004)
77. Pötschke P et al. *Fullerenes, Nanotubes, Carbon Nanostruct.* **13** 211 (2005)
78. Satapathy B K et al. *Compos. Sci. Technol.* **67** 867 (2007)
79. Kim K H, Jo W H *Carbon* **47** 1126 (2009)
80. Mitchell C A, Krishnamoorti R *Macromolecules* **40** 1538 (2007)
81. Saed K, Park S Y *J. Appl. Polym. Sci.* **104** 1957 (2007)
82. Worsley M A et al. *J. Mater. Chem.* **19** 3370 (2009)
83. Khosla A, Gray B L *Mater. Lett.* **63** 1203 (2009)
84. Mierczynska A, Mayne-L'Hermite M, Boiteux G *J. Appl. Polym. Sci.* **105** 158 (2007)
85. Lisunova M O et al. *Eur. Polym. J.* **43** 949 (2007)
86. Bin Y et al. *Macromolecules* **36** 6213 (2003)
87. Xi Y et al. *J. Appl. Polym. Sci.* **105** 2868 (2007)
88. Isaji S, Bin Y, Matsuo M *Polymer* **50** 1046 (2009)
89. Gorrasi G et al. *J. Polym. Sci. B* **45** 597 (2007)
90. Zhang Q H et al. *Carbon* **44** 778 (2006)
91. Jeon K et al. *Polymer* **48** 4751 (2007)
92. McNally T et al. *Polymer* **46** 8222 (2005)
93. Zhao D *Pigment Resin Technol.* **35** 341 (2006)
94. Munoz E et al. *Adv. Mater.* **17** 1064 (2005)
95. Grimes C A et al. *Chem. Phys. Lett.* **319** 460 (2000)
96. Isayev A I, Kumar R, Lewis T M *Polymer* **50** 250 (2009)
97. Fukushima T et al. *Small* **2** 554 (2006)
98. McCullen S D et al. *Macromolecules* **40** 997 (2007)
99. Awasthi K et al. *Nanotechnology* **17** 5417 (2006)
100. Chatterjee T et al. *Adv. Funct. Mater.* **15** 1832 (2005)
101. Anand A K, Agarwal U S, Rani J *J. Appl. Polym. Sci.* **104** 3090 (2007)
102. Hu G J et al. *Polymer* **47** 480 (2006)
103. Hernandez J J et al. *Compos. Sci. Technol.* **69** 1867 (2009)
104. Ghose S et al. *Compos. Sci. Technol.* **66** 1995 (2006)
105. Lanticse L J et al. *Carbon* **44** 3078 (2006)
106. Ounaies Z et al. *Compos. Sci. Technol.* **63** 1637 (2003)
107. Jiang X W, Bin Y Z, Matsuo M *Polymer* **46** 7418 (2005)
108. Srivastava R et al. *Macromol. Mater. Eng.* **294** 96 (2009)
109. Delozier D M et al. *Macromolecules* **39** 1731 (2006)
110. Yuen S M et al. *Compos. Sci. Technol.* **67** 2564 (2007)
111. Zhu B K et al. *Compos. Sci. Technol.* **66** 548 (2006)
112. Zhang D et al. *J. Phys. Chem. B* **110** 12910 (2006)
113. Wu D et al. *Biomacromolecules* **10** 417 (2009)
114. Schmidt R H et al. *Langmuir* **23** 5707 (2007)
115. Chen H et al. *Nanotechnology* **18** 415606 (2007)
116. Skakalova V, Dettlaff-Weglikowska U, Roth S *Synth. Met.* **152** 349 (2005)
117. Kim H M et al. *Phys. Rev. B* **74** 054202 (2006)
118. Benoit J M et al. *Synth. Met.* **121** 1215 (2001)
119. Du F, Fischer J E, Winey K I *Phys. Rev. B* **72** 121404(R) (2005)
120. Du F et al. *Macromolecules* **37** 9048 (2004)
121. Dai J F et al. *Mater. Lett.* **61** 27 (2007)
122. Regev O et al. *Adv. Mater.* **16** 248 (2004)
123. Du F, Fischer J E, Winey K I *J. Polym. Sci. B* **41** 3333 (2003)
124. Dettlaff-Weghkowska U et al. *Phys. Status Solidi B* **243** 3440 (2006)
125. Stephan C et al. *J. Mater. Res.* **17** 396 (2002)
126. Kim H M et al. *Curr. Appl. Phys.* **4** 577 (2004)
127. Kim H M et al. *Appl. Phys. Lett.* **84** 589 (2004)
128. Chauvet O, Benoit J M, Corraze B *Carbon* **42** 949 (2004)
129. Sundaray B et al. *Appl. Phys. Lett.* **88** 143114 (2006)
130. Peng H, Sun X *Chem. Phys. Lett.* **471** 103 (2009)
131. Kilbride B E et al. *J. Appl. Phys.* **92** 4024 (2002)
132. Curran S A et al. *Adv. Mater.* **10** 1091 (1998)
133. Coleman J N et al. *Synth. Met.* **102** 1174 (1999)
134. Andrews R et al. *Macromol. Mater. Eng.* **287** 395 (2002)
135. Kharchenko S B et al. *Nature Mater.* **3** 564 (2004)
136. Tjong S C, Liang G D, Bao S P *Scripta Mater.* **57** 461 (2007)
137. Seo M K, Park S J *Chem. Phys. Lett.* **395** 44 (2004)
138. Gorrasi G et al. *Nanotechnology* **18** 275703 (2007)
139. Micusik M et al. *J. Appl. Polym. Sci.* **113** 2536 (2009)
140. Yang J et al. *J. Appl. Polym. Sci.* **109** 720 (2008)
141. Aarab H et al. *Synth. Met.* **155** 63 (2005)
142. Fan J et al. *J. Appl. Polym. Sci.* **74** 2605 (1999)
143. Zhang X et al. *Chem. Phys. Chem.* **5** 998 (2004)
144. Yu Y et al. *J. Polym. Sci. A* **43** 6105 (2005)
145. Wu T M, Lin S H *J. Polym. Sci. B* **44** 1413 (2006)
146. Sluzarenko N et al. *Carbon* **44** 3207 (2006)
147. Chang T E et al. *Polymer* **47** 7740 (2006)
148. Grossiord N et al. *Chem. Mater.* **19** 3787 (2007)
149. Tchoul M N et al. *Chem. Mater.* **20** 3120 (2008)
150. Hermant M C et al. *Compos. Sci. Technol.* **69** 656 (2009)
151. Kim S T, Choi H J, Hong S M *Colloid Polym. Sci.* **285** 593 (2007)
152. Poa C H et al. *Appl. Phys. Lett.* **80** 3189 (2002)
153. Ha M L P et al. *Macromol. Chem. Phys.* **208** 446 (2007)
154. Dalmas F et al. *Compos. Sci. Technol.* **67** 829 (2007)
155. Antonucci V et al. *Macromol. Symp.* **247** 172 (2007)
156. Dufresne A et al. *J. Mater. Sci.* **37** 3915 (2002)
157. Li Y, Shimizu H *Macromolecules* **42** 2587 (2009)
158. Karim M R, Lee C J, Lee M S *J. Polym. Sci. A* **44** 5283 (2006)
159. Kim Y J et al. *IEEE Trans. Electromag. Compatibility* **47** 872 (2005)
160. Koerner H et al. *Polymer* **46** 4405 (2005)
161. Cho J W et al. *Macromol. Rapid Commun.* **26** 412 (2005)
162. Yoo H J et al. *J. Macromol. Sci. B* **45** 441 (2006)
163. You K M et al. *J. Mater. Sci.* **46** 6850 (2011)
164. Wang G et al. *Nanotechnology* **17** 5829 (2006)
165. Shaffer M S P, Windle A H *Adv. Mater.* **11** 937 (1999)
166. Hernandez Y R et al. *Scripta Mater.* **58** 69 (2008)
167. Grunlan J C et al. *Adv. Mater.* **16** 150 (2004)
168. Choi C S, Park B J, Choi H J *Diamond Relat. Mater.* **16** 1170 (2007)
169. Mamunya Y et al. *Compos. Sci. Technol.* **68** 1981 (2008)
170. Seoul C, Kim Y T, Baek C K *J. Polym. Sci. B* **41** 1572 (2003)
171. Dang Z M et al. *Adv. Mater.* **19** 852 (2007)
172. Wang L, Dang Z M *Appl. Phys. Lett.* **87** 42903 (2005)
173. Dalmas F et al. *J. Polym. Sci. B* **43** 1186 (2005)
174. Pedroni L G et al. *J. Appl. Polym. Sci.* **112** 3241 (2009)
175. Liu C H et al. *Appl. Phys. Lett.* **84** 4248 (2004)
176. Lahiff E et al. *Carbon* **44** 1525 (2006)
177. Vast L et al. *Compos. Sci. Technol.* **67** 880 (2007)
178. Gilmore K J, Moulton S E, Wallace G G *Carbon* **45** 402 (2007)
179. Bian C X et al. *Acta Chim. Sinica* **65** 525 (2007)
180. Battisti A, Skordos A A, Partridge I K *Compos. Sci. Technol.* **70** 633 (2010)
181. Kimura T et al. *Adv. Mater.* **14** 1380 (2002)
182. Gryshchuk O et al. *Composites A* **37** 1252 (2006)
183. Jiang M J, Dang Z M, Xu H P *Appl. Phys. Lett.* **90** 42914 (2007)
184. Kwon J Y, Kim H D *J. Appl. Polym. Sci.* **96** 595 (2005)
185. Logakis E et al. *J. Polym. Sci. B* **47** 764 (2009)
186. Mamunya Y P et al. *Polym. Eng. Sci.* **42** 90 (2002)
187. Ezquerra T A et al. *Adv. Mater.* **2** 597 (1990)
188. Balberg I et al. *Phys. Rev. B* **30** 3933 (1984)
189. Balberg I, Binenbaum N *Phys. Rev. A* **31** 1222(R) (1985)
190. Connor M T et al. *Phys. Rev. B* **57** 2286 (1998)
191. Barrau S et al. *Macromolecules* **36** 5187 (2003)
192. McLachlan D S et al. *J. Polym. Sci. B* **43** 3273 (2005)
193. Garboczi E J et al. *Phys. Rev. E* **52** 819 (1995)
194. Celzard A et al. *Phys. Rev. B* **53** 6209 (1996)
195. Eletskii A V *Phys. Usp.* **53** 863 (2010); *Usp. Fiz. Nauk* **180** 897 (2010)
196. Bocharov G S, Eletskii A V, Sommerer T J *Tech. Phys.* **56** 540 (2011); *Zh. Tekh. Fiz.* **81** (4) 111 (2011)
197. Schwarz M-K, Bauhofer W, Schulte K *Polymer* **43** 3079 (2002)
198. Kyritsis A, Pissis P, Grammatikakis J *J. Polym. Sci. B* **33** 1737 (1995)
199. Peoglos V et al. *J. Nanostruct. Polym. Nanocompos.* **3** 116 (2007)
200. Sheng P, Sichel E K, Gittleman J I *Phys. Rev. Lett.* **40** 1197 (1978)
201. Sichel E K, Gittleman J I, Sheng P, in *Carbon Black-Polymer Composites*: *the Physics of Electrically Conducting Composites* (Ed. E K Sichel) (New York: M. Dekker, 1982)
202. Mott N F, Davis E A *Electronic Processes in Non-Crystalline Materials* 2nd ed. (New York: Oxford Univ. Press, 1979)
203. Laredo E et al. *Macromolecules* **36** 9840 (2003)
204. Steeman P A M, Maurer F H J *Polymer* **33** 4236 (1992)

205. Thostenson E T, Ziaee S, Chou T W *Compos. Sci. Technol.* **69** 801 (2009)
206. Vera-Agullo J et al. *Compos. Sci. Technol.* **69** 1521 (2009)
207. Martin C A et al. *Polymer* **46** 877 (2005)
208. Liang G D, Bao S P, Tjong S C *Mater. Sci. Eng. B* **147** 55 (2007)
209. So H, Cho J W, Sahoo N G *Eur. Polym. J.* **43** 3750 (2007)
210. Haggenmueller R et al. *Macromolecules* **40** 2417 (2007)
211. Munson-McGee S H *Phys. Rev. B* **43** 3331 (1991)
212. Grujicic M, Cao G, Roy W N *J. Mater. Sci.* **39** 4441 (2004)
213. Dalmas F et al. *Acta Mater.* **54** 2923 (2006)
214. Hu N et al. *Nanotechnology* **19** 215701 (2008)
215. Hu N et al. *Composites A* **39** 893 (2008)
216. Vilcakova J, Saha P, Quadrat Q *Eur. Polym. J.* **38** 2343 (2002)
217. Yang Y et al. *Adv. Mater.* **17** 1999 (2005)
218. Gao B et al. *Phys. Rev. B* **74** 085410 (2006)
219. Salvato M et al. *Phys. Rev. Lett.* **101** 246804 (2008)
220. Cardoso P et al. *Phys. Status Solidi A* **207** 407 (2010)
221. Li C Y, Thostenson E T, Chou T W *Appl. Phys. Lett.* **91** 223114 (2007)
222. Li C, Thostenson E T, Chou T W *Compos. Sci. Technol.* **68** 1445 (2008)
223. Lu W, Chou T-W, Thostenson E T *Appl. Phys. Lett.* **96** 223106 (2010)
224. Behnam A et al. *Appl. Phys. Lett.* **89** 093107 (2006)
225. Behnam A et al. *J. Vac. Sci. Technol. B* **25** 348 (2007)
226. Foygel M et al. *Phys. Rev. B* **71** 104201 (2005)
227. Balberg I, Binenbaum N *Phys. Rev. B* **28** 3799 (1983)
228. Natsuki T, Endo M, Takahashi T *Physica A* **352** 498 (2005)
229. Behnam A, Guo J, Ural A *J. Appl. Phys.* **102** 044313 (2007)
230. Behnam A, Ural A *Phys. Rev. B* **75** 125432 (2007)
231. Kocabas C et al. *Nano Lett.* **7** 1195 (2007)
232. Hazama Y et al. *Phys. Rev. B* **82** 045204 (2010)
233. Derrida B, Vannimenus J *J. Phys. A Math. Gen.* **15** L557 (1982)
234. Bergman D J, Duering E, Murat M *J. Stat. Phys.* **58** 1 (1990)
235. Li J, Zhang S-L *Phys. Rev. E* **80** 040104(R) (2009)
236. Keblinski P, Cleri F *Phys. Rev. B* **69** 184201 (2004)
237. Narayanunni V, Gu H, Yu C *Acta Mater.* **59** 4548 (2011)
238. Simmons J D *J. Appl. Phys.* **34** 1793 (1963)
239. Yu Y, Song G, Sun L *J. Appl. Phys.* **108** 084319 (2010)
240. Bao W S et al. *Nanotechnology* **22** 485704 (2011)
241. Grimaldi C et al. *Appl. Phys. Lett.* **102** 223114 (2013)
242. Buia C, Buldum A, Lu J P *Phys. Rev. B* **67** 113409 (2003)
243. Tunney M A, Cooper N R *Phys. Rev. B* **74** 075406 (2006)
244. Uryu S, Ando T *Phys. Rev. B* **76** 155434 (2007)
245. Buldum A, Lu P J *Phys. Rev. B* **63** 161403(R) (2001)
246. Maarouf A A, Mele E J *Phys. Rev. B* **83** 045402 (2011)
247. Bell R A, Payne M C, Mostofi A A *Phys. Rev. B* **89** 245426 (2014)
248. Penazzi G et al. *J. Phys. Chem. C* **117** 8020 (2013)
249. Li E Y, Marzari N *ACS Nano* **5** 9726 (2011)
250. Ma P C, Tang B Z, Kim J-K *Carbon* **46** 1497 (2008)
251. DeVivo B et al., TNANO-00357-2012 (2012)
252. Park C et al. *Chem. Phys. Lett.* **364** 303 (2002)
253. Souier T, Stefancich M, Chiesa M *Nanotechnology* **23** 405704 (2012)
254. Souier T et al. *Carbon* **64** 150 (2013)
255. Alig I et al. *Polymer* **53** 4 (2012)
256. Faiella G et al. *Appl. Phys. Lett.* **95** 153106 (2009)
257. Zeng Y et al. *Carbon* **48** 3551 (2010)
258. Kuronuma Y et al. *Compos. Sci. Technol.* **72** 1678 (2012)
259. Taya M, Kim W J, Ono K *Mech. Mater.* **28** 53 (1998)
260. Rahman R, Servati P *Nanotechnology* **23** 055703 (2012)
261. Kashiwagi T et al. *Macromol. Rapid Commun.* **23** 761 (2002)
262. Kashiwagi T et al. *Nature Mater.* **4** 928 (2005)